

Strain engineering of H/transition metal systems

I. G. Shuttleworth,
School of Science and Technology,
Nottingham Trent University,
Nottingham NG11 8NS.
UK

E-mail: ian.shuttleworth@ntu.ac.uk

Abstract

The effects of both compressive and tensile surface strain on the hydrogenated low-index faces of Fe, Co, Ni, Cu, Ru, Rh, Pd, Ag, Os, Ir, Pt and Au has been investigated using density functional theory (DFT). Changes in the preferred H binding site have been observed on the Pd, Ir and Pt surfaces when the surface lattice constant is strained by up to 2%, and on Fe, Rh, Ag and Os surfaces for larger strains of up to 5%. A complete discussion of the variance of the hydrogen binding energy, charge, density of states and local geometry with strain is presented. The exchange-correlation, electrostatic and kinetic contributions to the binding energy are delineated and their respective contributions are discussed. The mechanism which determines the preferred binding site for each system under strain is shown to be complex.

Keywords

Hydrogen; Transition Metal; Strain Engineering; Density Functional Theory.

1. Introduction

The controllability of surface reactions has been a goal for surface science since its inception. The topic has developed significantly in the recent years as strain engineering has started to demonstrate some elements of the required controllability in an effective way [1-3].

One of the earlier studies of the effects of strain looked at oxygen adsorption on Ru(0001) [4] and showed that oxygen adsorbs preferentially in the on-top position in regions of tensile strain and generated the surface strain by forming sub-surface cavities using sputter-anneal cycles. Ar⁺ ion sputtering has been used more recently [5] to distribute stress across Au(100) surfaces and an increase in chemical reactivity was seen at the defected, or locally stressed, sites. Strain has also been seen across the surfaces of metallic nanoparticles – for example, Pd@Pt [6], Pt [7] and Au [8-9] - and both oxide nanoparticles and thin-films [10-11].

Comparative studies have addressed the behaviour of surface energies when the underlying bulk atoms are in a non-equilibrium, or stressed state. This behaviour can be induced by growing thick metallic layers on top of a support layer with a different lattice constant using, for example, repeated atomic layer deposition cycles [12], or by mechanically applying surface-parallel strain to the system [13]. This technology is established in the semiconductor and metal-oxide-semiconductor field [14] but is less well understood for purely metallic surfaces. Recent studies [15] have shown that the application of bulk strain is effective in controlling the binding site preference of H across catalytically active metallic surfaces and similar studies have shown H-binding site shifts in the bulk [16]. The binding energy of hydrogen to TiO₂ [17] has recently shown to be sensitive to the strain state of the surface.

The behaviour of surface energy when the bulk atoms are stressed is therefore not directly predictable, and also of considerable importance when looking towards the applications of surface technology. The interest of the current work is to look at the behaviour of hydrogen on strained transition metal surfaces. Hydrogen is a key component in numerous industrial processes as well as remaining at the forefront of proposed energy storage technologies [18]. Applications of hydrogen technology have commonly used nanoparticles as intermediates and the characteristics of these nanoparticles, including shape, size and composition, will affect their performance [19-22]. Controlling these characteristics will consequently alter the way that the nanoparticle will interact with the gaseous medium. Methods of affecting control are necessarily indirect and effected in part by changes to the way that the nanoparticles are grown. Global restructuring phenomena are becoming identified with recent studies [23] classifying a group of binary alloy materials as stable towards strain.

The current work will approach the effect of strain on surface reaction from a fundamental point view. The existing literature of fundamental hydrogen adsorption on unstrained systems is extensive - a recent review [24] contained 443 references. However, the current work will explore hydrogen adsorption on strained substrates by computationally deforming a sequence of low index transition metal surfaces and scrutinise the interactions of these surfaces with hydrogen. The remainder of this work is divided into three main sections: the computational details are outlined in Section 2; Section 3 will discuss the hydrogen binding energy E and its exchange-correlation part E_{XC} , structural investigations, and studies of the surface bonding and

the work function change that accompany hydrogenation. The key findings of the work will then be elucidated in the Section 4.

2. Computational details

The plane-wave density functional theory (DFT) simulations presented in this work were performed using the Quantum Espresso package [25]. Brillouin zone sampling was performed on a (6×6×1) grid using a first-order Methfessel-Paxton smearing of 0.02 Ry [26]. The Fe, Co and Ni simulations for spin-polarised whereas all other simulations were not as Fe, Co and Ni are the only magnetic substrates considered in the current work. Norm-conserving pseudopotentials were used for the Cu, Ru, Rh, Pd, Os, Ir or Pt simulations [27] and ultrasoft pseudopotentials were used for the Fe, Co, Ni, Ag and Au simulations [27-28]. Recent studies [29] have shown that these pseudopotentials give extremely high precision equilibrium (zero-strain) lattice constants for each of the elements considered in the current work, with variations between the computational and experimental values of the lattice parameter of <0.10 Å for all systems. A wave-function kinetic energy cut-off of 50-100 Ry was used for all simulations and a charge density/potential kinetic energy cut-off of 4× that amount was used for the simulations that used norm-conserving pseudopotentials, and 12× that amount for the simulations that used ultra-soft pseudopotentials. The GGA approximation was used exclusively throughout this work.

Fig. 1 shows the surface structures investigated in the current work. For a sequence of FCC systems – Ni, Cu, Rh, Pd, Ag, Ir, Pt and Au – the hydrogenated hexagonal (111) and square (100) surfaces were simulated, as well as the hydrogenated hexagonal HCP Co(0001), Ru(0001) and Os(0001), and the BCC Fe(100) surfaces. All investigations were performed using (2×2) surface unit cells and 7 layer slabs, separated by a vacuum of approximately 12 atomic layer spacings. The amount of lattice strain σ was defined as

$$\frac{L}{L_0} = 1 + \frac{\sigma}{100} \quad (1)$$

L and L_0 are the strained and un-strained lattice constants, respectively. Throughout the current work, strain σ was numerically treated as a percentage and $\sigma \in [-5\%, \dots, +5\%]$. During relaxation only the central layer of metal atoms were constrained. The remaining atoms were allowed to relax freely. Because of the small unit cell size the possibility of in-plane reconstructions was not investigated; however, significant reconstruction effects were not anticipated. This is because within the group of metals investigated, few would be expected to reconstruct under the range of strains used. The notable exception to this is Au though that only undergoes reconstruction for large surface unit cells.

The hydrogen binding energy was defined as

$$E = \frac{1}{2} (E_{\text{H/metal}} - E_{\text{metal}} - 2E_{\text{H}}) \quad (2)$$

$E_{\text{H/metal}}$ is the total energy of the (2×2) hydrogenated transition metal slab, E_{metal} is the total energy of a clean, fully relaxed (2×2) transition metal slab and E_{H} is the total energy of an isolated H atom. The factors of 2 and 1/2 account for the binding of H atoms on either side of the slab. E_{H} was determined to be -0.92 Ry and was obtained by placing a single H atom in a 10 Å×10 Å×10 Å cubic unit cell and performing a single self-consistent field calculation.

The total energy $E_{\text{KS}}[n]$ of a system described by Kohn-Sham density functional theory can be written

$$E_{\text{KS}}[n] = T_{\text{S}}[n] + \int n(\vec{r})v_{\text{ext}}(\vec{r})d\vec{r} + \frac{1}{2} \iint \frac{n(\vec{r})n(\vec{r}')}{|\vec{r} - \vec{r}'|} d\vec{r}d\vec{r}' + E_{\text{XC}}[n] \quad (3)$$

$T_{\text{S}}[n]$ is the kinetic energy of the system, $v_{\text{ext}}(\vec{r})$ is the external potential and $n(\vec{r})$ is the electron density. To elucidate the importance of the terms on the right hand side of Eq. (3) the hydrogen binding energy Eq. (2) can be re-written to only consider the exchange-correlation components

$$E_{\text{XC}} = \frac{1}{2} (E_{\text{H/metal,XC}} - E_{\text{metal,XC}} - 2E_{\text{H,XC}}) \quad (4)$$

E_{XC} , $E_{\text{H/metal,XC}}$, $E_{\text{metal,XC}}$ and $E_{\text{H,XC}}$ are the exchange-correlation components of E , $E_{\text{H/metal}}$, E_{metal} and E_{H} , respectively. Quantitatively, the relative importance of the exchange-correlation energy $E_{\text{XC}}[n]$ can be evaluated using by comparing its contribution to the binding energy against the kinetic $T_{\text{S}}[n]$ and electrostatic contributions. The electrostatic contributions are the external and Coulomb contributions, which are the single and double integrals on the right hand side of Eq. (3), respectively. The average fractional kinetic and electrostatic component of the binding energy is given by

$$\langle E_{\text{K+ES}} \rangle = \frac{1}{n} \sqrt{\sum_{j=1}^n \left(\frac{E_j - E_{j,\text{XC}}}{E_j} \right)^2} \quad (5)$$

E_j and $E_{j,XC}$ are the total and exchange-correlation energies at a particular value of strain σ and n is the total number of strains investigated. Specifically for the current work, $n=11$ corresponding to $\sigma \in [-5\%, \dots, +5\%]$ incrementing in steps of 1% and then, for example, E_1 and $E_{1,XC}$ are the total and exchange correlation energies for $\sigma=-5\%$.

The strain-dependant hydrogen-metal distance r_{H-Me} was modelled using

$$r_{H-Me} = r_{H-Me,0} + \left(\frac{dr_{H-Me}}{d\sigma} \right) \sigma \quad (6)$$

This model approximates the dependence of r_{H-Me} on σ to a linear form as terms in σ^2 and higher are ignored. A similar approach is used to model the surface lattice relaxation Δz_{surf} and work function change ϕ below.

Using the nomenclature defined in Fig. 1 vertical relaxation of the surface metal atoms is defined as

$$\Delta z_{surf} = \frac{z_{surf} - z_{surf,ideal}}{z_{hkl,ideal}} \times 100 \quad (7)$$

z_{surf} and $z_{surf,ideal}$ are the actual and ideal bulk terminated vertical positions of the surface metal atoms, respectively, and $z_{hkl,ideal}$ is the ideal bulk layer spacing. z_{surf} , $z_{surf,ideal}$ and $z_{hkl,ideal}$ vary with strain σ . The factor of 100 used in Eq. (7) converts Δz_{surf} to a percentage and is intended to provide consistency between the treatments of Δz_{surf} and σ . Δz_{surf} is numerically positive if the atoms have expanded outwards towards the vacuum, and negative if they are contracted inwards towards the bulk. In the current work, only the vertical relaxation of the surface metal atoms closest to the surface hydrogen atoms was investigated.

Δz_{surf} was modelled using the linear equation given in Eq. (8):

$$\Delta z_{surf} = \Delta z_{surf,0} + \left(\frac{d\Delta z_{surf}}{d\sigma} \right) \sigma \quad (8)$$

The work function ϕ of both the clean and the hydrogenated systems was defined by

$$\phi = V(\infty) - E_F \quad (9)$$

$V(\infty)$ was the potential at a height of approximately 6 lattice constants above the metal surface layer and E_F was the Fermi energy. The strain-dependence of ϕ was modelled linearly using

$$\phi = \phi_0 + \left(\frac{d\phi}{d\sigma} \right) \sigma \quad (10)$$

ϕ_0 is the work function of the hydrogenated system at zero strain ($\sigma = 0$) and $\left(\frac{d\phi}{d\sigma} \right)$ is the linear strain dependence.

3. Results and discussion

3.1 Binding energy and structural parameters

The investigations in this work first focus on the hydrogen binding energy E and its exchange-correlation part E_{XC} , structural investigations, and then will focus on studies of the surface bonding and the work function change that accompany hydrogenation.

Fig. 2 shows the variation of hydrogen binding energy E with σ for the (a) H/Ni(111) and (b) H/Cu(111) surfaces, and Fig. 3 shows E versus σ for the (a) H/Ir(111) and (b) H/Pt(111) systems. The remaining hydrogenated FCC (111) binding energy curves are presented in Fig. S1. The hydrogen binding energy curves for the FCC (100) systems were presented in Figs. 4 (a-c) for the H/Rh(100), H/Pd(100) and H/Ag(100) systems, respectively and Fig. S2 for the remaining hydrogenated FCC (100) systems. Further, the hydrogen binding energy curves for the HCP (0001) and BCC (100) systems were presented in Figs. 5 (a-b) for the H/Os(0001) and H/Fe(100) systems, respectively and Fig. S3 for the remaining hydrogenated HCP (0001) systems. The hydrogen binding energy curves are presented in this way to highlight systems which demonstrate significant peculiarities in the main part of this work whilst providing a complete record of these curves in the supplementary sections.

To test convergence, all of the binding energy curves presented in Figs. 2-5 and Figs. S1-S3 were evaluated for 4, 6 and 7 atomic layer slabs and consistency was observed between the 6 and 7 atomic layer simulations. This is consistent with recent work on the (100), (110) and (111) surfaces of Al, Pd, Pt and Au and Ti(0001) [30] which showed that 6-layer slabs were

required to achieve convergence in surface energy, relaxation and work function. In general, E lies between -2 and -4 eV and hydrogen binds more weakly to the low coordinated on-top sites, with the exception of Ir, Pt and, to a lesser extent, Os. The Ni and Cu curves presented in Figs. 2 (a) and (b), respectively, both show that the three fold adsorption sites are energetically preferred on the (111) surfaces for all σ , with a slight preference for the FCC site, and that the 4-fold hollow site is equally preferred for both metals on the (100) surfaces.

The binding energy of hydrogen to the FCC, HCP, 2-fold bridge and on-top sites of unstrained Ni(111) have been previously reported [31] -2.89, -2.88, -2.75 and -2.29 eV. A similar trend was seen by Kresse and Hafner [32] though in the latter study a molecular H_2 reference state rather than an atomic H state was used in their formulation of E . The same study [32] also showed a preference for H binding to the 4-fold rather than the 2-fold bridge site on the Ni(100) surface in agreement with the $\sigma=0\%$ case in the current work. Recent studies of the H/Cu(111) and H/Cu(100) systems [33] have shown that on the (111) surface the HCP and FCC sites are degenerate (within 0.05 eV) and that the H binds more strongly to the (111) than the (100) surface, in agreement with the $\sigma=0\%$ case in the current work.

A similar FCC/HCP binding site degeneracy is seen for Rh(111) and Pd(111) and is shown in Fig. S1. However, it has been lifted slightly when compared to the Ni and Cu degeneracy discussed in the previous paragraph, but the degeneracy is still present as the energy differences between the two sites are <0.05 eV for all σ . A degeneracy is observable between the HCP and 2-fold bridge sites of the H/Ir(111) and H/Pt(111) systems shown in Figs. 3 (a) and (b), respectively. However, in these latter cases the preferred binding sites are either FCC or on top and for these sites degeneracy is not present across all σ and a reversal of the trend seen in the previous two rows is now evident.

Fig. 4 shows the hydrogen binding energy for the FCC (a) H/Rh(100), (b) H/Pd(100) and (c) H/Ag(100) systems. The lowest energy binding positions for any of these systems is either the 2-fold bridge or 4-fold hollow sites, depending on the strain state. Differences in energy between these binding positions vary to approximately 100 meV between binding positions for the Rh(100) and Ag(100) cases, to the extreme right ($\sigma=+5\%$) and left ($\sigma=-5\%$) of the binding energy curves, respectively. This is above the level assigned to degeneracy defined in the FCC (111) cases indicating that a preferred binding position transition is possible with strain for each of the H/Rh(100), H/Pd(100) and H/Ag(100) systems.

Figs. 5 (a-b) show the hydrogen binding energy as a function of strain σ for the hydrogenated HCP Co(0001) and BCC Fe(100) surfaces, respectively. The H/Os(0001) and H/Ru(0001) hydrogen binding energy curves are presented in Fig. S3. Across the range of strain investigated the H/Co(0001) system demonstrates FCC/HCP degeneracy similar to the H/Ni(111) and H/Cu(111) degeneracy already discussed. The level of degeneracy is reduced for the H/Ru(0001) and then H/Os(0001). This is similar to the effect seen for the FCC (111) surfaces whereby as the row of the periodic table containing the elements changes, the degree of degeneracy between the lowest energy binding positions changes. For the FCC (111) systems, the Ir(111) and Pt(111) show a low average degeneracy which converges rapidly around a point where the lowest energy structure dramatically changes. For the HCP systems a preferred structure change is only seen for the H/Os(0001) system and then only at a large strains ($\sigma < -3\%$) and between energetically extreme binding positions. For the remaining FCC and HCP systems an increasing degree of degeneracy is seen as we progress up the periodic

table with the highest levels of degeneracy seen for the H/Ni(111), H/Cu(111) and H/Co(0001) systems.

H/Co(0001) has been investigated relatively little in the literature. The hydrogenated Ni(111) and Co(0001) surfaces have been investigated previously at zero strain [34] using DFT. Their studies showed that the FCC and HCP sites are preferred for H/Co(0001) and that the hydrogen bonding energy E on Co(0001) is -2.89 eV which compares well with the value presented in Fig. 2 (b). They also showed that the H-Co bond length was 1.69 – 1.70 Å in the preferred binding position, which also compares well with the values presented in the current work.

Table 1 shows the vertical relaxation of the surface metal atom which are closest to the hydrogen atom. The table contains two parameters: the vertical relaxation at zero strain $\Delta z_{\text{surf},0}$

and the rate of change of the vertical relaxation with strain $\left(\frac{d\Delta z_{\text{surf}}}{d\sigma}\right)$. Both of these parameters

were both defined in Eq. (5). The vertical relaxation is positive if metal atom moves from its ideal, bulk terminated position towards the vacuum and away from the bulk. Physically, $\Delta z_{\text{surf},0}$ is the outward expansion of the surface metal atom which is closest to the hydrogen atom and is positive (negative) if the metal atom moves towards the vacuum (bulk). Considering the hexagonal FCC (111) and HCP (0001) surfaces a significant outward expansion $\Delta z_{\text{surf},0}$ on hydrogenation is seen for the H/Pd(111), H/Pt(111) and H/Au(111) systems. This expansion is reminiscent of the outward expansion seen for clean Pd(111) [35]. However the clean Au(111) surface reconstructs in plane forming large domain ‘herringbone’ structures suggesting that the outward expansion is more consequential of the hydrogenation rather than being inherent to the surface. The relative H-metal interaction strengths between this group of systems can be investigated by looking at the H-metal atom bond lengths. Table 2 shows the hydrogen-metal bond length and its variation with strain σ for hexagonal FCC (111) and HCP (0001) surfaces, and the square FCC (100) and BCC (100) surfaces. The variation in $r_{\text{H-Me},0}$ between the hydrogenated Pd(111), Pt(111) and Au(111) surfaces is relatively small compared to the variation of $r_{\text{H-Me},0}$ with H binding position for these three surfaces. The metals themselves have different equilibrium lattice constants so geometrically the H/Pd(111) surfaces will be distinct from the H/Pt(111) and H/Au(111) surfaces, and similarly between the H/Pt(111) and H/Au(111) surfaces. The common strong outward expansion and $r_{\text{H-Me},0}$ is not necessarily suggestive of a common bonding mechanism between the systems.

Constancy in the H-metal bond is also evident in the $\left(\frac{dr_{\text{H-Me}}}{d\sigma}\right)$ parameter. The values of this

parameter in table 2 indicate that the H-metal bond length experiences changes of the order of 0.005 – 0.020 Å across the range $\sigma \in [-5\%, \dots, +5\%]$. These range of values can be compared to the variance in H-metal bond length with binding position. This latter variation is significantly greater and is clearly evident when comparing the bond lengths between the on-top and FCC/HCP or 2-fold bridge site on the hexagonal surfaces, or when comparing the bond lengths for H binding to the on-top site and either the 2-fold or 4-fold sites on the orthogonal FCC (100) and BCC (100) surfaces. The H-metal bond length is clearly more sensitive on binding position rather than strain state.

A key observation in the binding energy E and structural studies presented so far has been the observation of preferred site degeneracy and of transitions in the preferred binding position as the strain state of the system changes. The orthogonal surfaces – Rh(100), Pd(100) and Ag(100) – show strain dependence. For the Pd(100) surface a strain-induced transition in the preferred hydrogen binding position occurs at approximately $\sigma=0\%$. The Rh(100) and Ag(100) surfaces demonstrate similar characteristics as the strain becomes increasingly compressive (σ approaches -5%) for Rh(100) and as the strain becomes increasingly tensile (σ approaches $+5\%$) for Ag(100). In both cases, changes in σ cause the 2-fold bridge and 4-fold hollow H binding positions to become increasingly degenerate.

A transition in the minimum energy structure has been seen in the Ir(111) and Pt(111) binding energy curves. In this sequence a strain of $+2\%$ or $+1\%$, respectively, is sufficient to cause the preferred binding position to change from the on-top to the FCC site. In this third sequence of energies the FCC-HCP degeneracy has been almost removed compared to the degeneracy seen across these binding positions for the Ni, Cu and Ag systems, as well as to a lesser extent on the Rh and Pd systems.

Other studies have addressed the response of metallic surfaces to sources of stress which arise from sources other than the relaxation of surface atoms due to their loss of symmetry during surface formation. Pao et al [36] have shown that as surface defects grown on Cu(001) and (111) the surface stress increases, but starts to reduce back to the un-defected value when the defect density increases above 25%. Studies on Ir(001) [37] have shown that a reduction of surface energy induces the (1×1) to (5×1) -hex reconstruction as the surface stress concurrently increases. Investigations of same system shows a reduction in tensile surface stress during hydrogen adsorption. Comparatively, both H and O adsorption on Pt(111) [38] has been seen to induce a compressive surface stress. This latter result cannot be simply explained using simple electro-positivity arguments – H is electropositive, so during adsorption charge would be expected to flow towards the H-centre, depopulating charge in the surface and enabling an in-plane contraction of the surface metal atoms. Conversely, O is electronegative and by equal argument would be expected to induce an out-of-plane expansion of the surface metal atoms. Structural Pt-Pt changes [39] have been proposed to explain this phenomenon. This explanation highlights the complexity of the interplay between the geometric and the electronic determination of surface energy and stress.

3.2 Charge population and energy partitioning

Fig. 6 shows the hydrogen s state population as a function of strain σ for the (a) H/Pt(111), (b) H/Co(0001) and (c) H/Fe(100) surfaces. The hydrogen s state population curves for the remaining FCC (111), FCC (100) and HCP (0001) surfaces are given in supplementary Fig. S4. Generally on FCC substrates charge flows towards the H atom as strain σ increases whereas for the HCP and BCC substrates the charge on the H atom increases as strain increases, then reaches a maximum point and decreases for higher strains. This behaviour is seen for Co(0001) and Fe(100) for strains σ of approximately 2-4% and 0%, respectively, and for Ru(0001) and Os(0001) for strains $\sigma > 4\%$ for on-top bound hydrogen. The effect is also suggested for some of the other surfaces including Ni(111), Pt(100) and Au(100) though position of the turning

point is at $\sigma > 5\%$. The magnitude of the hydrogen population is also seen to change grossly with periodic table row; the Ni and Cu H s state populations are larger than the Rh, Pd and Ag populations, which in turn are larger than the H s s state populations of Ir, Pt and Au. This behaviour is less well pronounced for the HCP systems, with the Ru and Os surfaces containing similarly populated H s states.

Hydrogen-transition metal bonds can be described using the concepts of hyper-conjugation and re-hybridisation [40]. In hyper-conjugation charge flows to an anti-bonding H-metal state and weakens the bond. Conversely, to Bent's rule requires that for H atoms to form bonds with metal centres charge needs to flow from the H atom towards the metal centre lowering population centred at the H atom. The two effects can consequently be thought of as increase or lower their importance depending on how strain is varying. As the system experiences increasingly tensile strain charge will flow towards the H centres and the hyper-conjugation will tend to weaken the bond; conversely, as the strain becomes increasingly compressive strain charge will flow away from the H centres and the bond will tend to strengthen. The relative constancy of the hydrogen-metal bond lengths presented in for the hexagonal systems in table 2 suggests that the two contributions – or their variation with strain – is comparable. The reason for this is that hyper-conjugation will tend to lengthen the H-metal bond length whereas re-hybridisation will tend to shorten it.

Fig. 7 shows the projected density of states (PDOS) for the hydrogenated (a) H/Pt(111), (b) H/Co(0001) and (c) H/Fe(100) surfaces. The projected density of states (PDOS) curves for the remaining hydrogenated FCC (111), FCC (100) and HCP(0001) surfaces are given in supplementary Fig. S5. For further brevity, only the zero strain ($\sigma = 0\%$) curves are shown in both figures. Generally, the H 1s states are seen to overlap with the metal d states for H adsorption in the on-top site whereas the H 1s states are at different energies to the metal d states for H adsorption in other binding positions. During strain ($\sigma \neq 0\%$) these alignments persisted and the H 1s remained overlapped with the metal d states for the on-top adsorption, and energetically separated from the metal d states for the other binding positions, though both sets of peaks are seen to shift relative to the Fermi level as the strain becomes either increasingly tensile or compressive.

The PDOS curves show some evidence of hybridisation between the H s and metal d states as peaks in these s and d curves generally occur at the same energy. The degree of hybridisation between the on-top and the other, higher coordinated sites is proposed to be different as the H s states for the on top site lie significantly closer to the centre of the metal d states whereas the H s states for the other, higher coordinated binding positions lie at or below the trailing edge of the d states. This observation can be made for adsorption on both the primitive FCC (111) and HCP (0001) systems and the orthogonal FCC (100) and BCC (100).

These observations support the presence of re-hybridisation. The distinct behaviour of the on-top position has also been seen in some of the other data presented in the current work; the H s population curves presented in Figs. 6 and S1 showed that the on-top bound hydrogen systematically carried either the greatest or the least charge (the latter in the case of orthogonal, square surfaces) independent of the strain state. The importance of the sites has been highlighted in the hydrogen binding energy curves shown in Fig. 3 where the sites became the preferred binding positions for compressively strained Pt(111) and Ir(111).

To gain an insight into the energetic reasons for the charge transfer, density of states and binding energy E behaviour under strain the total energy of each of the hydrogenated surfaces was partitioned and these partitions separately analysed. There are numerous energy decomposition algorithms [41] which focus on extracting chemical information. In the current study the partitioning of energy between the average kinetic and electrostatic components $\langle E_{K+ES} \rangle$ and the exchange-correlation component E_{XC} during hydrogenation is analysed.

The total energy $E_{KS}[n]$ of a system described by Kohn-Sham density functional theory was given in Eq. (3). In this equation the final term E_{XC} is the exchange correlation potential and the remaining terms are combined to form an average kinetic and electrostatic energy $\langle E_{K+ES} \rangle$ using the procedure outlined in Eq. (5). The reason for this partitioning is because the exchange correlation interaction may be interpreted as the cohesion of the system [42-43]. This interpretation is quite general and can be applied to any system, including adsorption onto a metallic surface. In the absence of E_{XC} the energy of the system will be defined by $\langle E_{K+ES} \rangle$ alone and this will necessarily underestimate E .

Table 3 shows that on-top binding position for both the groups of hexagonal and orthogonal surfaces has proportionally higher $\langle E_{K+ES} \rangle$ than binding at any of the other, higher coordinated positions. This difference between binding positions is less for the orthogonal FCC (100) and BCC (100) surfaces. The difference between binding positions is also less for hydrogen adsorption on the Cu(111), Ag(111) and Au(111) surfaces but in these cases the a proportionally higher $\langle E_{K+ES} \rangle$ is seen for hydrogen binding at the higher coordinated FCC, HCP and 2-fold bridge sites.

E_{XC} , its corollary $\langle E_{K+ES} \rangle$ and the charge transfer during strain are subtly interlinked. Fig. 6 shows almost with no exceptions that the H s state population for hydrogen atoms bound in the on-top site is larger than for other, higher coordination sites, independent of the strain state of the surface - proportionally more charge is drawn away from the surface to the on-top H than for hydrogen bound in any of the other sites. The exchange-correlation energy for this charge has been lowered. The converse (that $\langle E_{K+ES} \rangle$ has increased) is not proposed as a general case because Figs. 2-5 have shown that, with some notable exceptions, the on-top H binding energy is numerically smaller than the binding energy for the other sites. In cases where the binding energies of all the binding positions are more comparable – e.g. Ir(111) and Pt(111) – the converse may be true and $\langle E_{K+ES} \rangle$ may be increasing. This has to be demonstrated in a fully system and strain-state resolved way.

The hyper-conjugation and re-hybridisation arguments were insufficient to fully explain the behaviour in Figs. 2-5. This was because the predictions surrounding the H s state population analysis implied an bond weakening as strain increases which clearly was not seen generally in the hydrogen binding energy curves shown in Fig. 2-5. The decomposition of the total energy into $\langle E_{K+ES} \rangle$ and by inference E_{XC} has suggested an energetic reason for this behaviour which has been correlated with the charge transfer during hydrogenation, strain and with the projected density of states curves.

3.3 Work function studies

These effects of surface strain and electron distribution are combined when considering the work function change of a system. This parameter has been investigated across strained semiconductor systems [14] where device characteristics can be tuned sensitively, and investigated, using the work function. In catalytic applications, the work function may be considered, at least approximately, as a barrier towards reaction allowing charge transfer between the substrate and the surface reactants. It's study is consequently germane in the current work.

Table 4 summarises strain dependence of the work function change during hydrogenation $\left(\frac{d\phi}{d\sigma}\right)$ for all the systems investigated in the current work. For all clean surfaces the work function is seen to decrease as the strain became increasingly tensile and increase as the strain became increasingly compressive, i.e. $\left(\frac{d\phi}{d\sigma}\right) < 0$ for all clean surfaces. Therefore it can be generally commented that the work function changes for the systems investigated in the current work are not simply predicted by the strain state, as $\left(\frac{d\phi}{d\sigma}\right)$ is seen to take both positive and negative values in table 4.

In most cases, a strong correlation between $\left(\frac{d\phi}{d\sigma}\right)$ and the substrate, independent of the hydrogen binding position. This trend is reversed in the case of on-top adsorption to the hexagonal HCP (0001) and FCC (111) surfaces. The second general observation is that $\left(\frac{d\phi}{d\sigma}\right) < 0$ for most (100) surfaces and a mixture of $\left(\frac{d\phi}{d\sigma}\right) < 0$ and $\left(\frac{d\phi}{d\sigma}\right) > 0$ exist across the (0001) and (111) surfaces presented in table 4 with the most notable region of $\left(\frac{d\phi}{d\sigma}\right) > 0$

existing across the Os(0001), Ir(111), Pt(111) and Au(111) surfaces. Conventionally, work function of a surface is expected to increase if the adsorbate is more electronegative than the substrate. This is because electrons will be transferred from the substrate to the adsorbate layer causing a negative dipole. Fig. 6 shows that the H atom becomes increasingly electronegative as the strain becomes increasingly tensile. However, the section of table 2 that presents results from hexagonal systems has shown that r_{H-M_e} remains approximately constant during strain. This will allow H atoms bound in the FCC, HCP, 2-fold and 4-fold hollow sites to lie lower within the surface as the surface strain increases, and effectively reducing the effect of the charge flow towards the H atom. Geometrically this effect will be absent for the on-top site. Also, the change in the surface density due to strain will affect the work function of the clean surfaces for similar reasons – the charge ‘spill out’ layer and it's resulting surface dipole will change character (dipole moment) as the surface experiences different levels of strain. This has

already been evidenced in the general observation above that $\left(\frac{d\phi}{d\sigma}\right) < 0$ for all clean surfaces.

The two types of surface dipole will combine in the hydrogenated system generating the observed $\left(\frac{d\phi}{d\sigma}\right)$ behaviour.

4. Conclusions

The current study has investigated the effects of strain on the hydrogenated Fe, Co, Ni, Cu, Ru, Rh, Pd, Ag, Os, Ir, Pt and Au surfaces using density functional theory (DFT). The hexagonal FCC (111) and HCP (0001) surfaces and the square FCC (100) and BCC (100) and a fixed surface hydrogen coverage of 0.25 ML was used in all investigations. A range of both compressive and tensile strains σ were applied to these systems, in the range of -5% to +5%, and both the surface and seldge metal atoms as well as the surface hydrogen atoms were allowed to completely relax before any analytical investigations were made.

The preferred binding position of the H/Ir(111) and H/Pt(111) changes under a tensile strain of $\sigma = +2\%$. For both systems the H atom preferentially occupies the on-top binding position for more compressive strains and the FCC site for more tensile strains. A similar effect is also seen for hydrogen adsorbing on the strained Pd(100) surface where the preferential hydrogen binding position changes from the 4-fold hollow when the system is under compressive strain to the 2-fold bridge when it is under tensile strain. Other changes in preferred binding position are also seen for the Fe(100) and Os(0001) surfaces, and may be reasonably inferred for the Rh(100) and Ag(100) surfaces, but for larger strains of up to 5%.

The mechanism by which this change in binding position proceeds has been investigated and has been seen to be complex. The charge transfer mechanisms hyper-conjugation and re-hybridisation have been evaluated against the observation that general observation that charge flows towards (away from) the H atom as the strain becomes increasingly compressive (tensile). A general decrease in the exchange-correlation energy is proposed for charge drawn from the surface towards the on-top bound H atom across all strain states, though some exceptions to this have been seen in the unstrained ($\sigma=0\%$) cases of H/Ir(111) and H/Pt(111).

The significance of the effect of a change in the binding position of the H atom on a surface is profound. It has been demonstrated that the charge state, energetic state and degree of electron localisation can change significantly during strain. This action on catalytically active materials such as Pt may explain fundamentally why moieties attached to these surfaces – in this case hydrogen – behave as they do when the material they are bound to experiences either a compressive or a tensile strain. The current work has addressed this question and has presented a thorough survey of the H-transition metal systems to provide a reference for future studies where the strain state of the system – for example, across a nanoparticle surface – is not clearly defined or at equilibrium with reference to the bulk – and the possibility of alternative adsorbate binding positions may be proposed.

Acknowledgements

This work was supported by the author's membership of the UK's HEC Materials Chemistry Consortium, which is funded by the EPSRC (**EP/L000202**) and used the ARCHER UK National Supercomputing Service (<http://www.archer.ac.uk>).

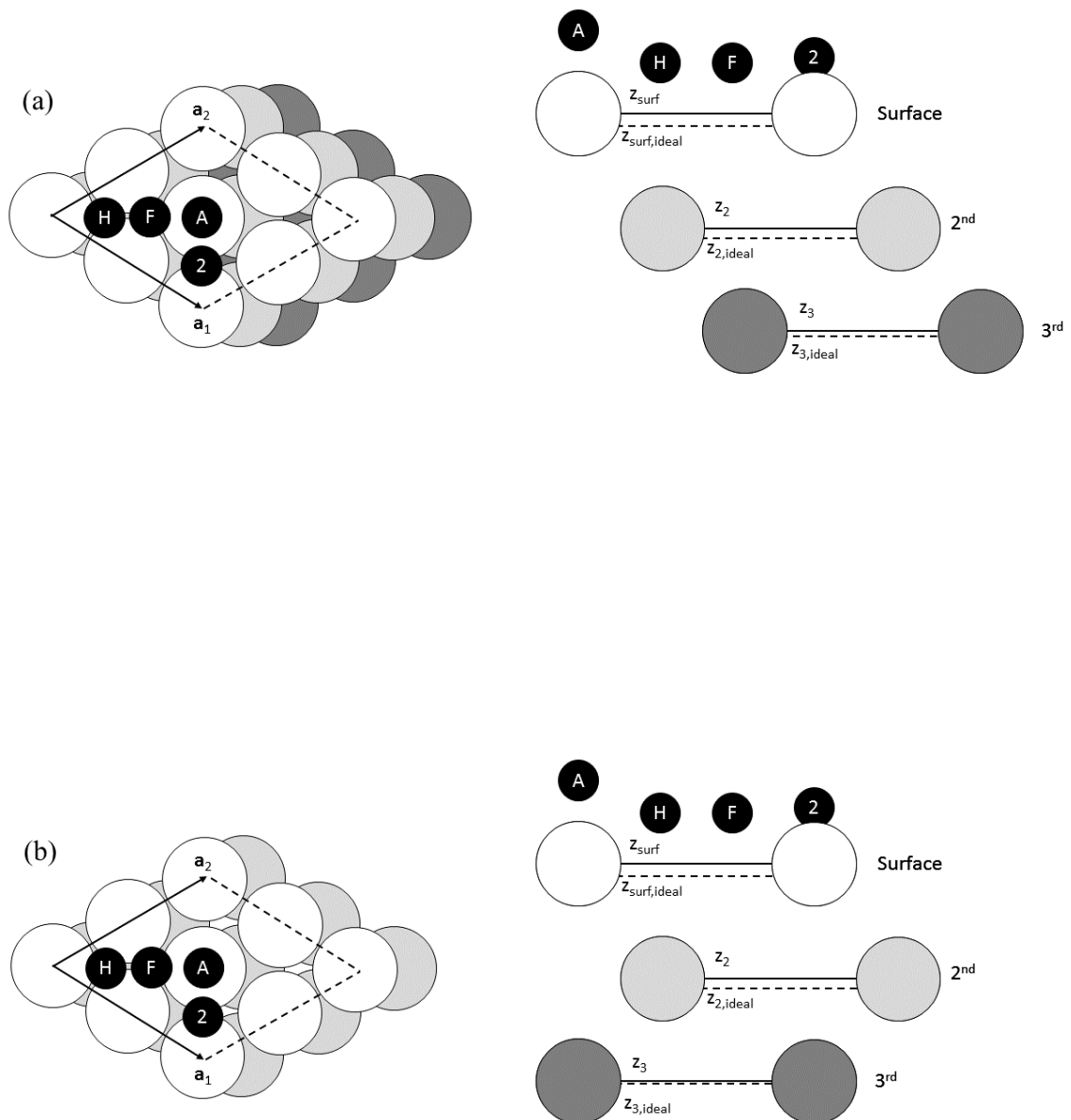
References

- [1] K. Yan, T. A. Maark, A. Khorshidi, V. A. Sethuraman, A. A. Peterson, and P. R. Guduru. *Angew. Chem. Int. Ed.* **55** (2016) 6175–6181.
- [2] S. Yang, F. Liu, C. Wu, and S. Yang. *Small* **12(30)** (2016) 4028-4047.
- [3] B.R. Cuenya. *Thin Solid Films* **518** (2010) 3127–3150.
- [4] M. Gsell, P. Jakob, and D. Menzel. *Science* **280** (1998) 717-720.
- [5] O. R. de la Fuente, M. A. González-Barrio, V. Navarro, B. M. Pabón, I. Palacio, and A. Mascaraque. *J. Phys.: Condens. Matter* **25** (2013) 484008.
- [6] W. An, and P. Liu. *J. Phys. Chem. C* **117(31)** (2013) 16144-16149.
- [7] Y. Nie, L. Li, and Z. Wei. *Chem. Soc. Rev.* **44** (2015) 2168–2201.
- [8] Q. Deng, V. Gopal, and J. Weissmüller.
Angew. Chem. Int. Ed. **54** (2015) 12981–12985.
- [9] J. Biener, A. Wittstock, L. A. Zepeda-Ruiz, M. M. Biener, V. Zielasek, D. Kramer, R. N. Viswanath, J. Weissmüller, M. Bäumer and A. V. Hamza.
Nat. Mater. **8** (2009) 47 – 51.
- [10] N. F. Quackenbush, H. Paik, M. J. Wahila, S. Sallis, M. E. Holtz, X. Huang, A. Ganose, B. J. Morgan, D. O. Scanlon, Y. Gu, F. Xue, L.-Q. Chen, G. E. Sterbinsky, C. Schlueter, T.-L. Lee, J. C. Woicik, J.-H. Guo, J. D. Brock, D. A. Muller, D. A. Arena, D. G. Schlom, and L. F. J. Piper.
Phys. Rev. B: Condens. Matter **94** (2016) 085105.
- [11] D. V. Potapenko, Z. Li, J. W. Kysar, and R. M. Osgood.
Nano Lett. **14(11)** (2014) 6185–6189.
- [12] J. Lu, J. W. Elam, and P. C. Stair. *Surf. Sci. Repts.* **71** (2016) 410-472.
- [13] G. K. Pálsson, M. Wälde, M. Amft, Y. Wu, M. Ahlberg, M. Wolff, A. Pundt, and B. Hjörvarsson. *Phys. Rev. B: Condens. Matter* **85** (2012) 195407.
- [14] Y. Sun, S. E. Thompson, and T. Nishida. *J. Appl. Phys.* **101** (2007) 104503.
- [15] I. G. Shuttleworth. *Appl. Surf. Sci.* **378** (2016) 286-292.
- [16] R. Johansson, R. Ahuja, O. Eriksson, B. Hjörvarsson, and R. H. Scheicher.
Scientific Reports **5** (2015) 10301.
- [17] Z. Li, D. V. Potapenko, and R. M. Osgood. *ACS Nano* **9 (1)** (2015) 82–87.
- [18] A. G. Olaibi. *Int. J. Hydrogen Energy* **41** (2016) 16323-16329.

- [19] L. Zhang, R. M. Anderson, R. M. Crooks, and G. Henkelman. *Surf. Sci.* **640** (2015) 65-72.
- [20] L. Zhang, and G. Henkelman. *ACS Catal.* **5** (2015) 655-660.
- [21] A. Staykov, D. Derekar, and K. Yamamura. *Int. J. Quantum Chem.* **116** (2016) 1486-1492.
- [22] D. Li, H. Lv, Y. Kang, N. M. Markovic, and V. R. Stamenkovic. *Annu. Rev. Chem. Biomol. Eng.* **7** (2016) 509-532.
- [23] E. Panizon, and R. Ferrando. *Nanoscale* **8** (2016) 15911-15919.
- [24] K. Christmann. *Surf. Interface Sci.* **5** (2016) 255-356.
- [25] P. Giannozzi, S. Baroni, N. Bonini, M. Calandra, R. Car, C. Cavazzoni, D. Ceresoli, G.L. Chiarotti, M. Cococcioni, I. Dabo, A. Dal Corso, S. Fabris, G. Fratesi, S. deGironcoli, R. Gebauer, U. Gerstmann, C. Gougoussis, A. Kokalj, M. Lazzeri, L. Martin-Samos, N. Marzari, F. Mauri, R. Mazzarello, S. Paolini, A. Pasquarello, L. Paulatto, C. Sbraccia, S. Scandolo, G. Sclauzero, A.P. Seitsonen, A. Smogunov, P. Umari, and R.M. Wentzcovitch. *J. Phys. Condens. Matter.* **21** (2009) 395502.
- [26] M. Methfessel, and A.T. Paxton. *Phys. Rev. B: Condens. Matter* **40** (1989) 3616–3621.
- [27] The Fe.pbe-spn-rrkjus_psl.0.2.1.UPF, x.pbe-nd-rrkjus.UPF, where x= Co or Ni, y.pbe-mt fhi.UPF, where y= Cu, Ru, Rh, Pd, Os, Ir or Pt, and z.pbesol-dn-rrkjus_psl.0.1.UPF, where y= Ag or Au, pseudopotentials, and their corresponding H pseudopotentials, were used from the Quantum ESPRESSO pseudopotential data base: <http://www.quantum-espresso.org/pseudopotentials>.
- [28] A. Dal Corso. *Comput. Mater. Sci.* **95** (2014) 337-350.
- [29] I. G. Shuttleworth, *Chem. Phys. Lett.* **666** (2016) 51-57.
- [30] N. E. Singh-Miller, and N. Marzari. *Phys. Rev. B: Condens. Matter* **80** (2009) 235407.
- [31] J. Greeley, and M. Mavrikakis. *Surf. Sci.* **540** (2003) 215-229.
- [32] G. Kresse, and J. Hafner. *Surf. Sci.* **459** (2000) 287-302.
- [33] P. Ferrin, S. Kandoi, A. U. Nilekar, and M. Mavrikakis. *Surf. Sci.* **606** (2012) 679-689.
- [34] D. J. Klinke II, and L. J. Broadbelt. *Surf. Sci.* **429** (1999) 169-177.

- [35] X.Q. Qi, Z.D. Wei, L. Li, M.B. Ji, L.L. Li, Q. Zhang, M.R. Xia, S.G. Chen, and L.J. Yang. *Comput. Theo. Chem.* **979** (2012) 96-101.
- [36] C. -W. Pao, D. J. Srolovitz, and C. V. Thompson. *Phys. Rev. B: Condens. Matter* **74** (2006) 155437.
- [37] M. K. Bradley, D. P. Woodruff, and J. Robinson. *Phys. Rev. B: Condens. Matter* **84** (2011) 075438.
- [38] Z. Tian, D. Sander, N. N. Negulyaev, V. S. Stepanyuk, and J. Kirschner. *Phys. Rev. B: Condens. Matter* **81** (2010) 113407.
- [39] P. J. Feibelman. *Phys. Rev. B: Condens. Matter* **56** (1997) 2175.
- [40] N. V. Belkova, L. M. Epstein, O. A. Filippov, and E. S. Shubina. *Chem. Rev.* **116** (2016) 8545-8587.
- [41] M. J. S. Phipps, T. Fox, C. S. Tautermann, and C.-K. Skylaris. *Chem. Soc. Rev.* **44** (2015) 3177.
- [42] S. Kurth, and J. P. Perdew. *Int. J. Quantum Chem.* **77** (2000) 814-818.
- [43] H. T. Tran, and J. P. Perdew. *Am. J. Phys.* **71** (2003) 1048-1061.

Fig. 1. Structures of the (a) FCC (111), (b) HCP (0001), and the (c) FCC (100) and BCC (100) (2×2)-H/transition metal systems investigated in this work. The surface, second and third layer transition metal atoms are shown by white, light grey and dark grey circles, respectively. The black circles represent H atoms whose labels denote binding in the ‘H’ HCP, ‘F’ FCC, ‘A’ atop, and ‘2’ 2-fold bridge sites for structures (a-b), and the ‘2’ 2-fold bridge, ‘4’ 4-fold hollow and ‘A’ atop sites for structure (c). z_{surf} and $z_{\text{surf,ideal}}$ are the actual and ideal bulk terminated surface layer heights, respectively, and similar notation is used for the height of the atoms in the second and third layers.



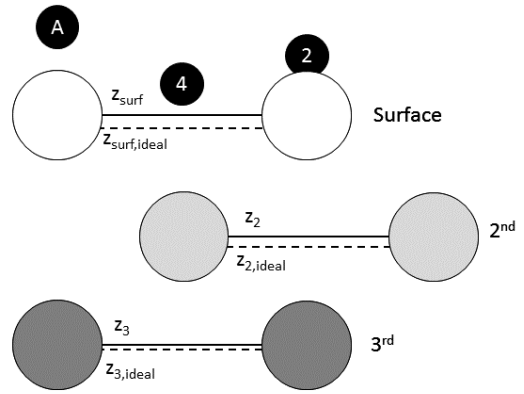
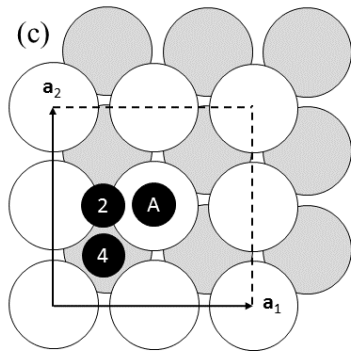
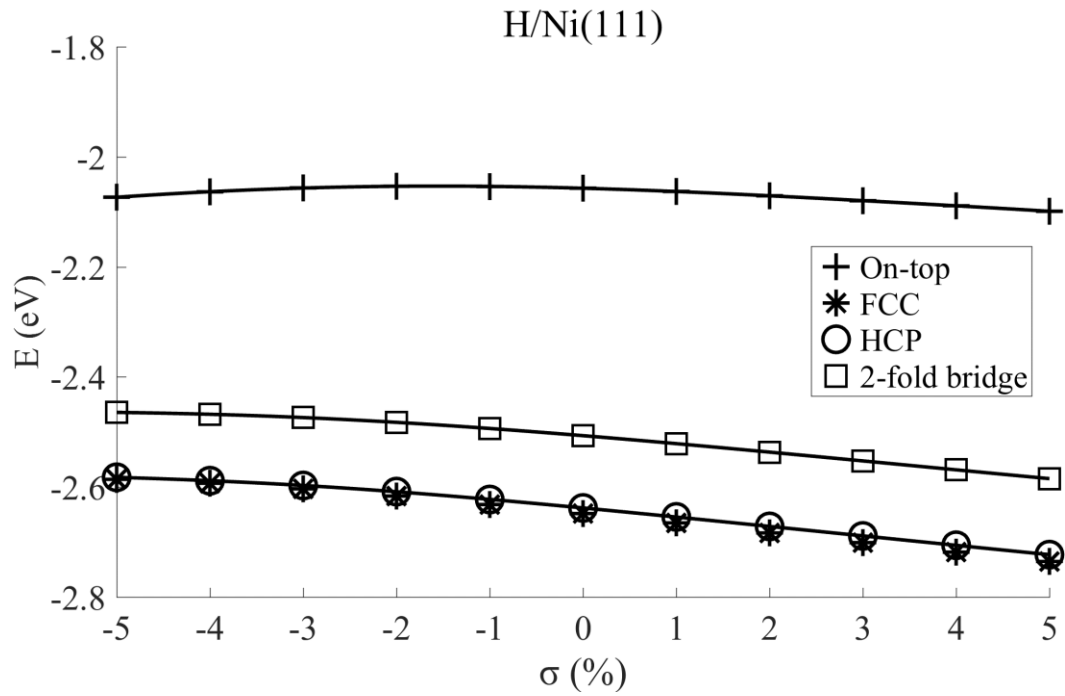


Fig. 2. Hydrogen binding energy E as a function of strain σ for the hydrogenated (a) Ni(111) and (b) Cu(111) surfaces. The legend indicates the H binding position, which is defined in Fig. 1. The solid connecting lines are a guide to the eye.

(a)



(b)

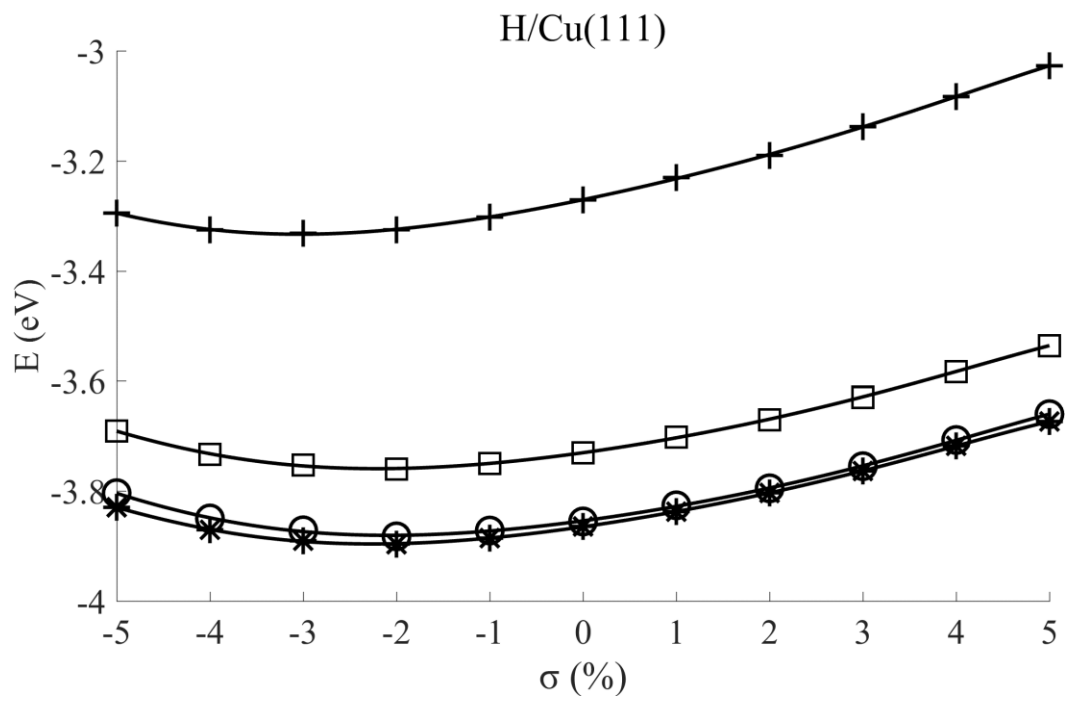
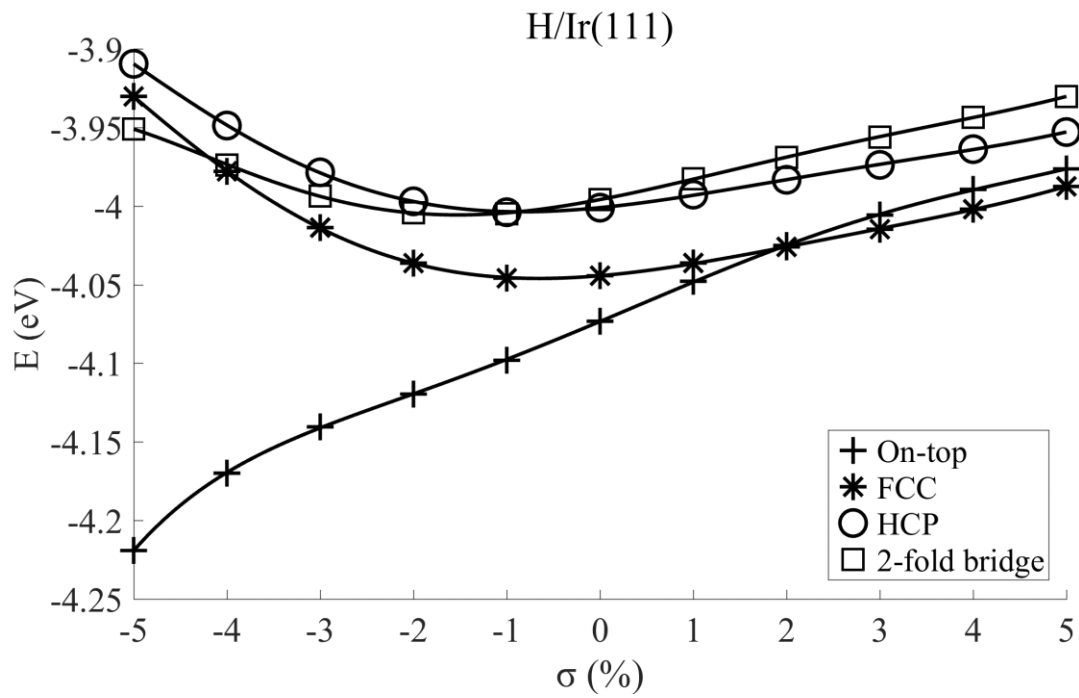


Fig. 3. Hydrogen binding energy E as a function of strain σ for the hydrogenated (a) Ir(111) and (b) Pt(111) surfaces. The legend indicates the H binding position, which is defined in Fig. 1. The solid connecting lines are a guide to the eye.

(a)



(b)

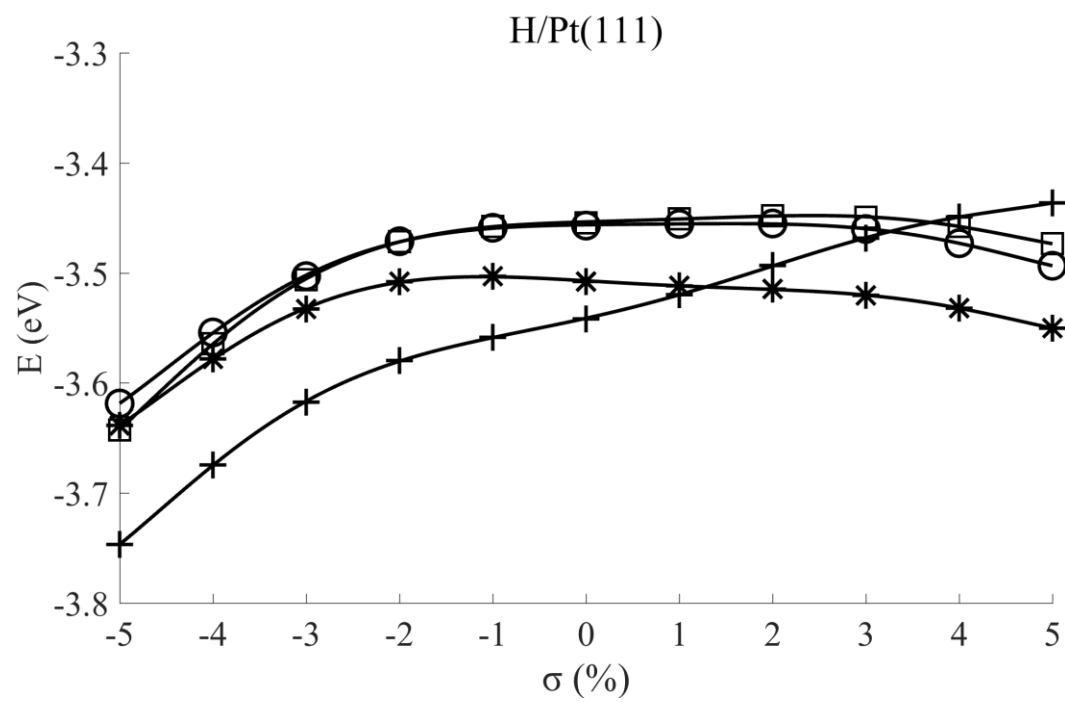
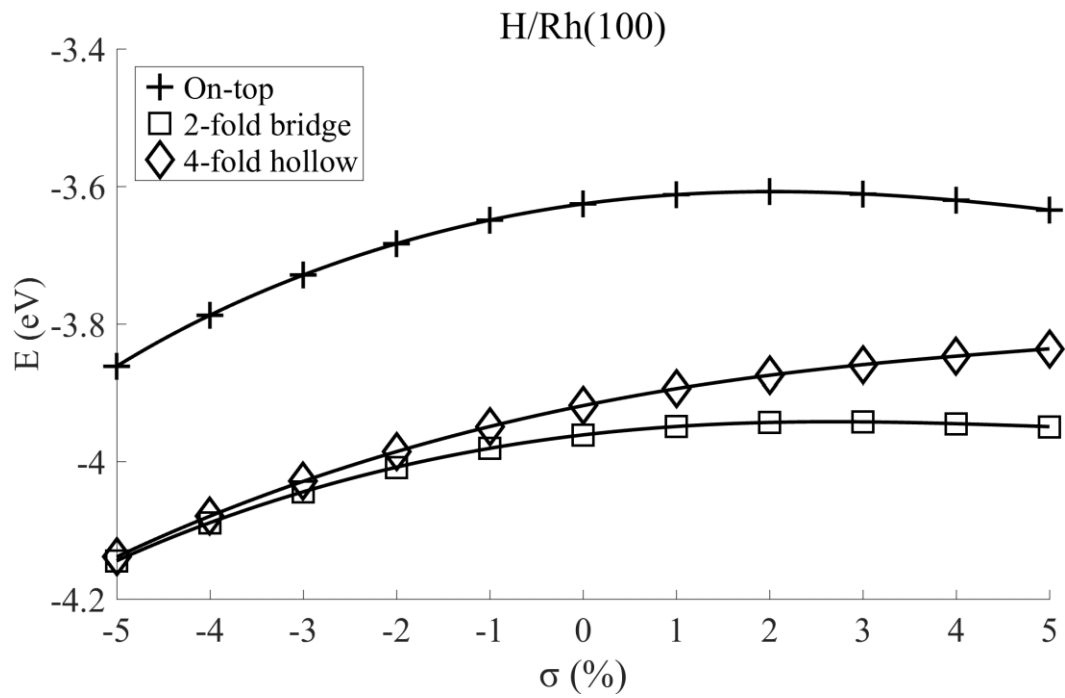
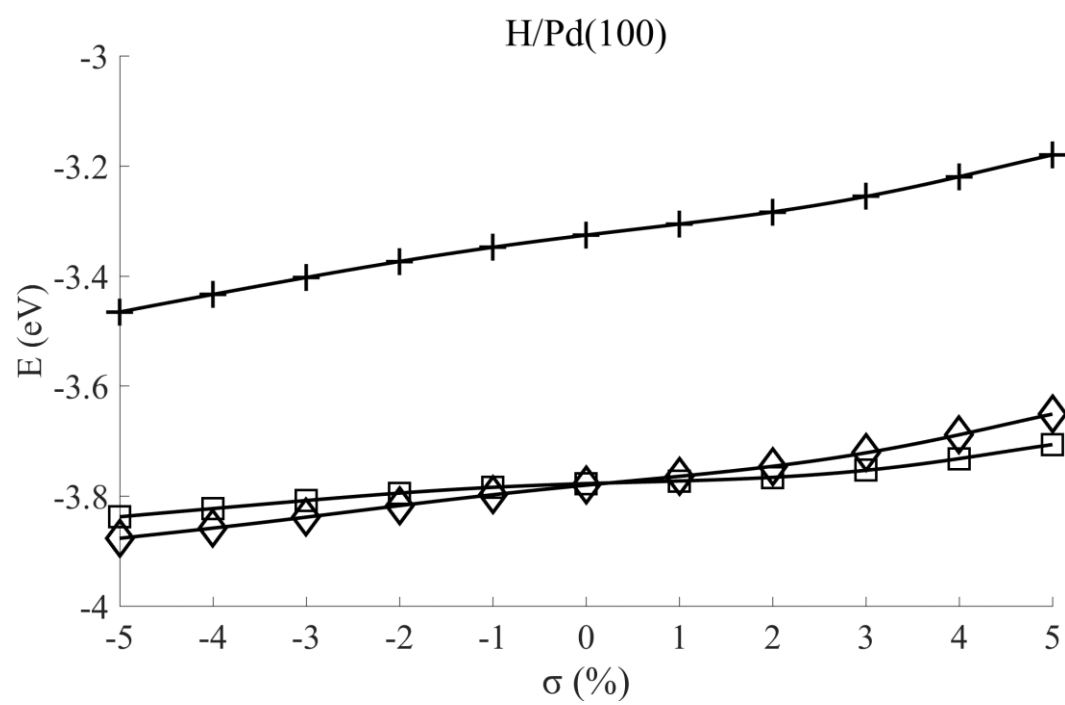


Fig. 4. Hydrogen binding energy E as a function of strain σ for the hydrogenated (a) Rh(100), (b) Pd(100) and (c) Ag(100) surfaces. The legend indicates the H binding position, which is defined in Fig. 1. The solid connecting lines are a guide to the eye.

(a)



(b)



(c)

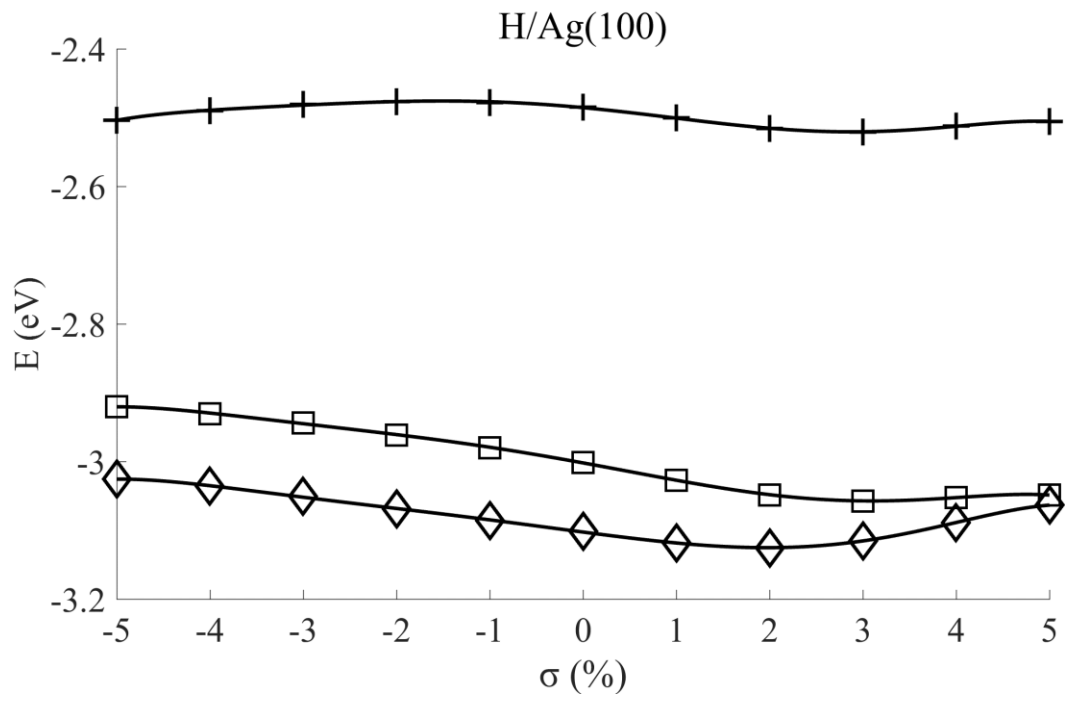
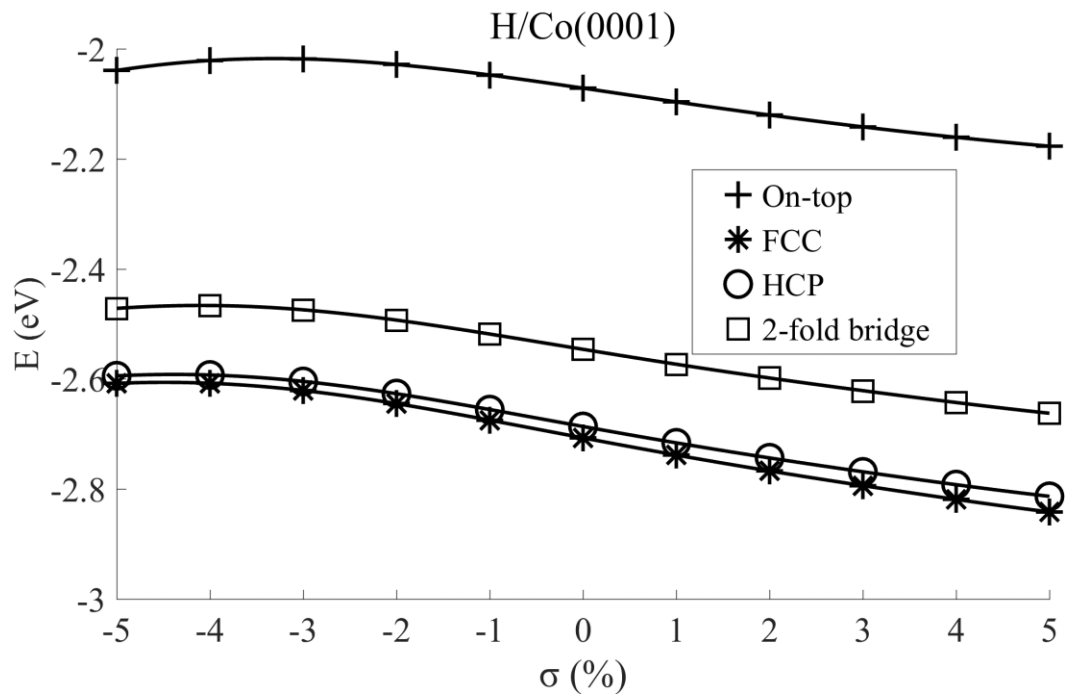


Fig. 5. Hydrogen binding energy E as a function of strain σ for the hydrogenated (a) Co(0001) and (b) Fe(100) surfaces. The legend indicates the H binding position, which is defined in Fig. 1. The solid connecting lines are a guide to the eye.

(a)



(b)

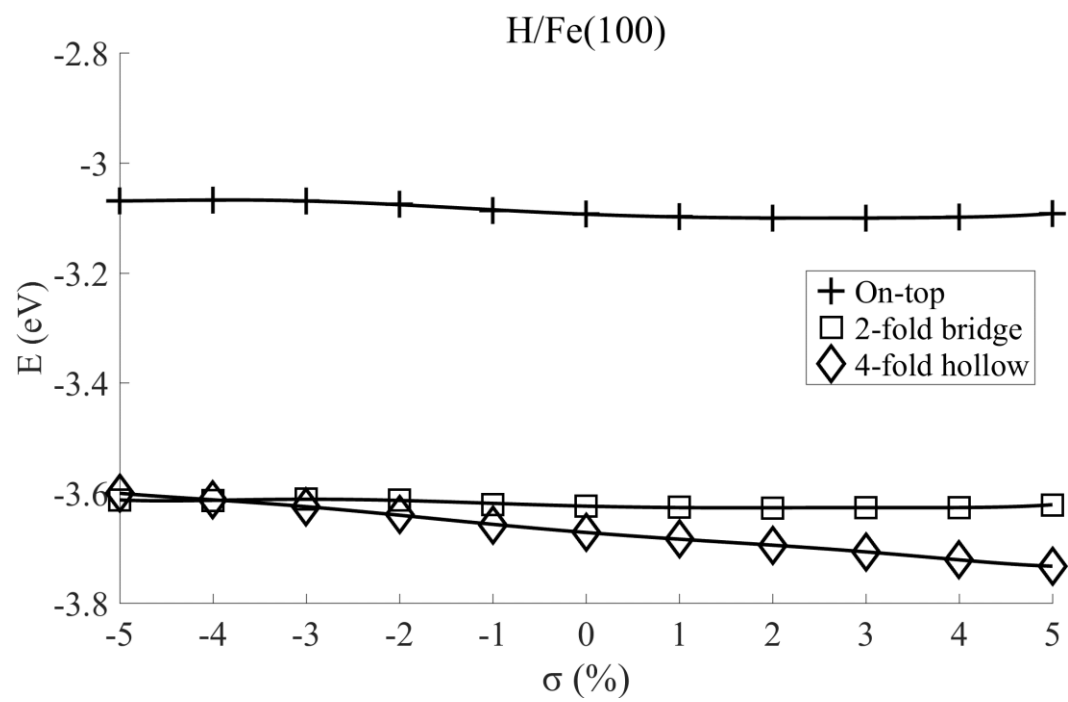
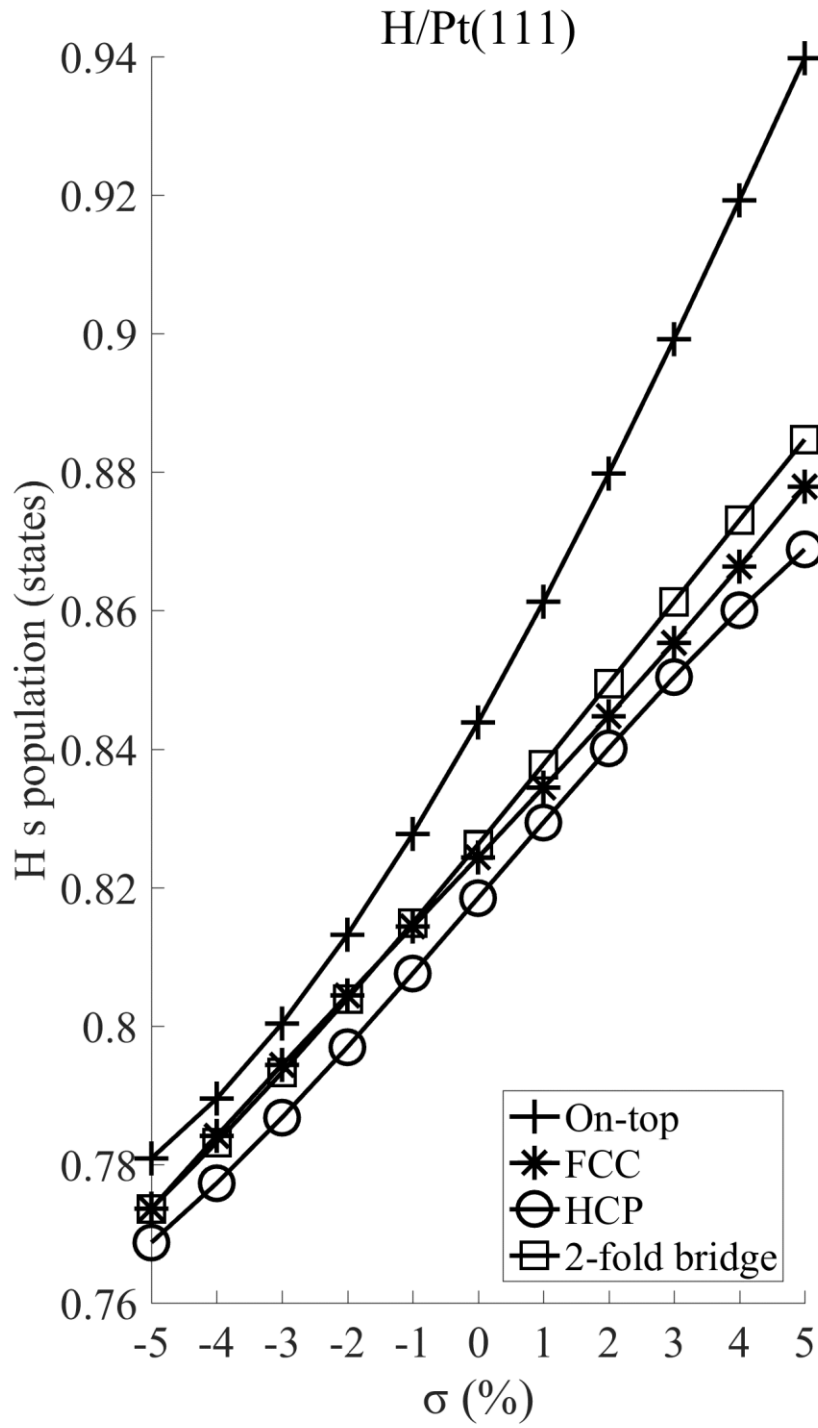
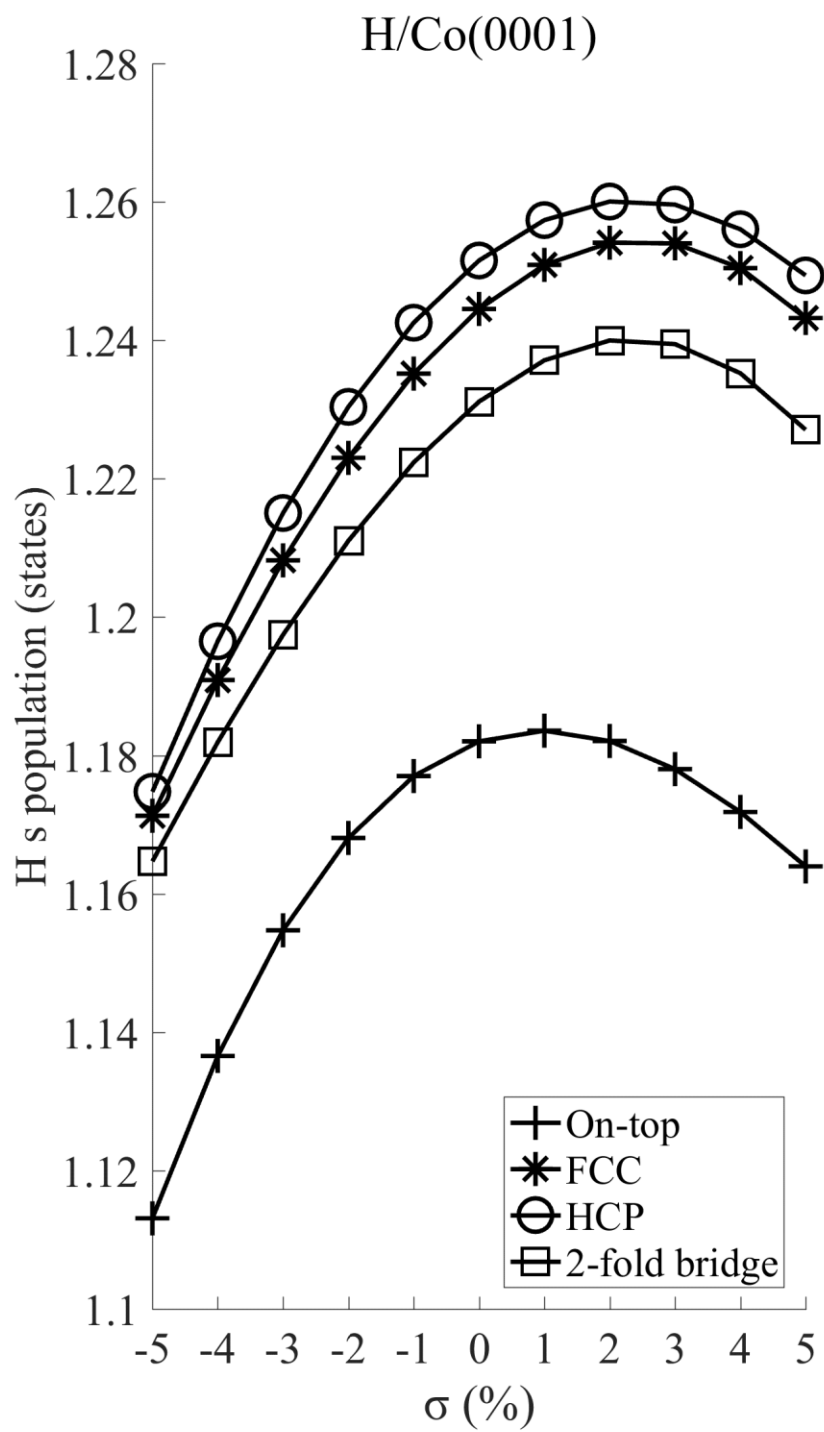


Fig. 6. The hydrogen s state population as a function of strain σ for the (a) H/Pt(111), (b) H/Co(0001) and (c) H/Fe(100) surfaces. The legend indicates the H binding position, which are defined in Fig. 1. The solid connecting lines are a guide to the eye.

(a)



(b)



(c)

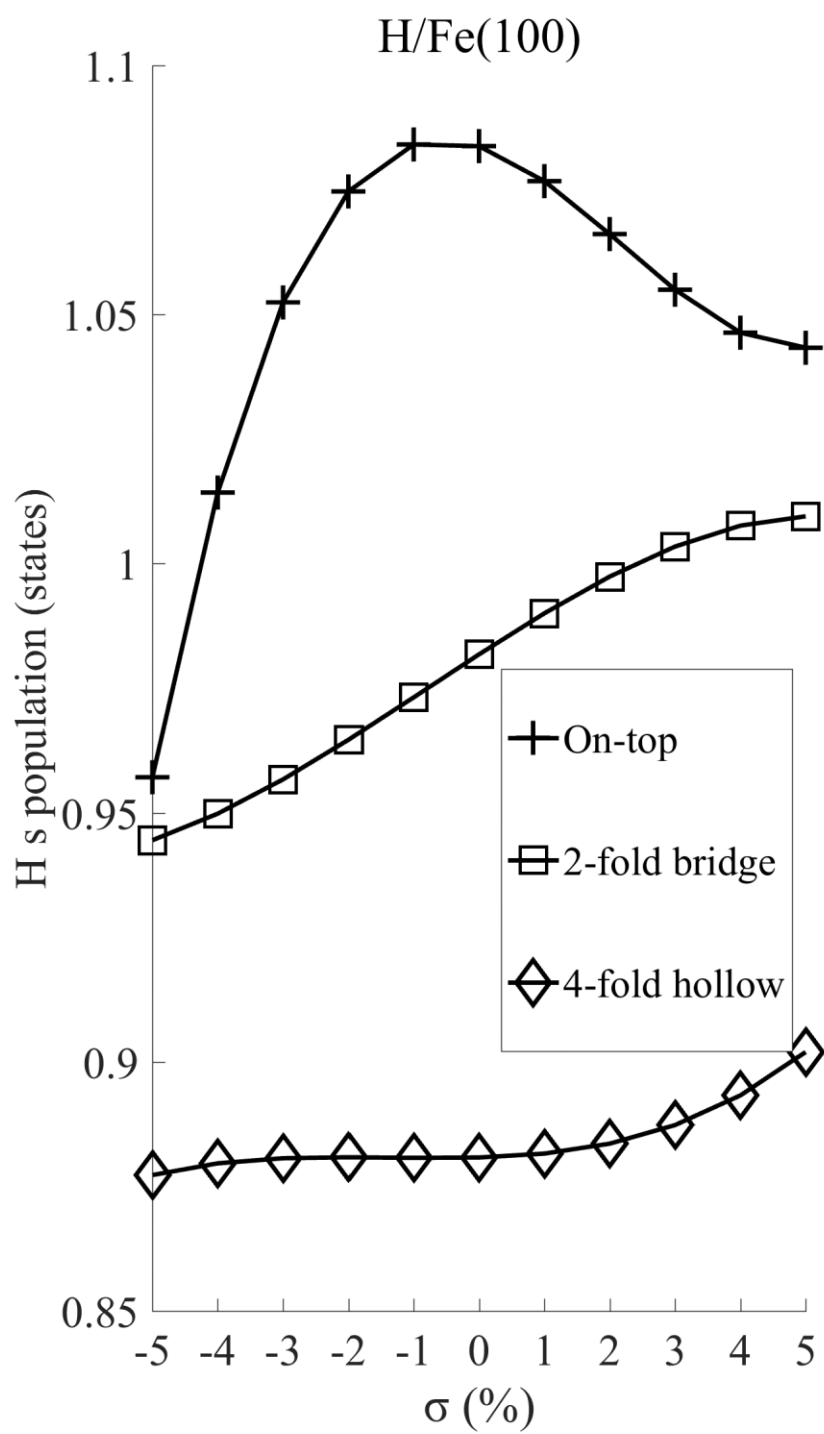
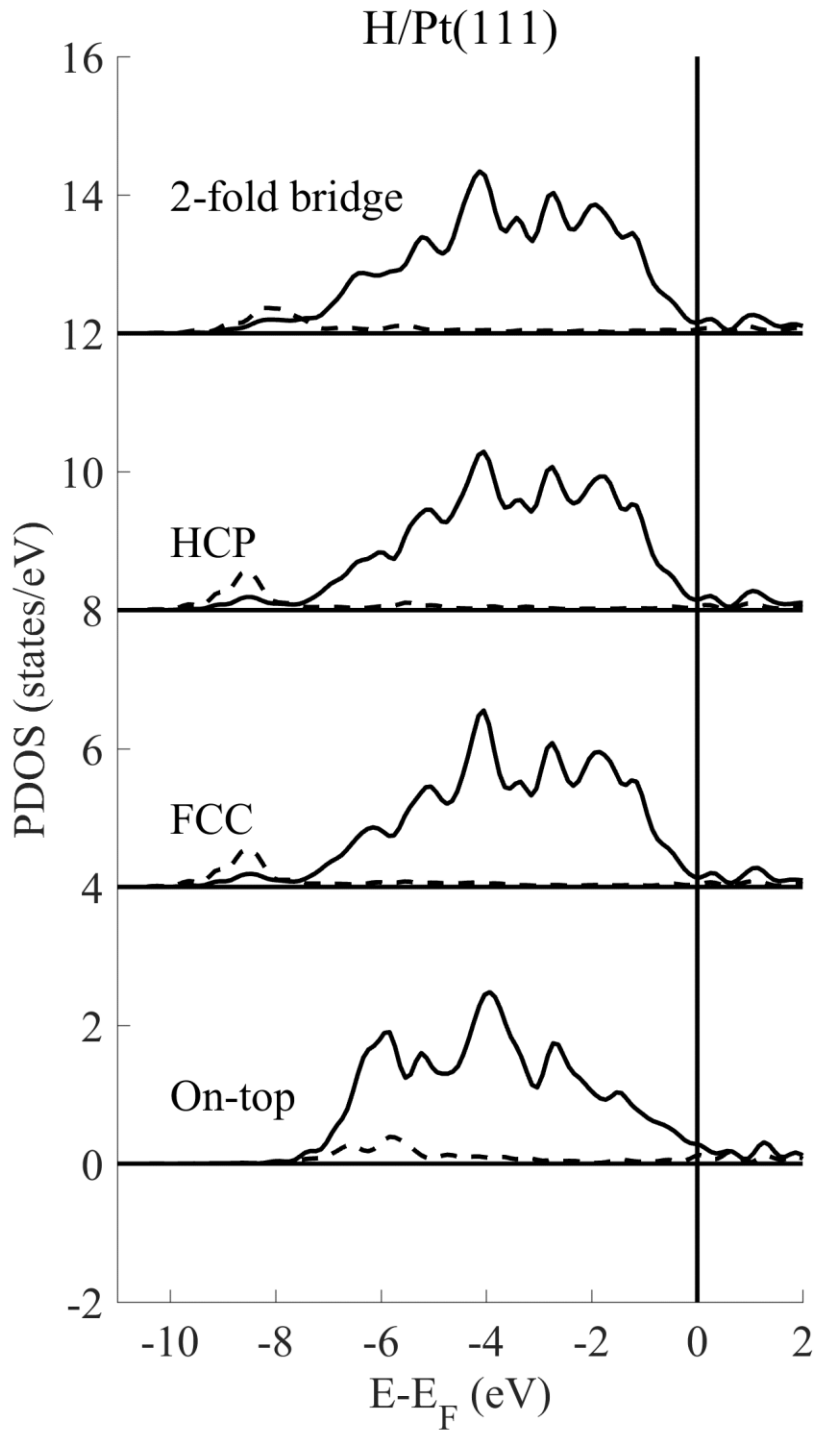
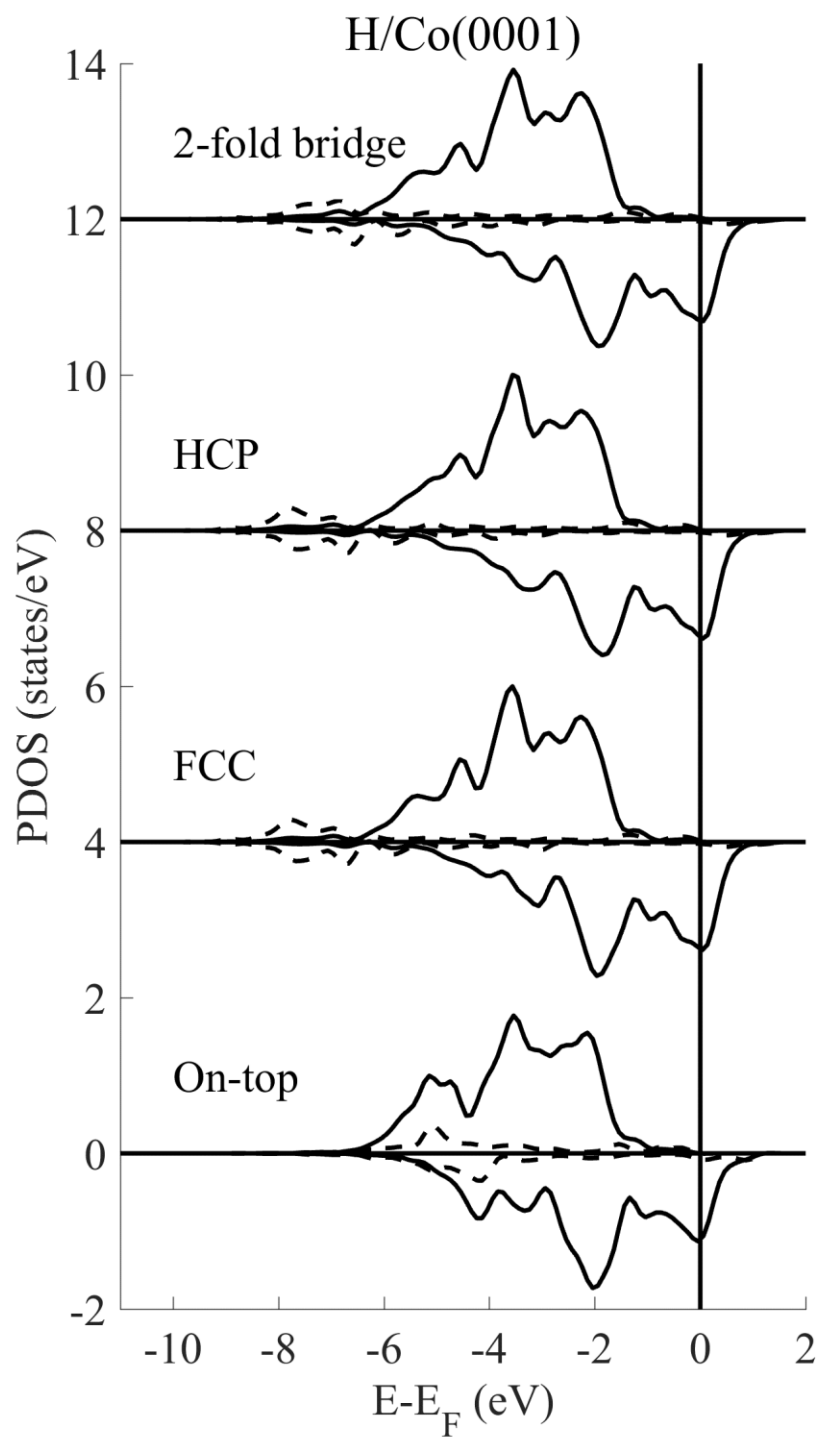


Fig. 7. The projected density of states (PDOS) at equilibrium ($\sigma=0\%$) for the hydrogenated (a) H/Pt(111), (b) H/Co(0001) and (c) H/Fe(100) surfaces. The dashed (solid) curves denote H s (metal d) states. The labels denote the hydrogen binding position which are defined in Fig. 1. Curves for different hydrogen binding sites are offset vertically for clarity.

(a)



(b)



(c)

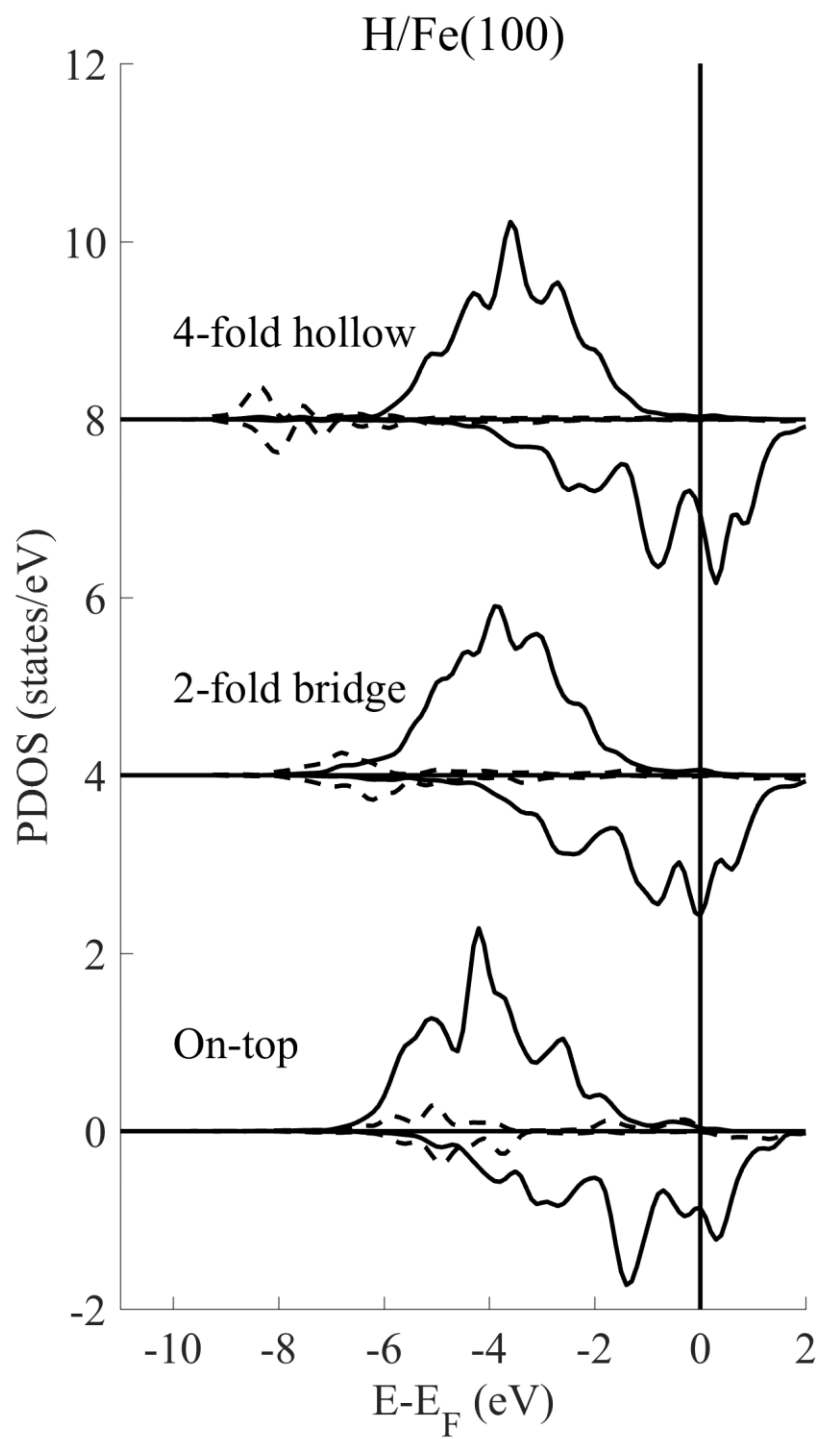


Table 1. Vertical relaxation of the nearest-neighbour surface metal atoms to the surface H atom for hydrogenated FCC (111), HCP (0001), FCC (100) and BCC (100) metal surfaces. $\Delta z_{\text{surf},0}$ is the vertical relaxation at zero strain and $\left(\frac{d\Delta z_{\text{surf}}}{d\sigma}\right)$ is the rate of change of the vertical relaxation with strain. ‘On-top’, ‘FCC’, ‘HCP’, ‘2-fold bridge’ and ‘4-fold hollow’ indicate the H binding position defined in Fig. 1.

System	$\Delta z_{\text{surf},0}$				$\left(\frac{d\Delta z_{\text{surf}}}{d\sigma}\right)$			
	On-top	FCC	HCP	2-fold bridge	On-top	FCC	HCP	2-fold bridge
H/Co(0001)	-2.56	-2.09	-2.17	-2.42	-3.25	-3.24	-3.23	-3.18
H/Ni(111)	0.03	0.38	0.54	0.40	-3.36	-3.34	-3.33	-3.35
H/Cu(111)	-1.52	-0.08	-0.86	-0.40	-3.35	-3.71	-3.59	-3.64
H/Ru(0001)	-3.18	-5.08	-4.71	-4.47	-3.91	-3.07	-3.09	-3.19
H/Rh(111)	2.36	-1.30	-0.64	-0.44	-4.40	-3.21	-3.28	-3.37
H/Pd(111)	3.22	2.60	3.12	2.98	-4.00	-4.09	-4.10	-4.10
H/Ag(111)	-1.37	0.32	-0.32	0.02	-3.52	-3.97	-3.80	-3.86
H/Os(0001)	-0.87	-4.95	-4.70	-4.05	-4.38	-3.11	-3.09	-3.24
H/Ir(111)	3.20	-1.04	-0.58	0.28	-4.43	-3.19	-3.23	-3.45
H/Pt(111)	7.00	4.60	4.80	6.01	-4.90	-4.83	-4.82	-5.06
H/Au(111)	2.49	2.51	2.35	3.38	-4.48	-5.21	-5.16	-5.20
System	On-top	2-fold bridge	4-fold hollow	On-top	2-fold bridge	4-fold hollow		
H/Fe(100)	3.32	6.63	2.50	-4.84	-5.13	-5.17		
H/Ni(100)	-1.70	-0.61	-1.18	-4.50	-4.35	-4.40		
H/Cu(100)	0.18	-0.09	-2.32	-4.70	-5.04	-4.97		
H/Rh(100)	-2.53	-2.55	-3.02	-4.50	-3.98	-3.95		
H/Pd(100)	2.13	1.46	1.20	-5.29	-5.07	-5.11		
H/Ag(100)	1.02	0.49	-1.32	-4.81	-5.09	-4.96		
H/Ir(100)	-2.39	-2.95	-3.27	-4.21	-3.79	-3.76		
H/Pt(100)	6.21	1.34	0.56	-6.13	-5.20	-5.18		
H/Au(100)	3.48	1.05	-0.44	-5.21	-5.61	-5.63		

Table 2. H-metal atom bond lengths for hydrogenated FCC (111), HCP (0001), FCC (100) and BCC (100) metal surfaces. $r_{\text{H-Me},0}$ is the H-metal atom bond length at zero strain and $\left(\frac{dr_{\text{H-Me}}}{d\sigma}\right)$ is the rate of change of the H-metal atom bond length with strain. All lengths are in Angstrom (\AA) and $\left(\frac{dr_{\text{H-Me}}}{d\sigma}\right)$ has units of \AA per %. ‘On-top’, ‘FCC’, ‘HCP’, ‘2-fold bridge’ and ‘4-fold hollow’ and indicate the H binding position defined in Fig. 1.

System	$r_{\text{H-Me},0}$				$\left(\frac{dr_{\text{H-Me}}}{d\sigma}\right)$			
	On-top	FCC	HCP	2-fold bridge	On-top	FCC	HCP	2-fold bridge
H/Co(0001)	1.51	1.74	1.74	1.66	1.58×10^{-3}	2.28×10^{-3}	2.76×10^{-3}	1.51×10^{-3}
H/Ni(111)	1.47	1.71	1.70	1.62	1.47×10^{-3}	2.45×10^{-3}	2.13×10^{-3}	1.80×10^{-3}
H/Cu(111)	1.52	1.75	1.75	1.67	0.16×10^{-3}	1.66×10^{-3}	1.84×10^{-3}	0.13×10^{-3}
H/Ru(0001)	1.64	1.90	1.89	1.82	1.17×10^{-3}	2.50×10^{-3}	2.78×10^{-3}	1.06×10^{-3}
H/Rh(111)	1.58	1.86	1.85	1.77	1.66×10^{-3}	1.42×10^{-3}	0.85×10^{-3}	0.96×10^{-3}
H/Pd(111)	1.55	1.83	1.82	1.73	0.31×10^{-3}	0.62×10^{-3}	0.09×10^{-3}	-0.22×10^{-3}
H/Ag(111)	1.65	1.89	1.90	1.81	-0.06×10^{-3}	1.00×10^{-3}	1.01×10^{-3}	-0.70×10^{-3}
H/Os(0001)	1.66	1.95	1.94	1.85	2.31×10^{-3}	2.94×10^{-3}	4.12×10^{-3}	1.59×10^{-3}
H/Ir(111)	1.60	1.91	1.90	1.81	2.13×10^{-3}	2.18×10^{-3}	2.14×10^{-3}	1.33×10^{-3}
H/Pt(111)	1.56	1.87	1.88	1.77	1.81×10^{-3}	2.43×10^{-3}	2.33×10^{-3}	0.75×10^{-3}
H/Au(111)	1.59	1.88	1.88	1.77	-0.43×10^{-3}	2.21×10^{-3}	2.66×10^{-3}	-0.57×10^{-3}
System	On-top	2-fold bridge	4-fold hollow		On-top	2-fold bridge	4-fold hollow	
H/Fe(100)	1.58	1.71	2.08		0.09×10^{-3}	1.02×10^{-3}	18.7×10^{-3}	
H/Ni(100)	1.48	1.62	1.84		0.51×10^{-3}	1.01×10^{-3}	5.93×10^{-3}	
H/Cu(100)	1.53	1.66	1.90		-0.26×10^{-3}	-0.15×10^{-3}	7.56×10^{-3}	
H/Rh(100)	1.58	1.77	2.02		-0.97×10^{-3}	0.38×10^{-3}	6.82×10^{-3}	
H/Pd(100)	1.55	1.73	2.00		-0.02×10^{-3}	-0.01×10^{-3}	9.74×10^{-3}	
H/Ag(100)	1.65	1.79	2.07		-0.28×10^{-3}	-0.72×10^{-3}	10.4×10^{-3}	
H/Ir(100)	1.61	1.81	2.09		-1.01×10^{-3}	0.65×10^{-3}	7.86×10^{-3}	
H/Pt(100)	1.57	1.77	2.06		0.89×10^{-3}	0.93×10^{-3}	9.13×10^{-3}	
H/Au(100)	1.59	1.76	2.08		-0.66×10^{-3}	0.38×10^{-3}	10.0×10^{-3}	

Table 3. Average fractional kinetic and electrostatic component of the binding energy $\langle E_{K+ES} \rangle$ for the hydrogenated FCC (111), HCP (0001), FCC (100) and BCC (100) systems. ‘On-top’, ‘FCC’, ‘HCP’, ‘2-fold bridge’ and ‘4-fold hollow’ and indicate the H binding position defined in Fig. 1.

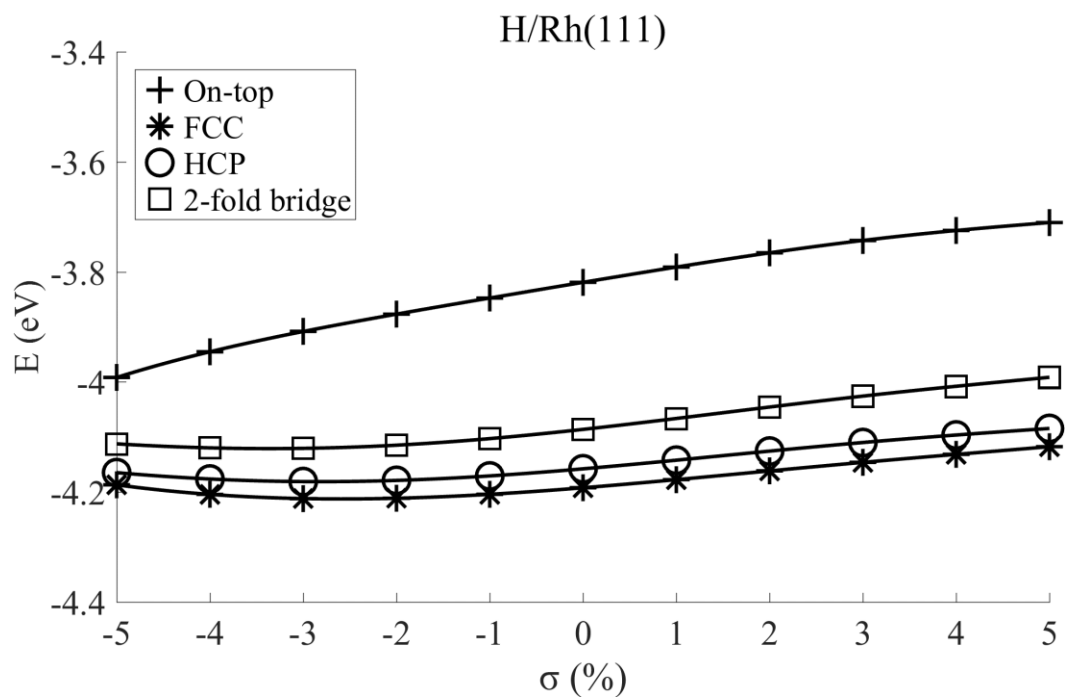
System	H binding position			
	On-top	FCC	HCP	2-fold bridge
H/Co(0001)	0.184	0.098	0.095	0.113
H/Ni(111)	0.194	0.076	0.075	0.090
H/Cu(111)	0.159	0.107	0.100	0.109
H/Ru(0001)	0.109	0.072	0.066	0.076
H/Rh(111)	0.105	0.058	0.061	0.069
H/Pd(111)	0.074	0.025	0.026	0.029
H/Ag(111)	0.174	0.115	0.118	0.124
H/Os(0001)	0.153	0.077	0.074	0.087
H/Ir(111)	0.121	0.055	0.056	0.066
H/Pt(111)	0.142	0.070	0.076	0.097
H/Au(111)	0.225	0.218	0.216	0.218
System	On-top	2-fold bridge	4-fold hollow	
H/Fe(100)		0.169	0.129	0.033
H/Ni(100)		0.311	0.212	0.135
H/Cu(100)		0.125	0.080	0.044
H/Rh(100)		0.137	0.106	0.095
H/Pd(100)		0.167	0.113	0.098
H/Ag(100)		0.092	0.053	0.043
H/Ir(100)		0.162	0.128	0.126
H/Pt(100)		0.153	0.090	0.088
H/Au(100)		0.060	0.051	0.063

Table 4. The strain dependence of the work function change during hydrogenation $\left(\frac{d\phi}{d\sigma}\right)$ for the hydrogenated FCC (111), HCP (0001), FCC (100) and BCC (100) systems. All quantities in this table are in meV per %. ‘On-top’, ‘FCC’, ‘HCP’, ‘2-fold bridge’ and ‘4-fold hollow’ indicate the H binding position defined in Fig. 1.

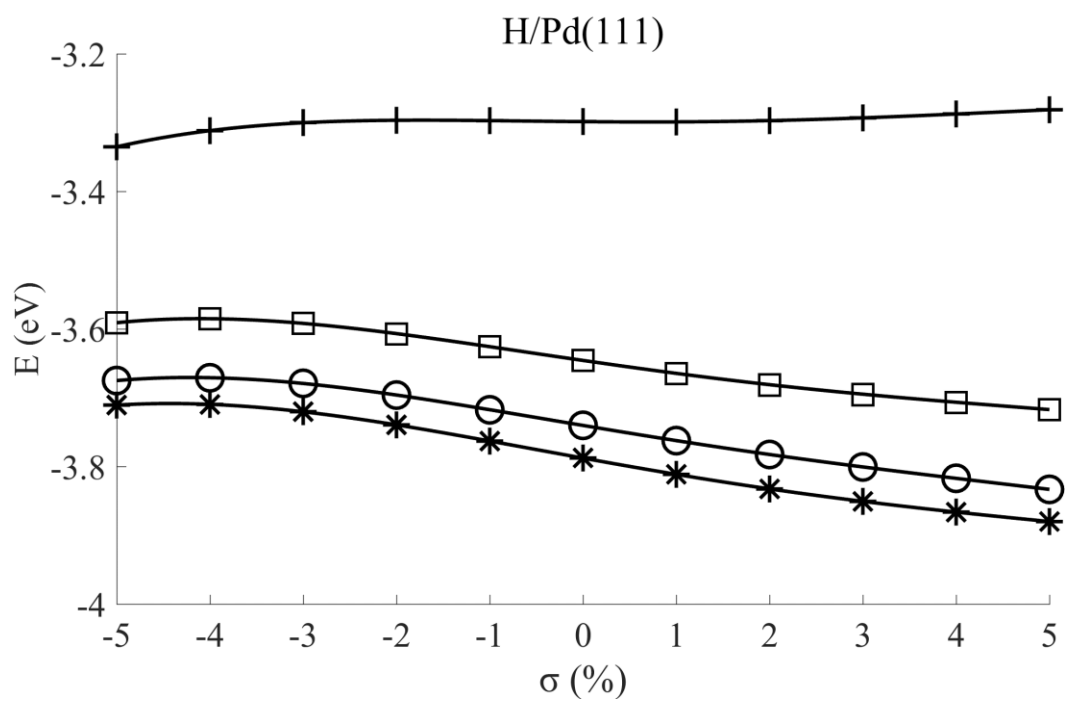
System	On-top	FCC	HCP	2-fold bridge
H/Co(0001)	0.77	-18.67	-19.56	-13.44
H/Ni(111)	2.57	-12.27	-12.64	-10.07
H/Cu(111)	-0.43	-17.67	-16.92	-16.64
H/Ru(0001)	-35.26	-3.05	-1.63	-3.65
H/Rh(111)	-16.45	-5.42	-5.24	-1.31
H/Pd(111)	-0.05	-14.71	-14.81	-9.76
H/Ag(111)	4.20	-17.83	-13.15	-13.01
H/Os(0001)	-12.83	9.22	13.34	5.76
H/Ir(111)	2.88	17.21	14.14	11.42
H/Pt(111)	6.02	-17.36	-17.05	-16.70
H/Au(111)	26.00	13.15	13.44	17.47
System	On-top	2-fold bridge	4-fold hollow	
H/Fe(100)	-7.39	-25.55	-35.31	
H/Ni(100)	-6.52	-7.63	-12.85	
H/Cu(100)	-27.89	-36.60	-40.72	
H/Rh(100)	-13.71	-5.02	-8.45	
H/Pd(100)	-13.14	-15.74	-20.12	
H/Ag(100)	-30.03	-31.85	-27.80	
H/Ir(100)	-3.77	3.35	-2.28	
H/Pt(100)	-11.37	-10.87	-14.61	
H/Au(100)	-23.53	-21.32	-31.32	

Fig. S1. Hydrogen binding energy E as a function of strain σ for the hydrogenated FCC (111) surfaces. The legend indicates the H binding position, which is defined in Fig. 1. The solid connecting lines are a guide to the eye.

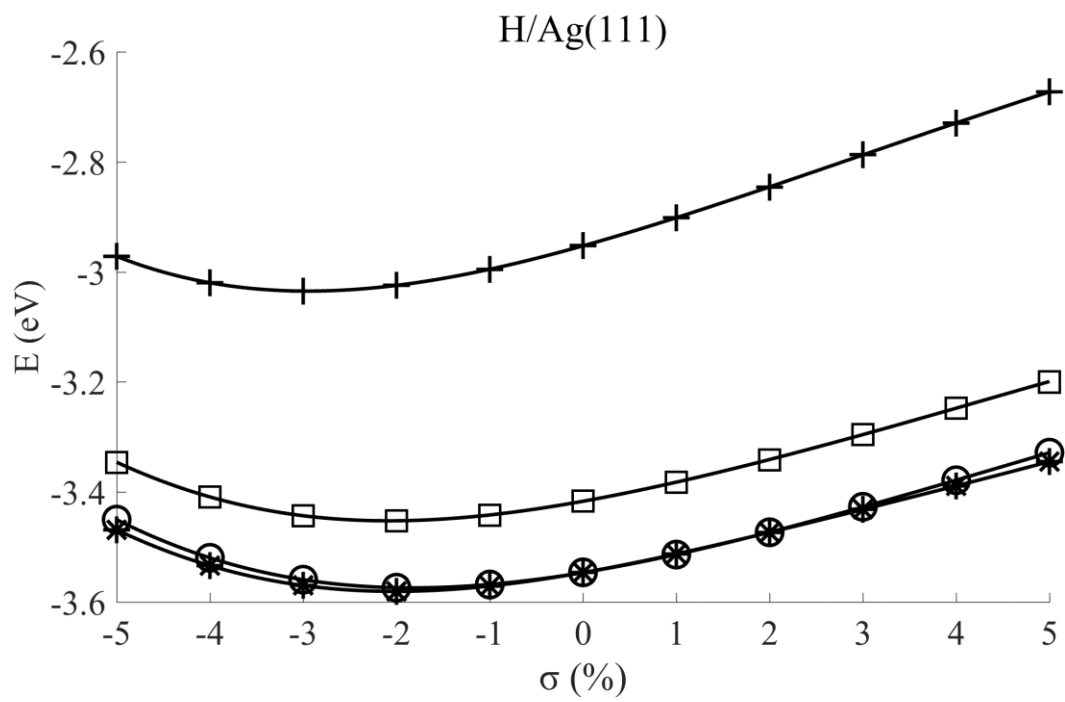
(a)



(b)



(c)



(d)

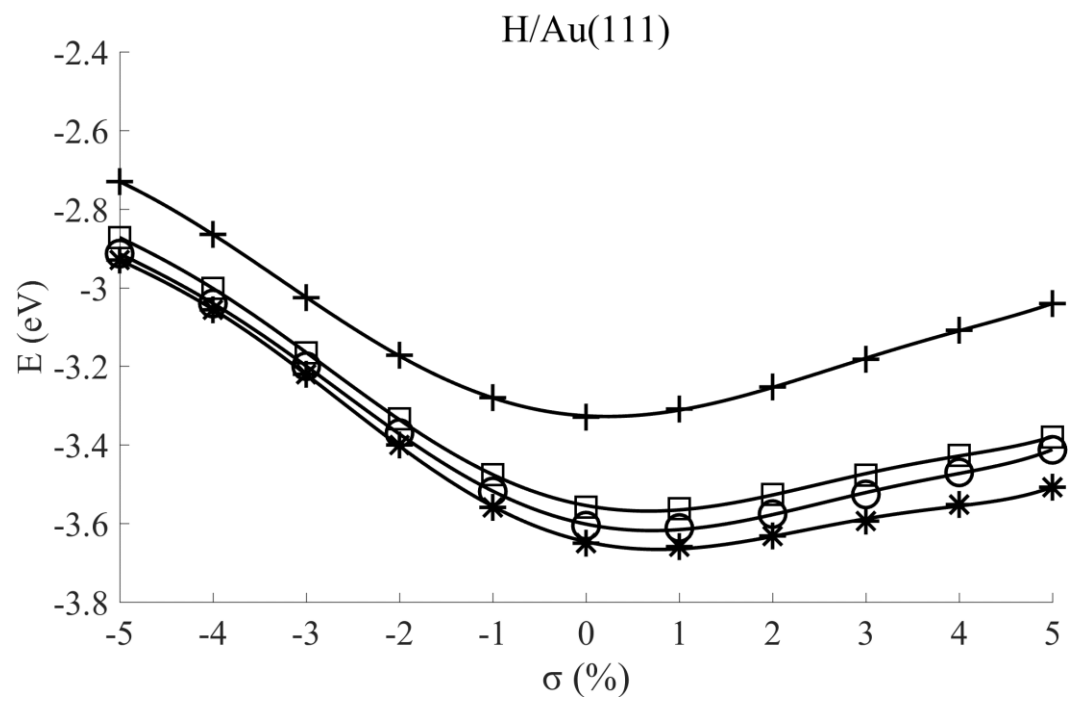
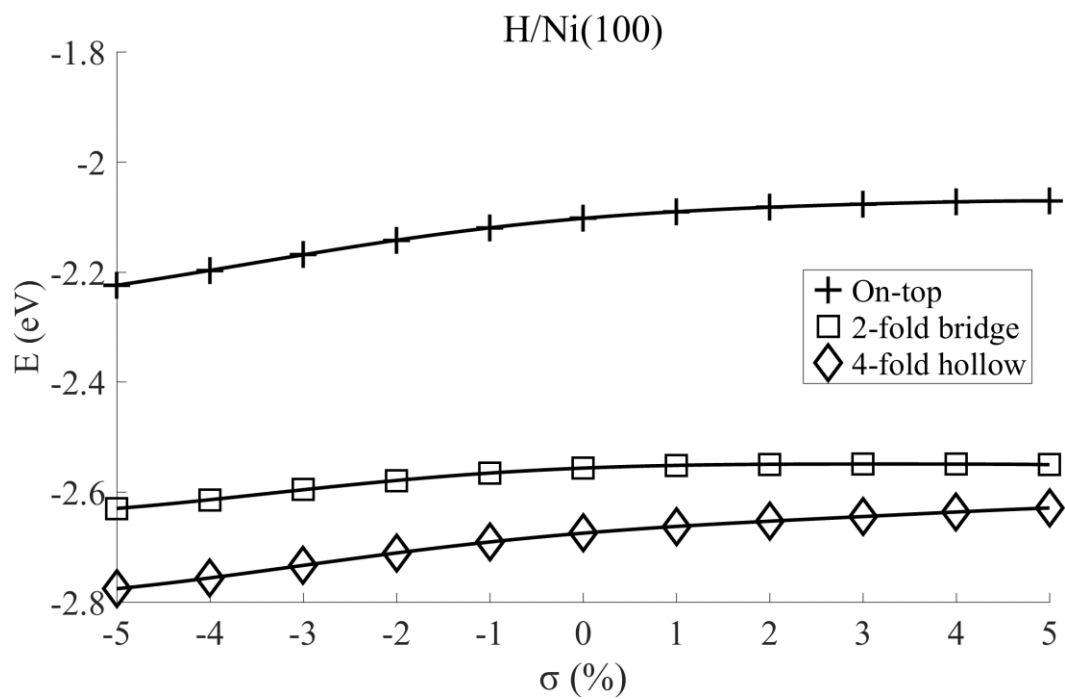
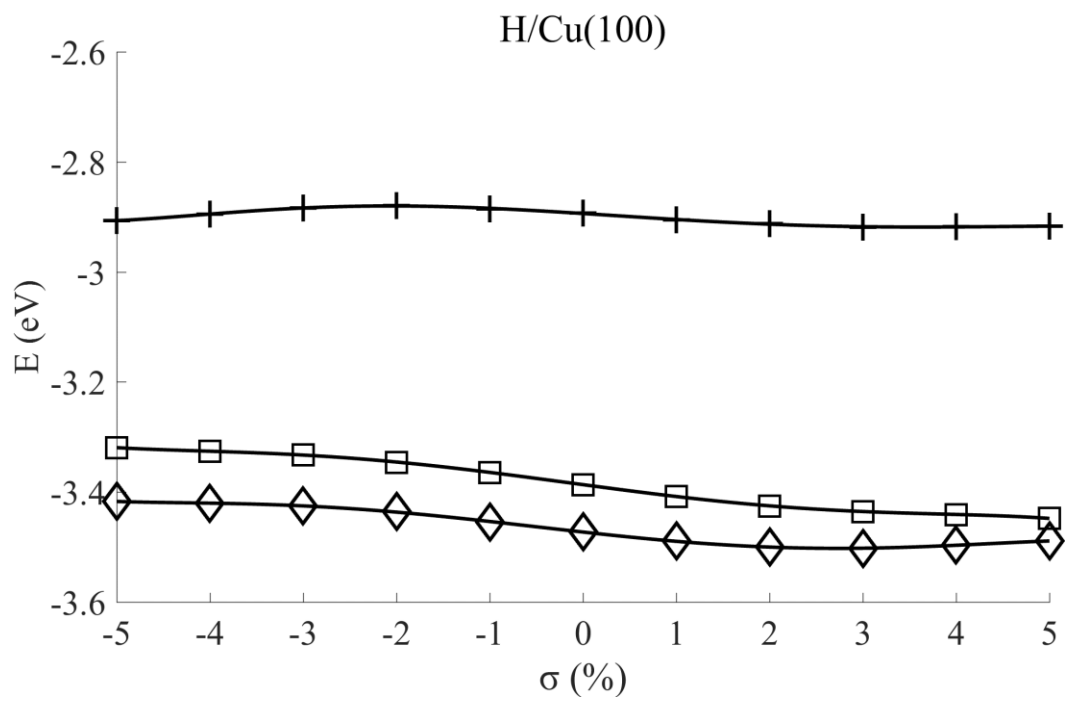


Fig. S2. Hydrogen binding energy E as a function of strain σ for the hydrogenated FCC (100) surfaces. The legend indicates the H binding position, which is defined in Fig. 1. The solid connecting lines are a guide to the eye.

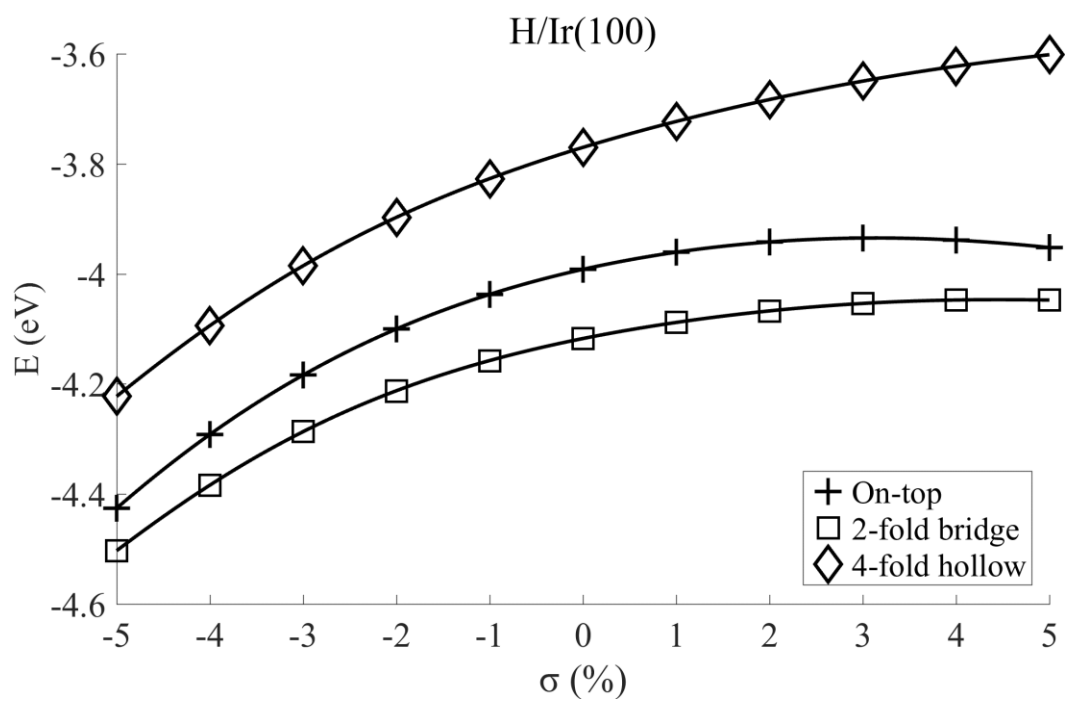
(a)



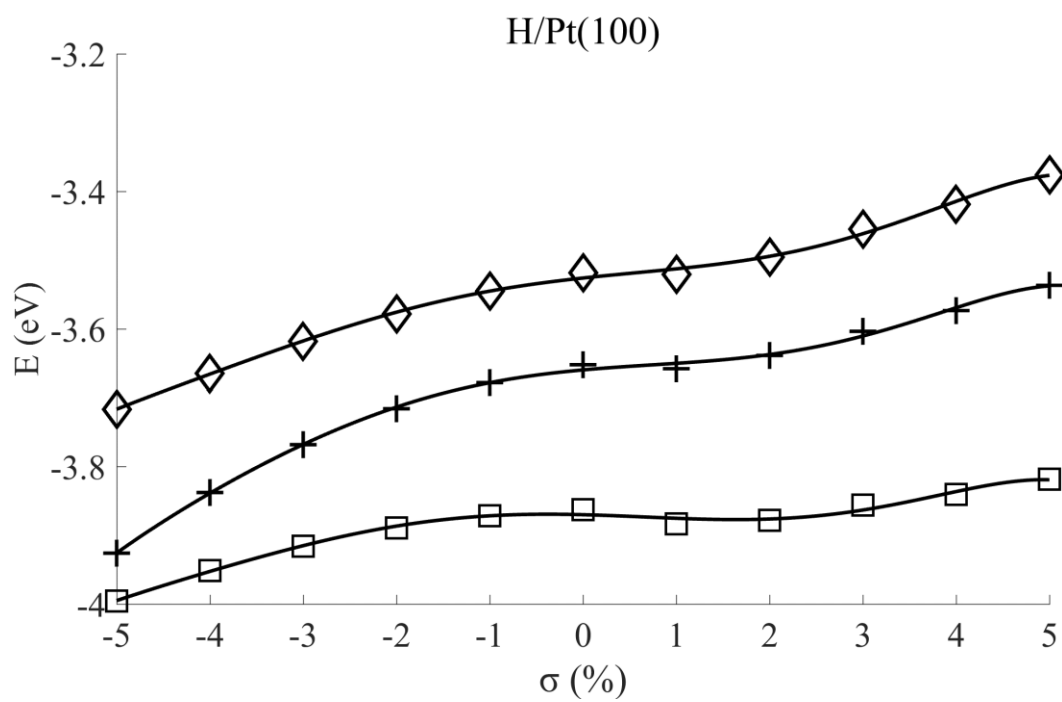
(b)



(c)



(d)



(e)

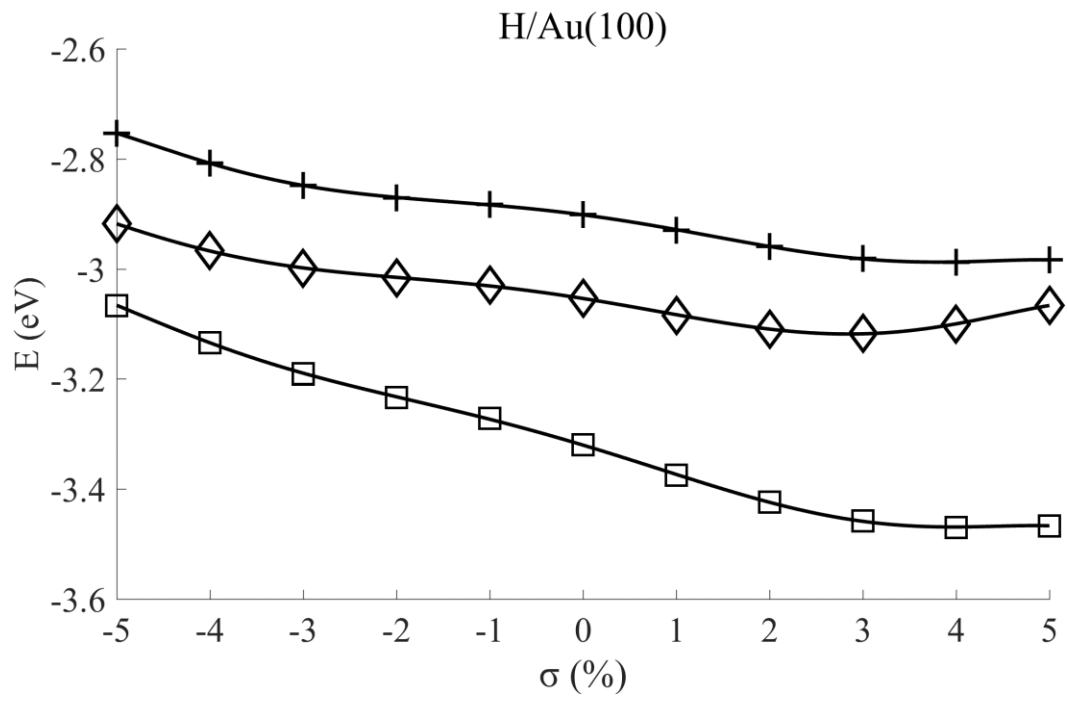
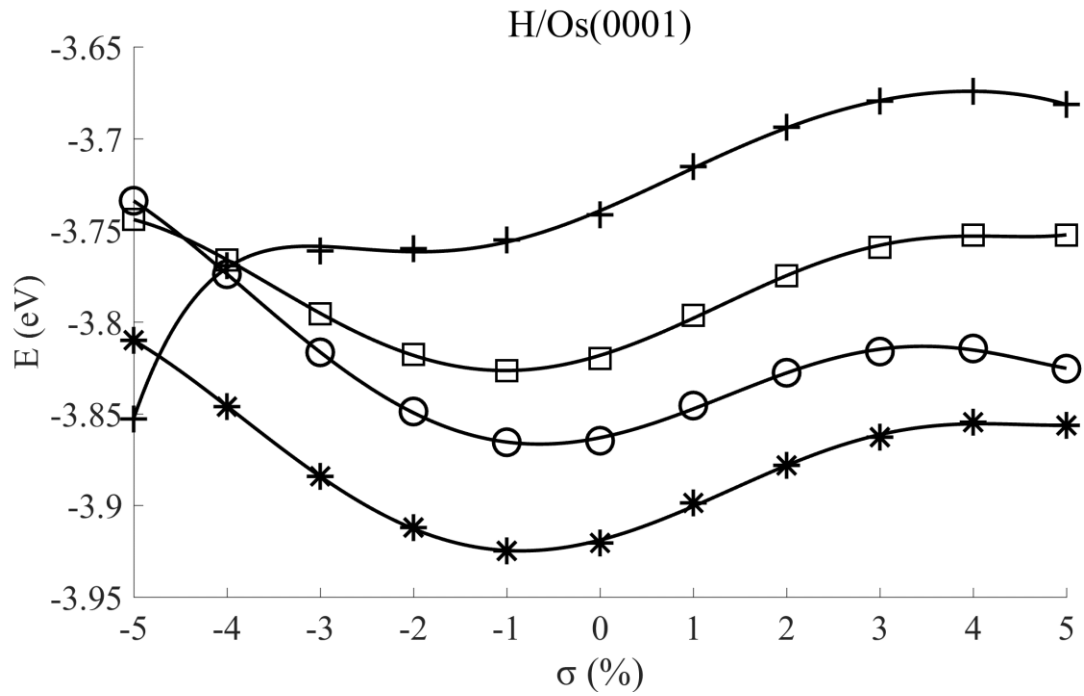


Fig. S3. Hydrogen binding energy E as a function of strain σ for the hydrogenated HCP(0001) surfaces. The legend indicates the H binding position, which is defined in Fig. 1. The solid connecting lines are a guide to the eye.

(a)



(b)

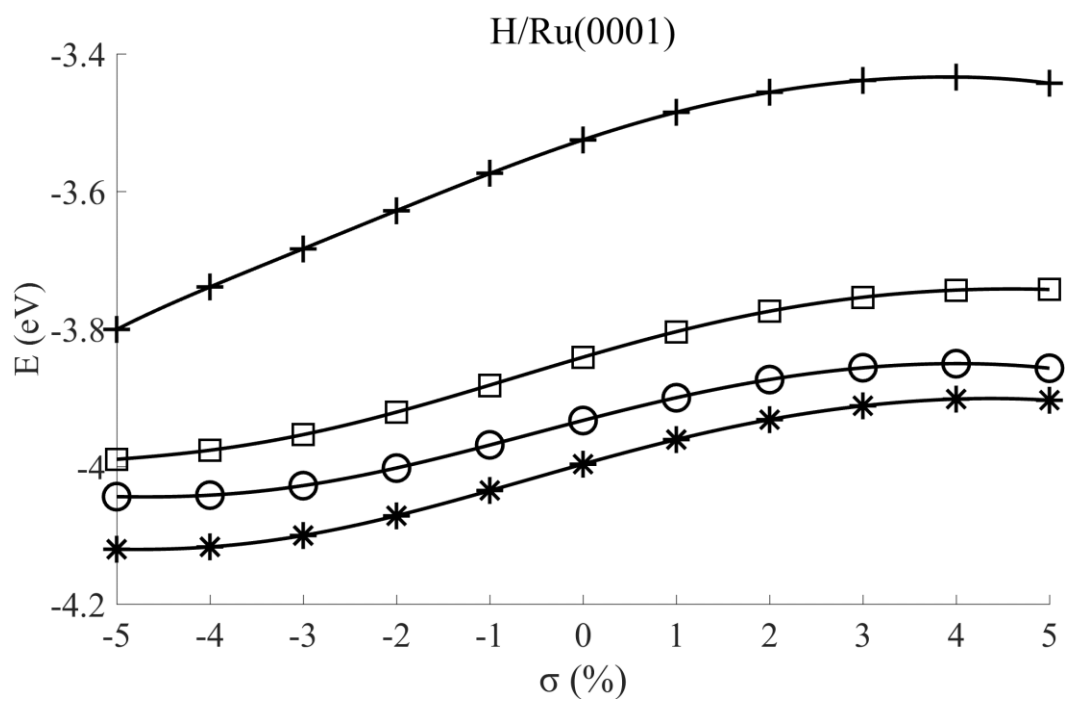
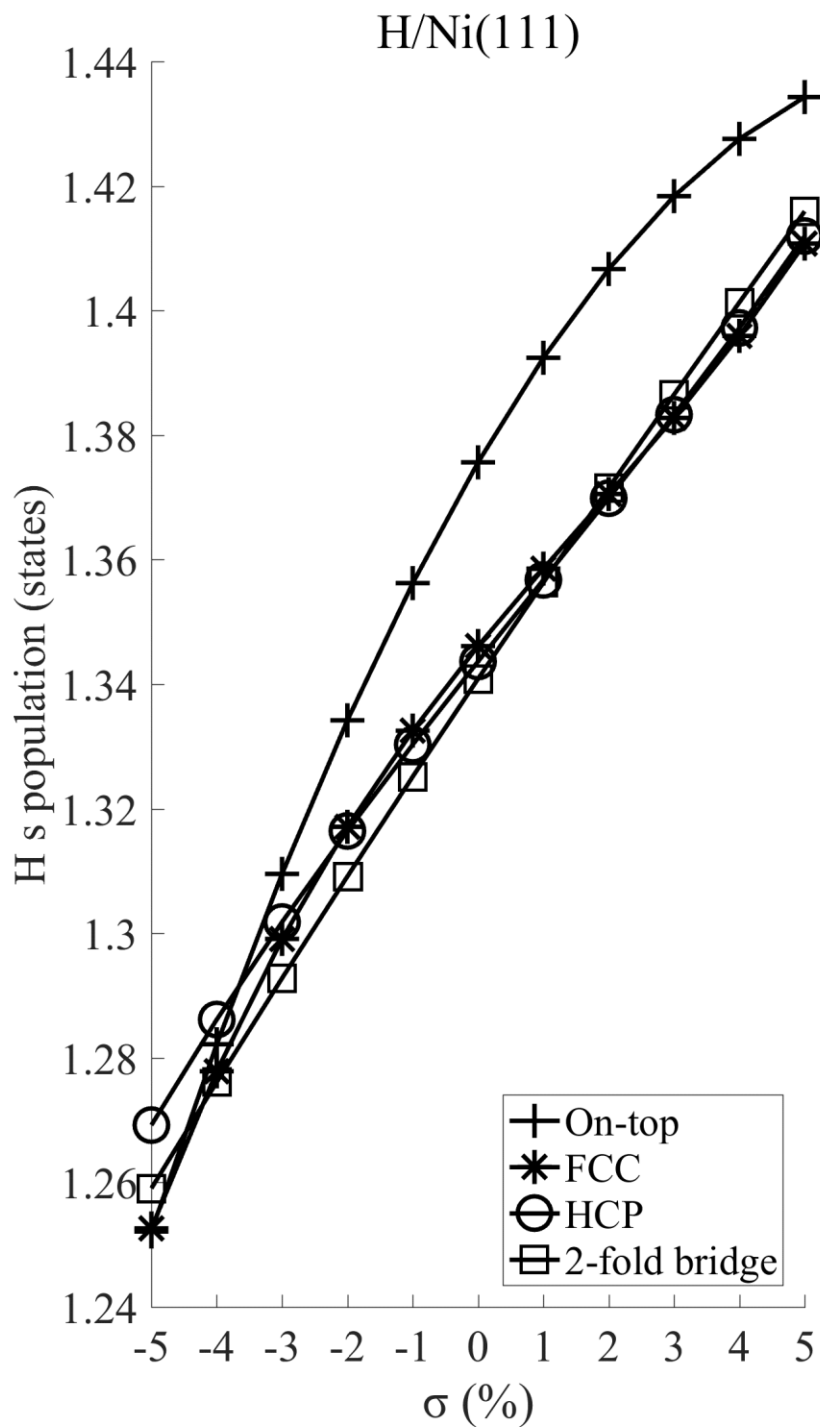
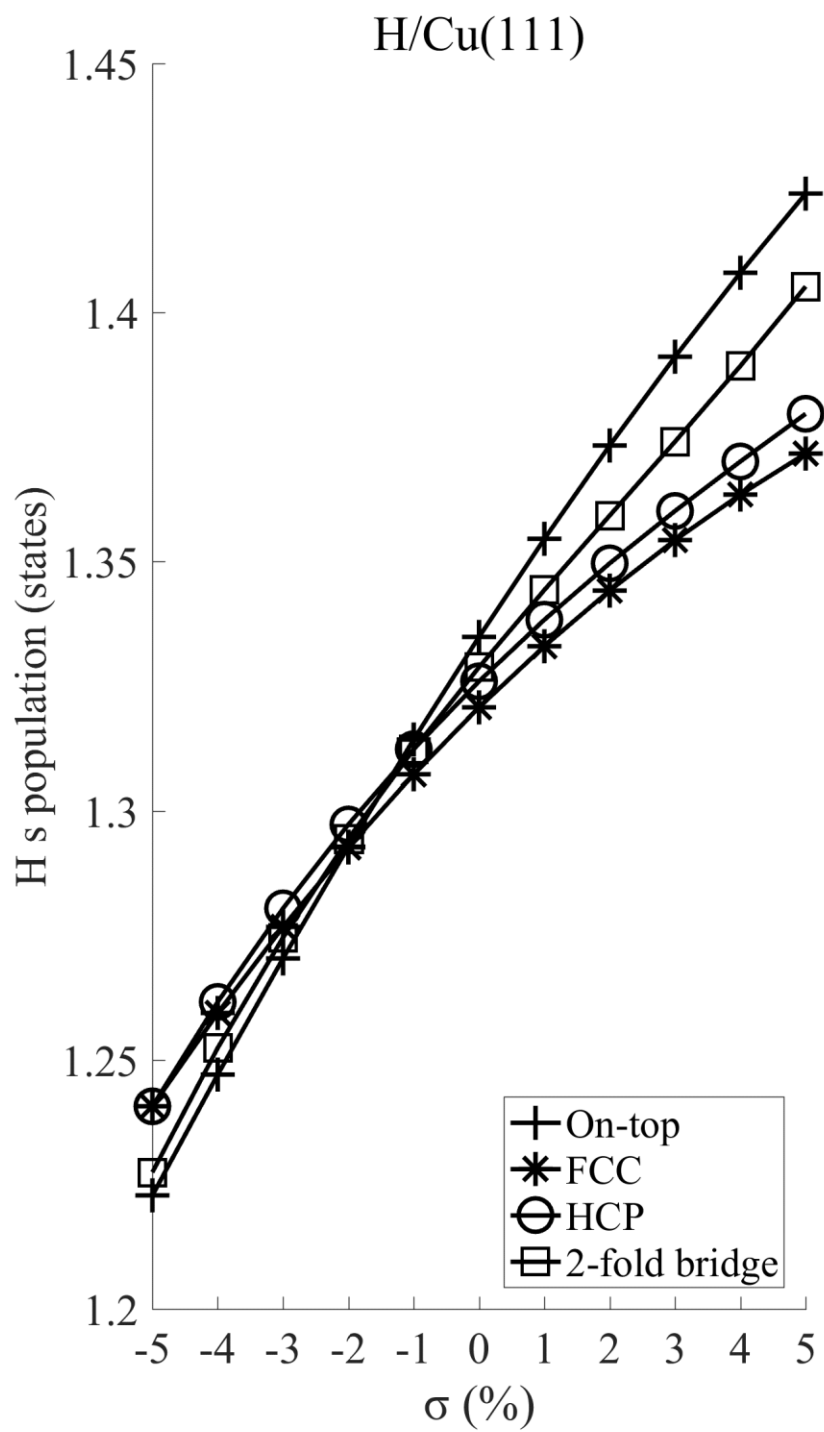


Fig. S4. The hydrogen s state population as a function of strain σ for the hydrogenated (a-g) FCC (111), (h-o) FCC (100), and (p-q) HCP(0001) surfaces. The legend indicates the H binding position, which are defined in Fig. 1. The solid connecting lines are a guide to the eye.

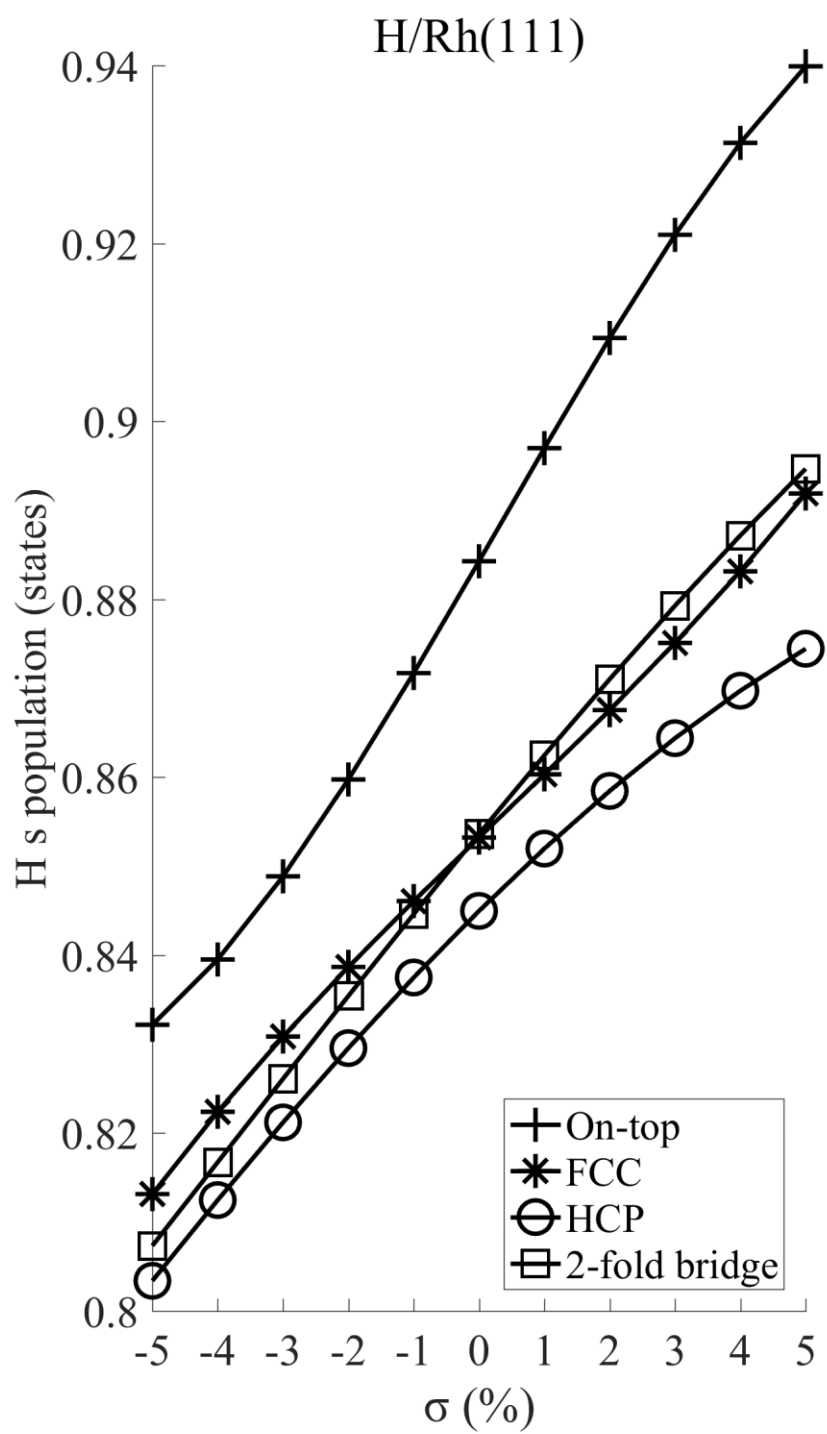
(a)



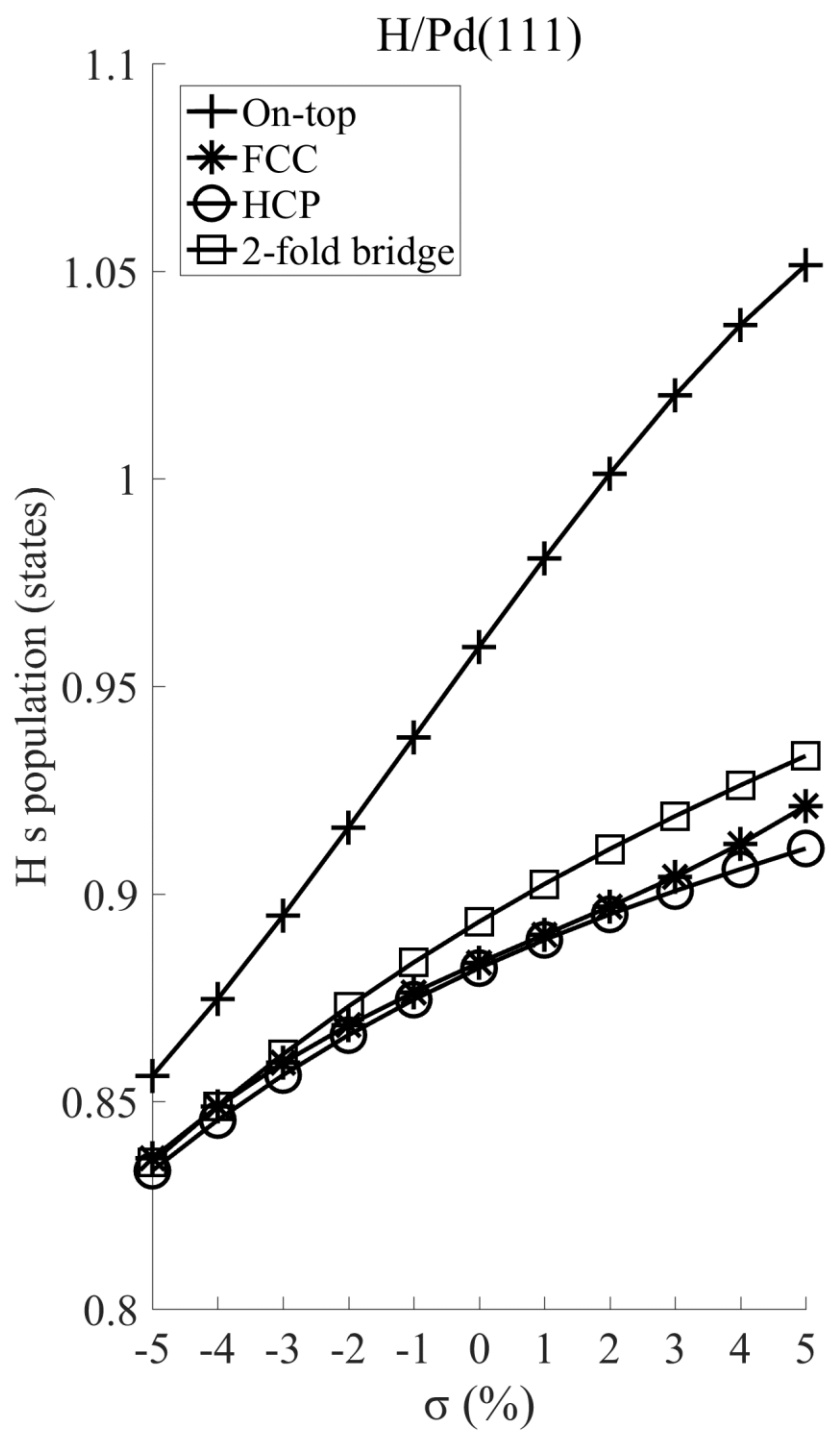
(b)



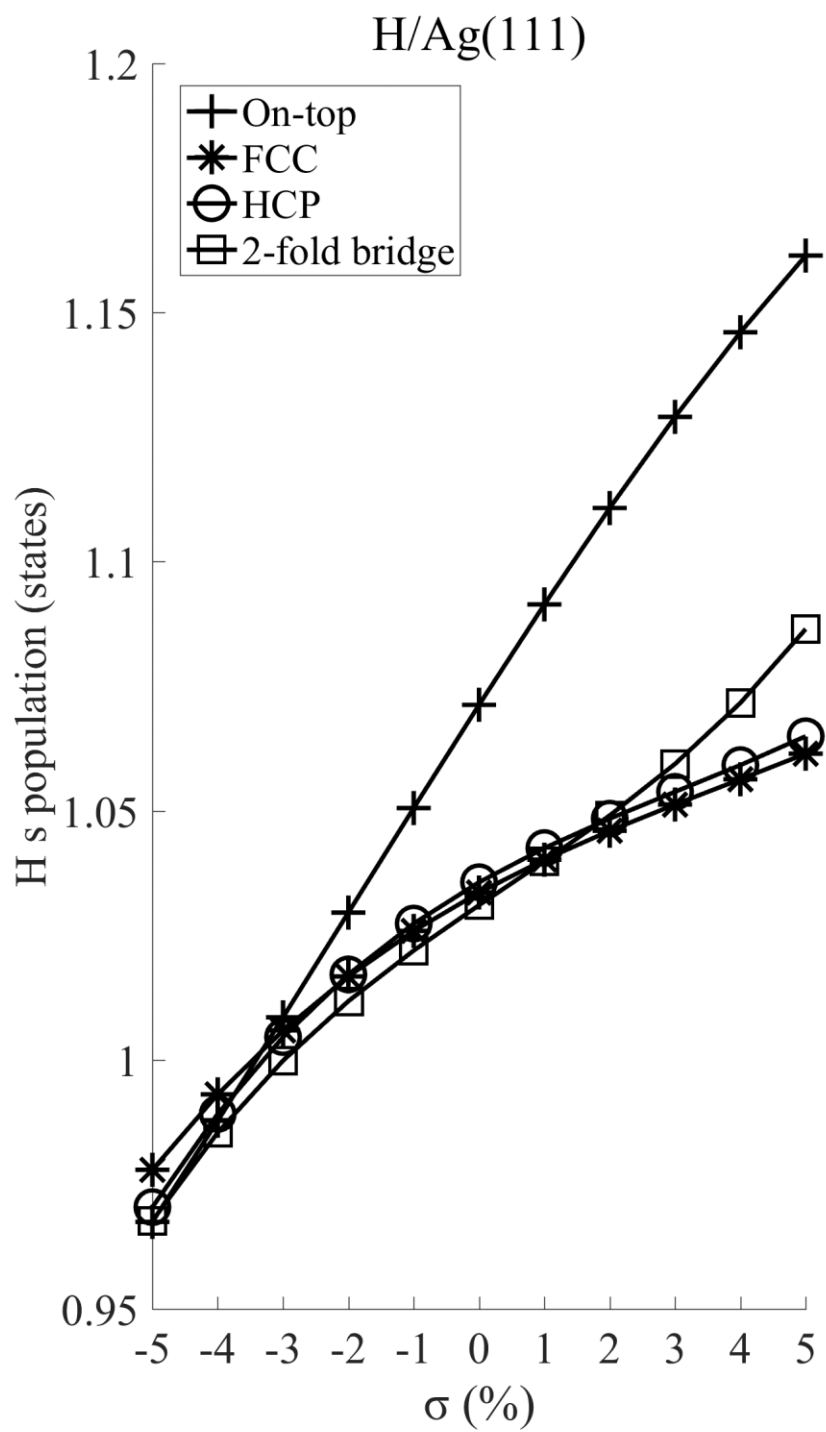
(c)



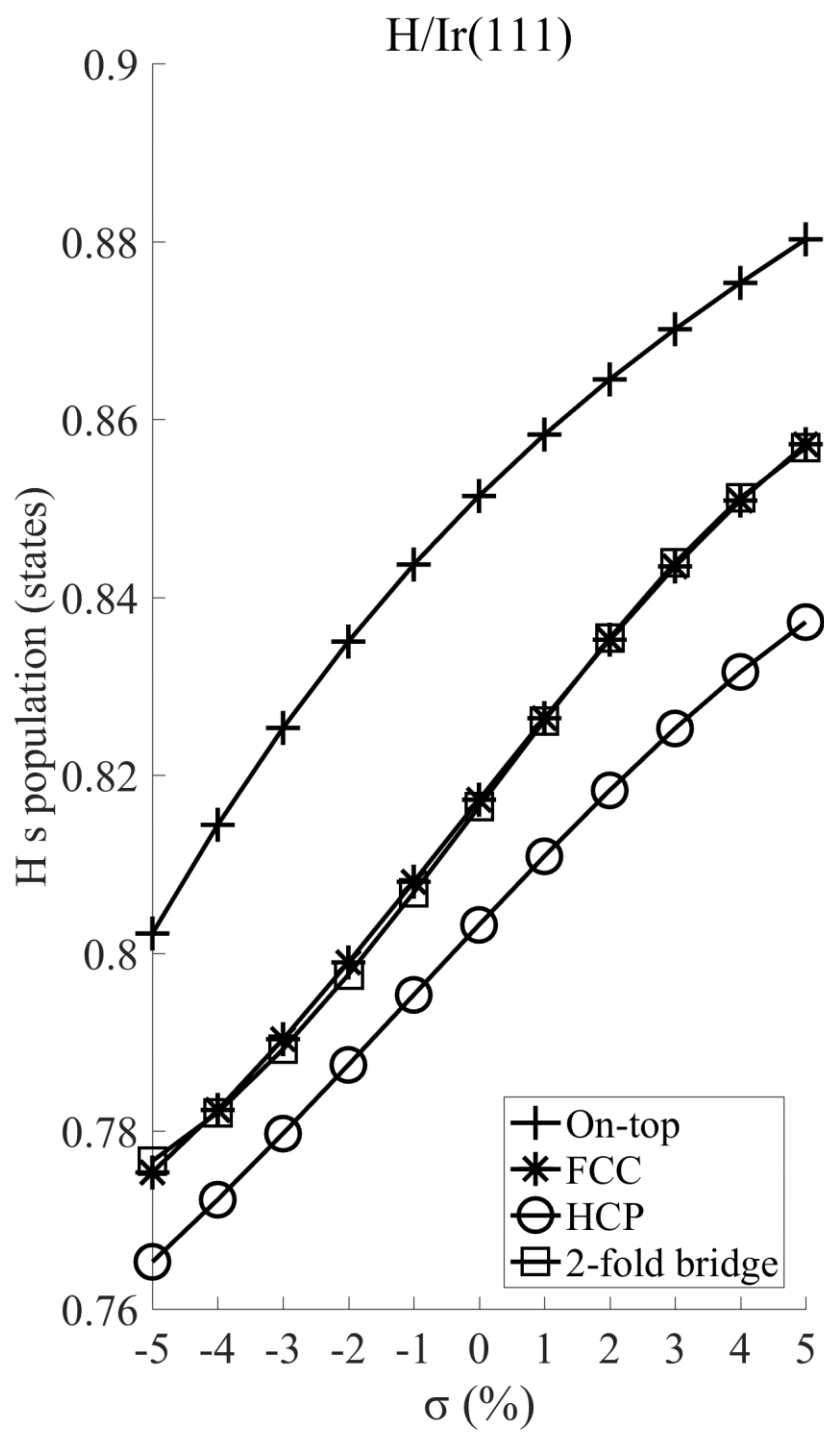
(d)



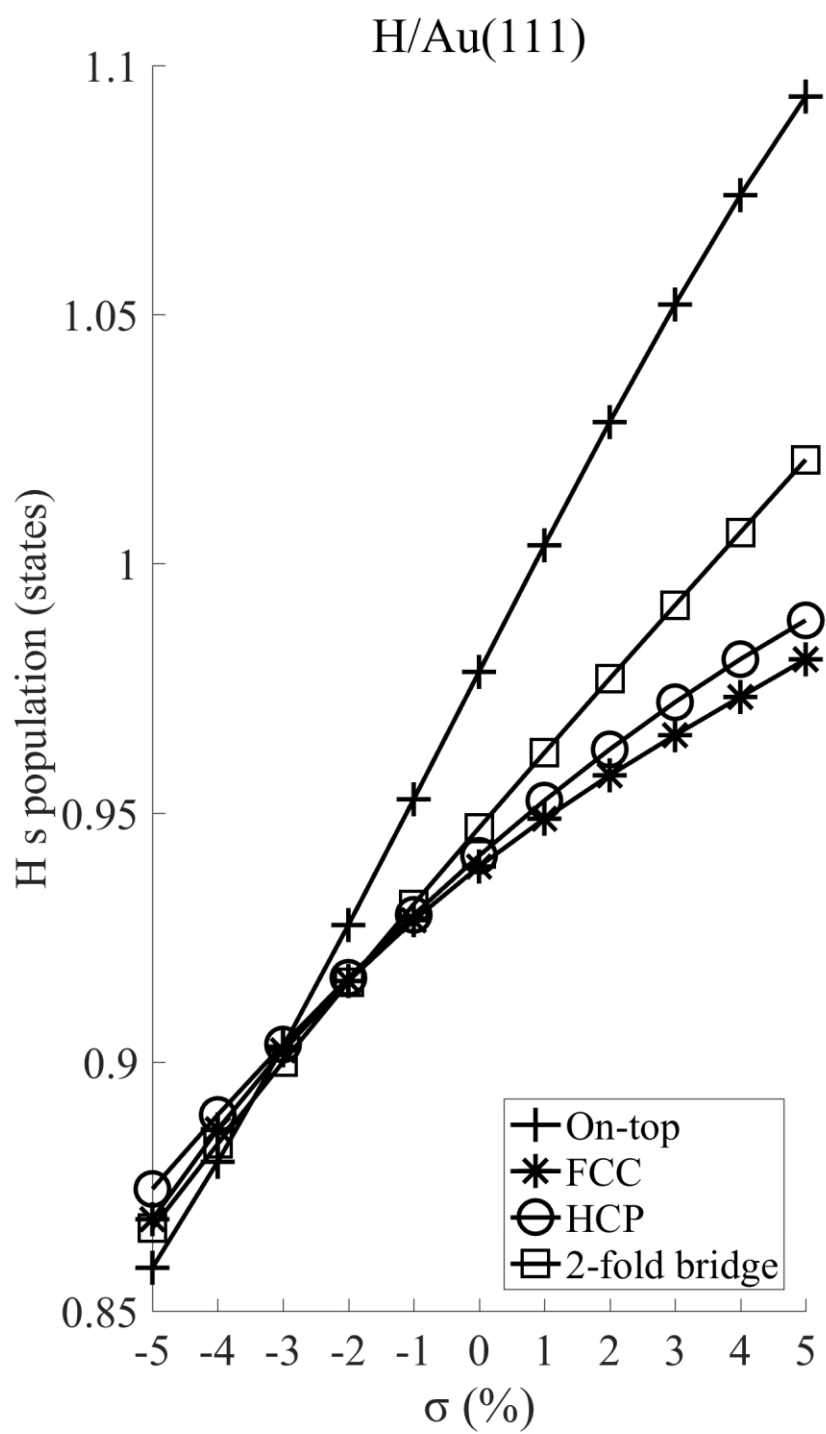
(e)



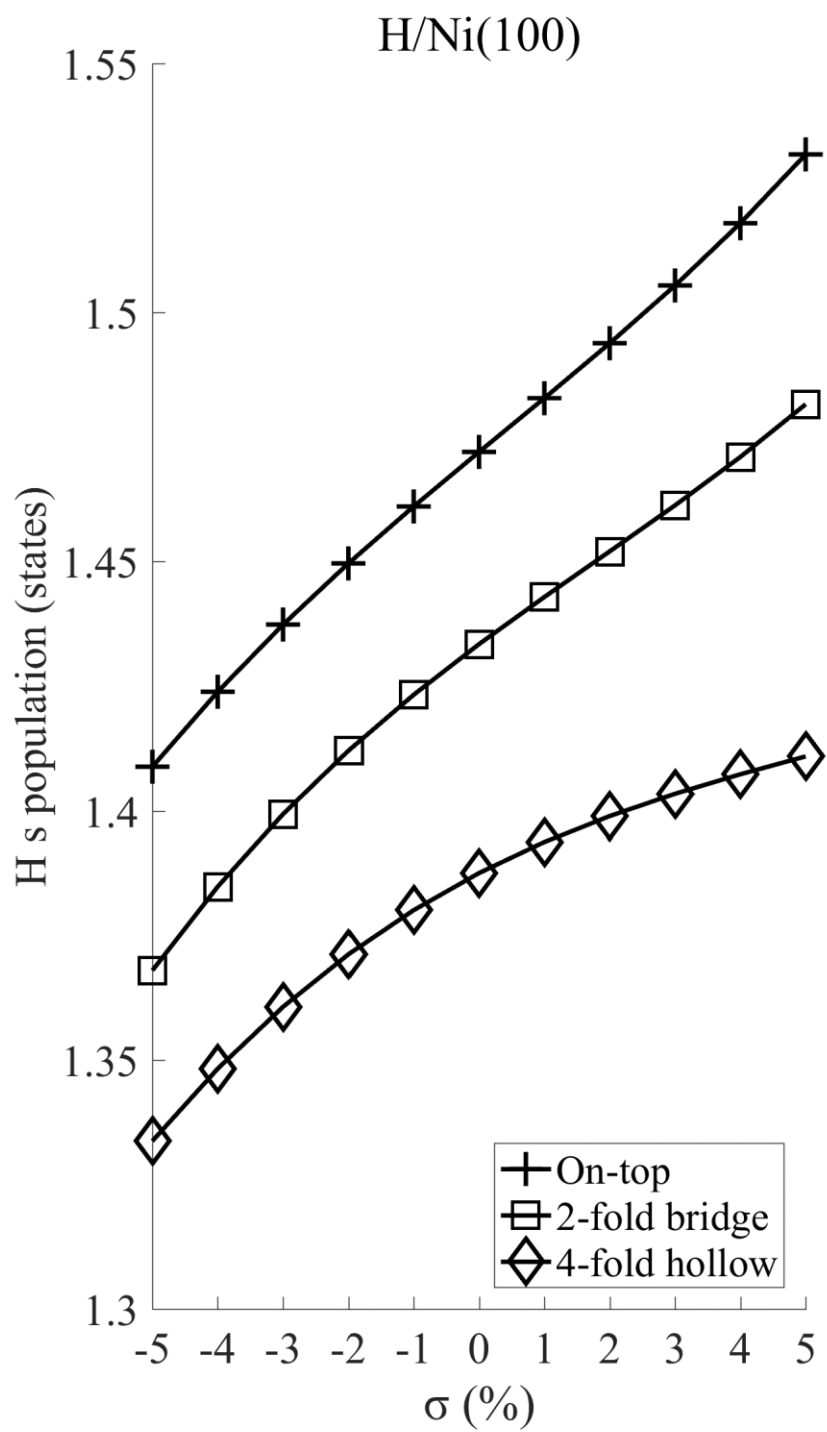
(f)



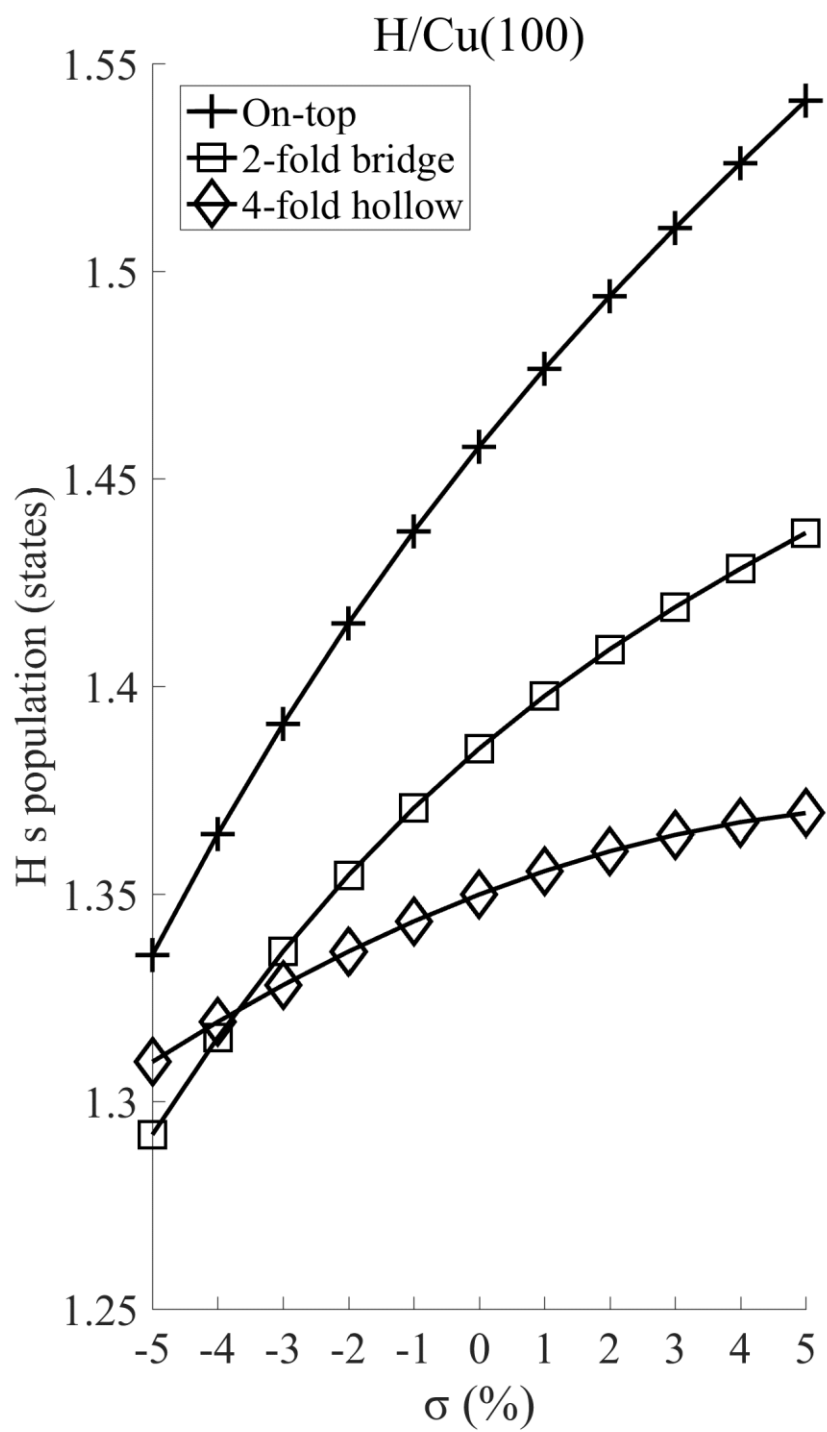
(g)



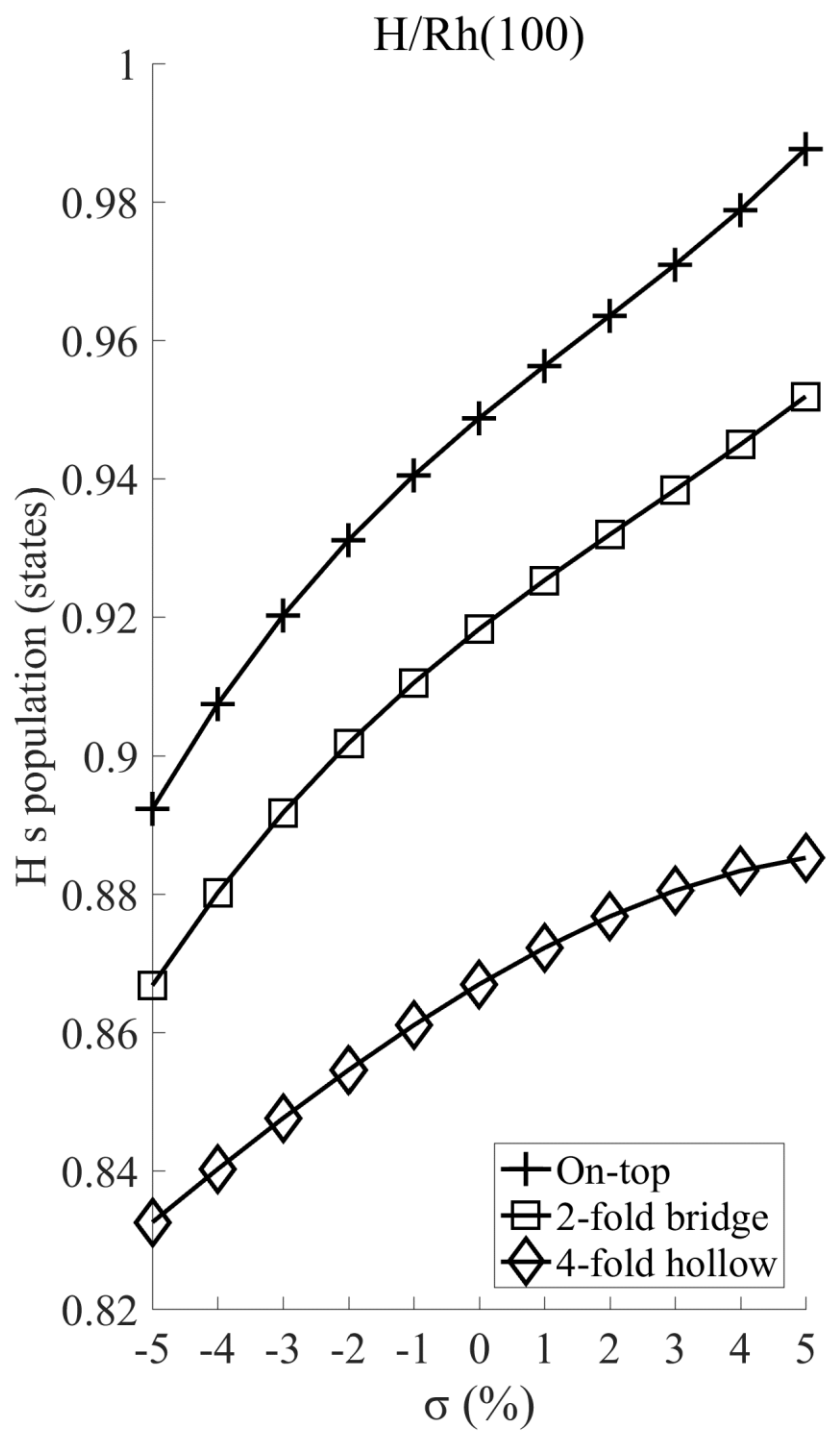
(h)



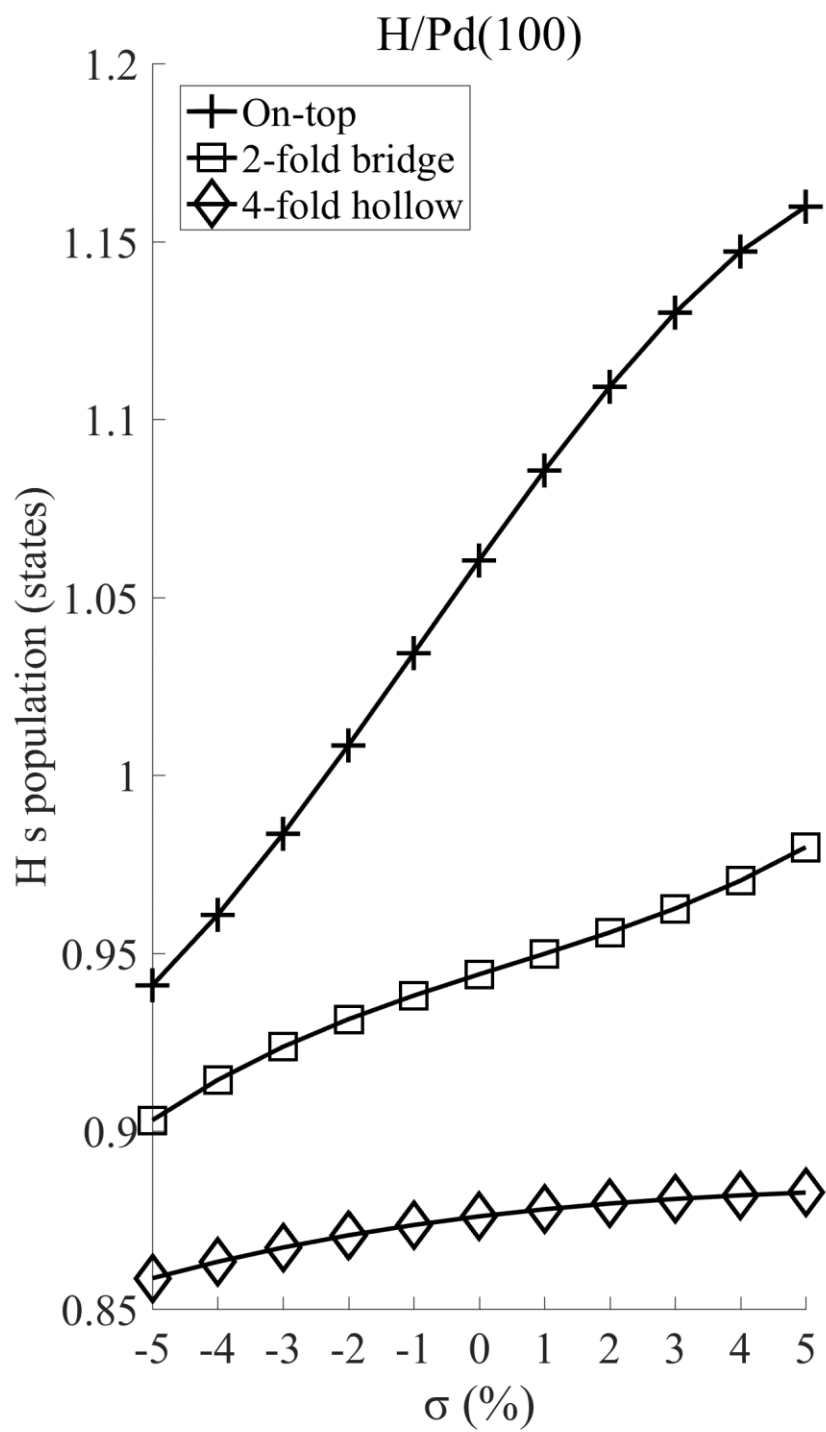
(i)



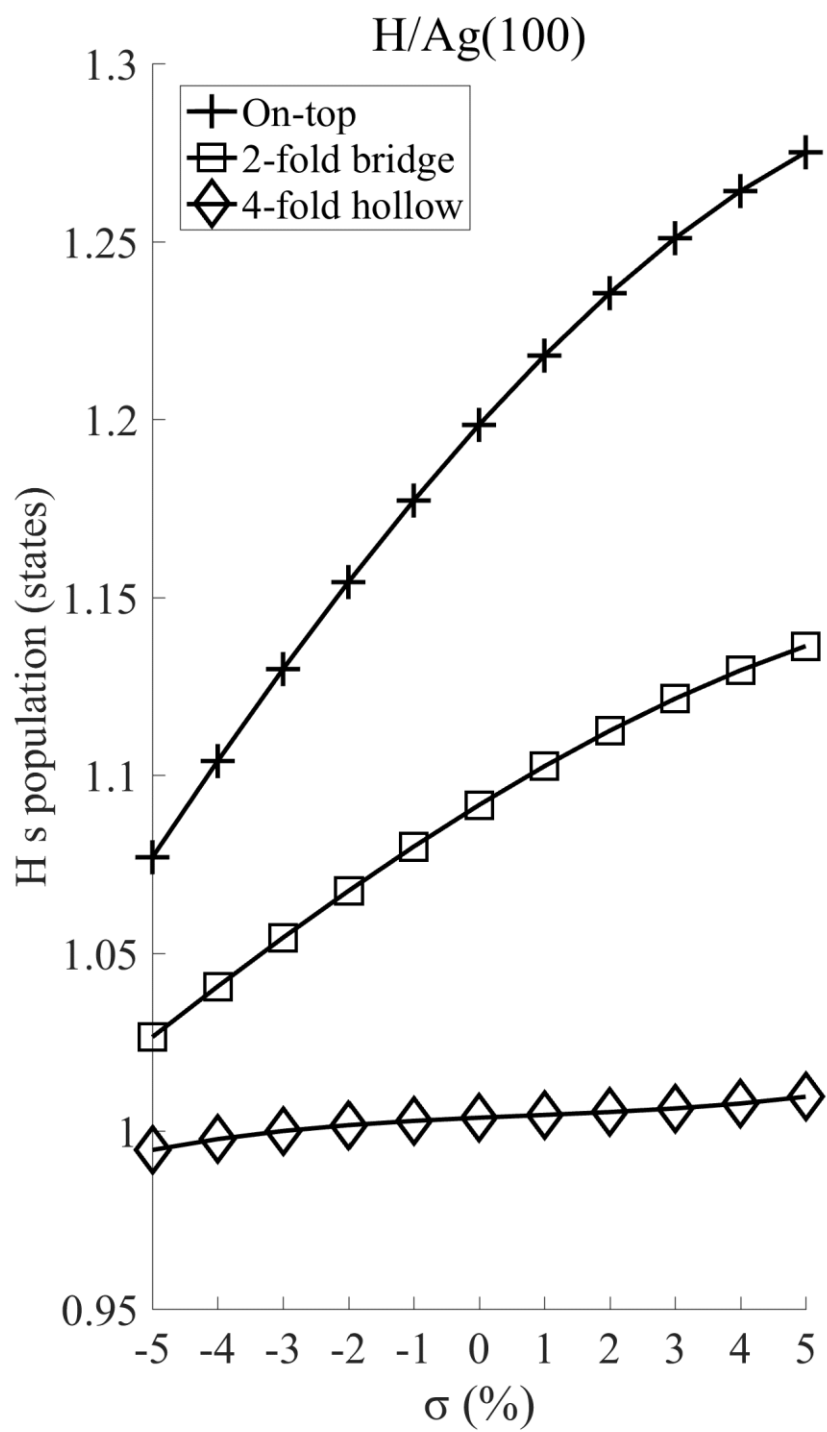
(j)



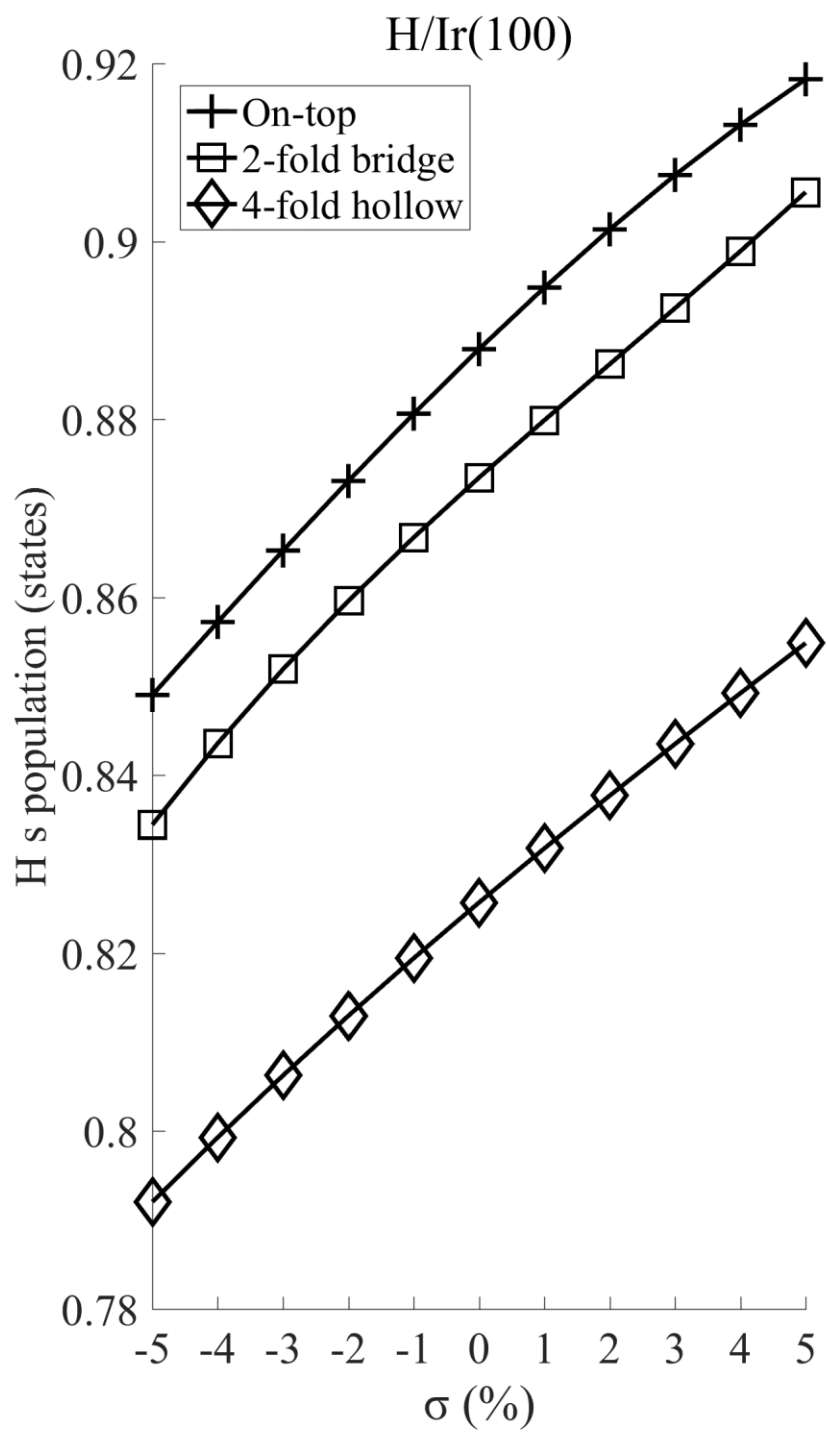
(k)



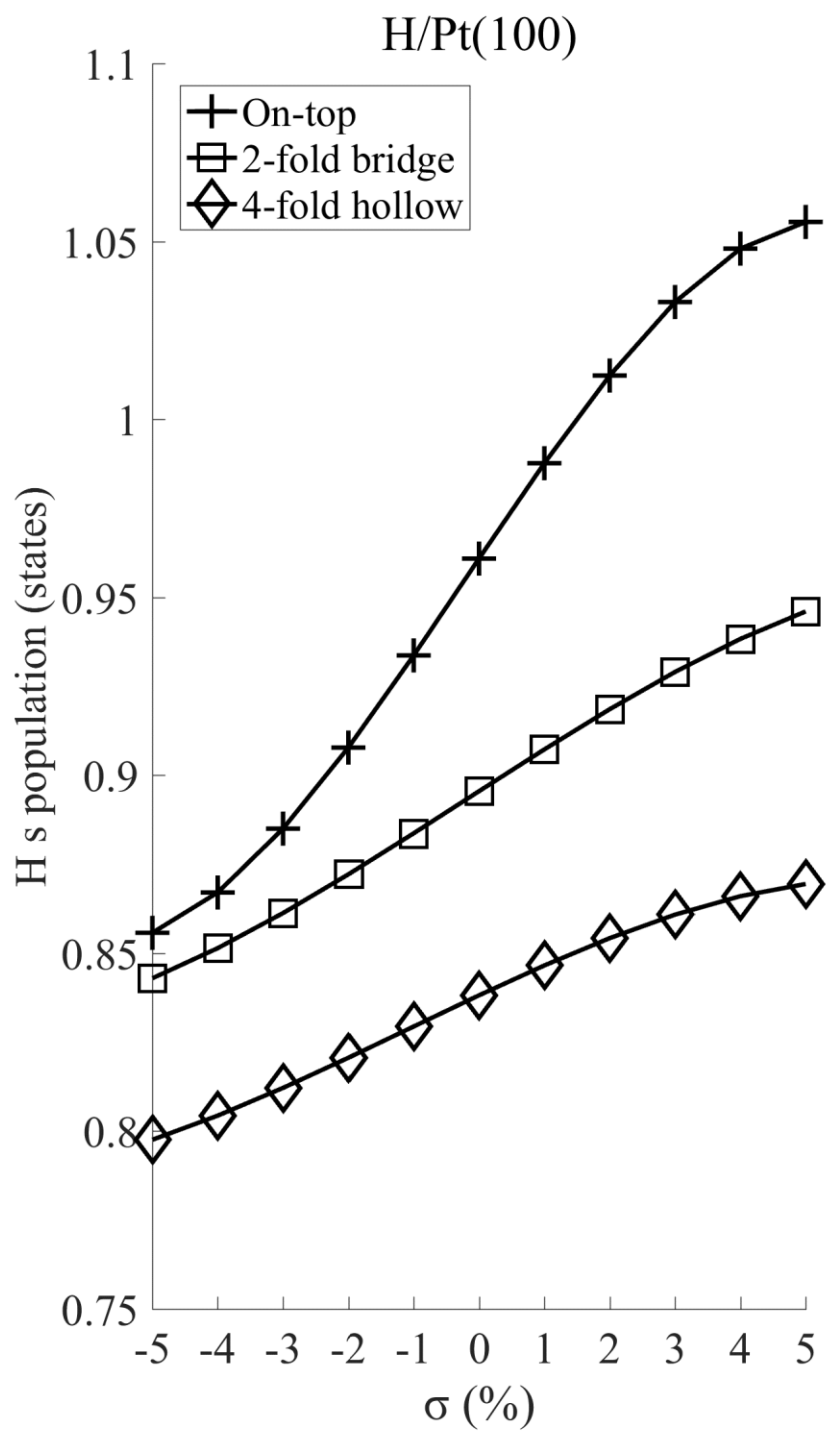
(1)



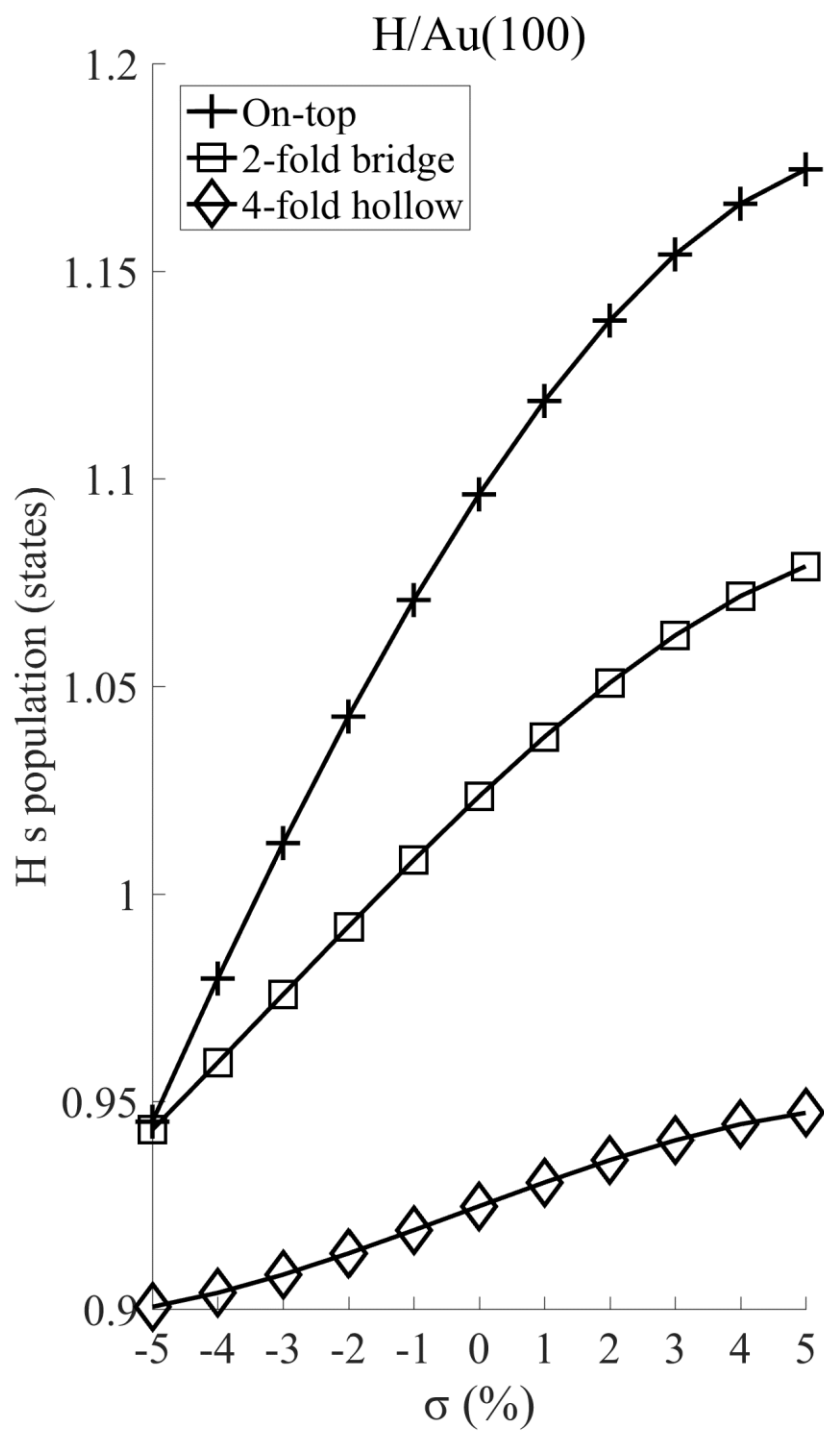
(m)



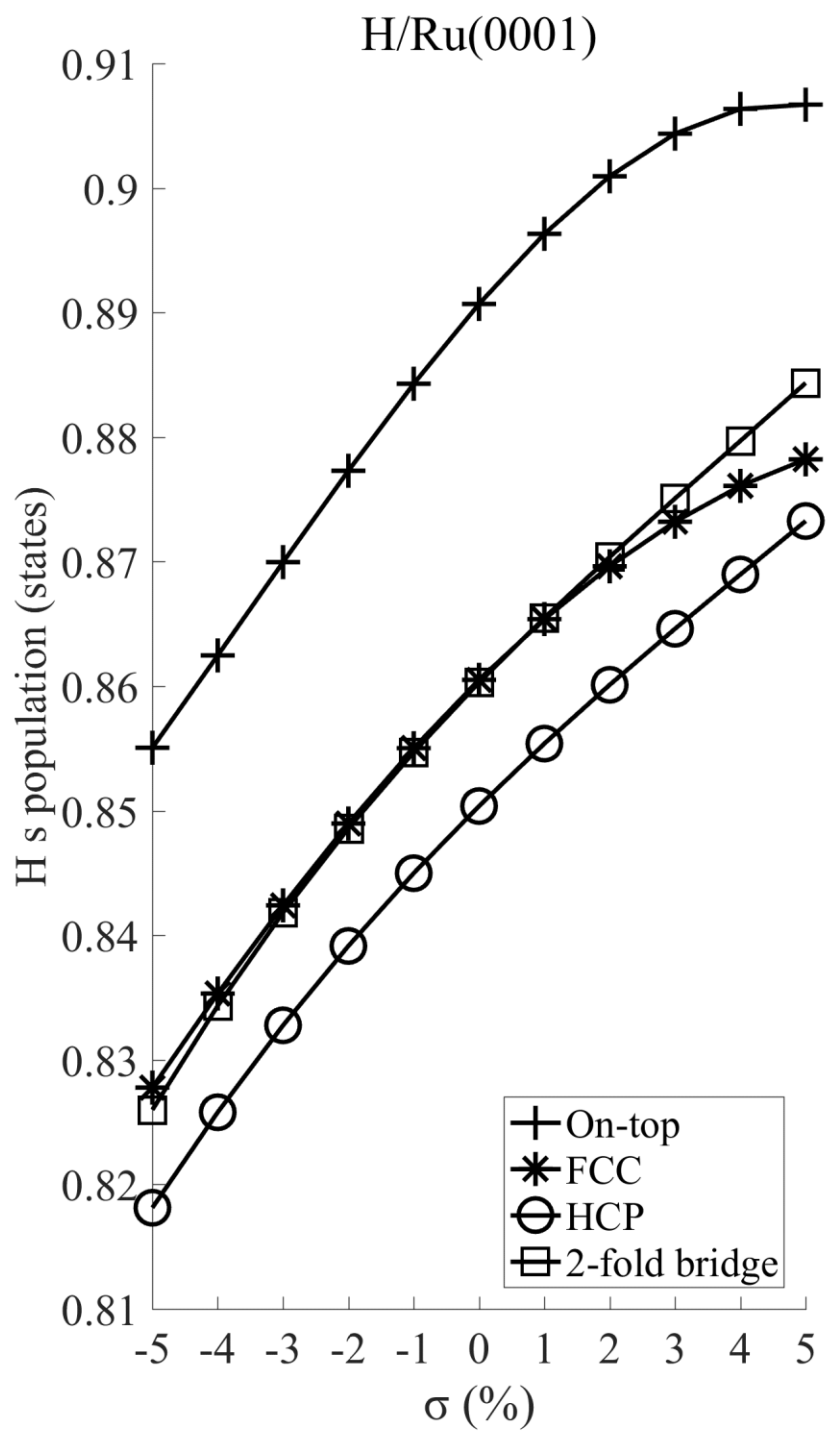
(n)



(o)



(p)



(q)

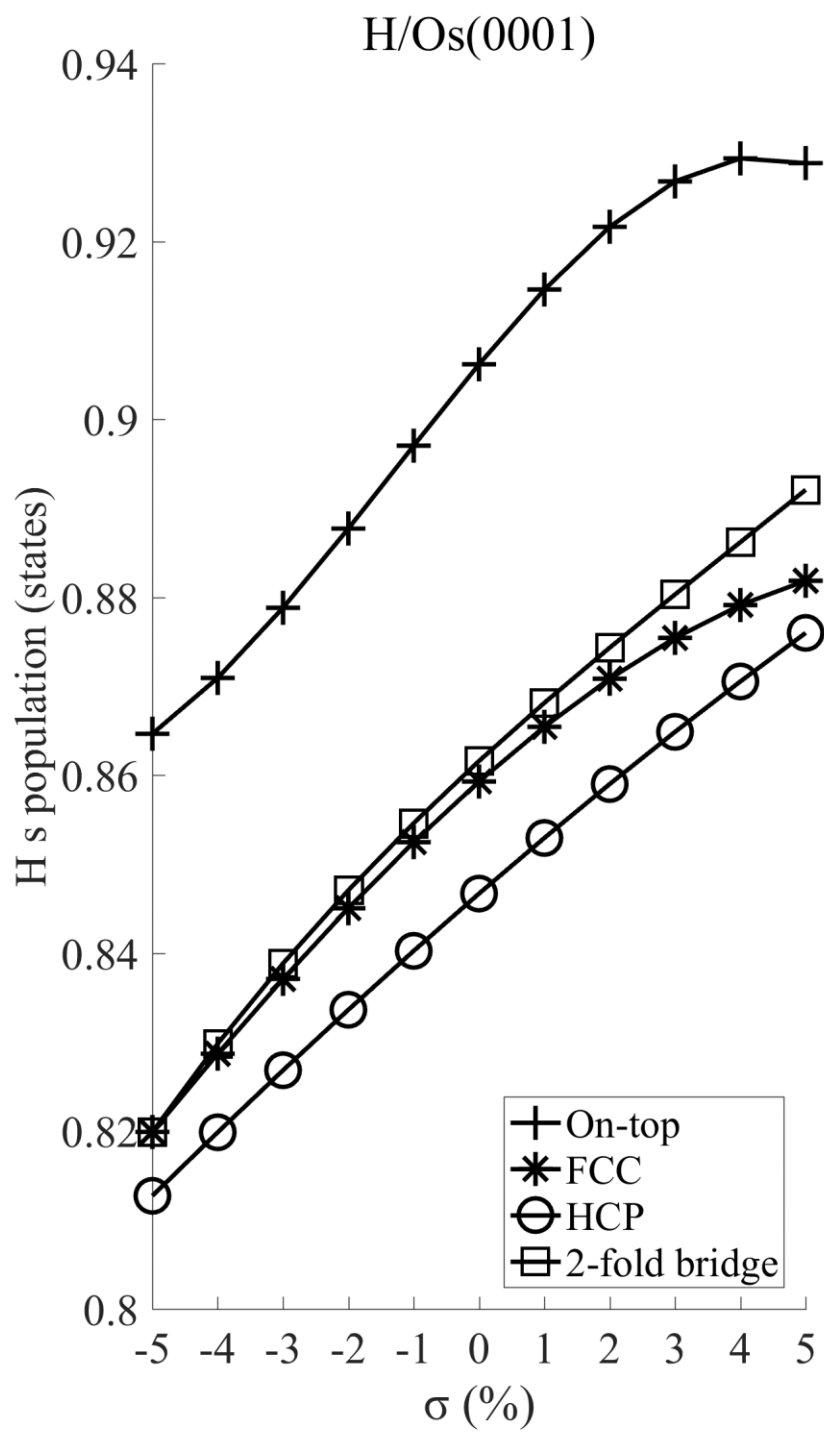
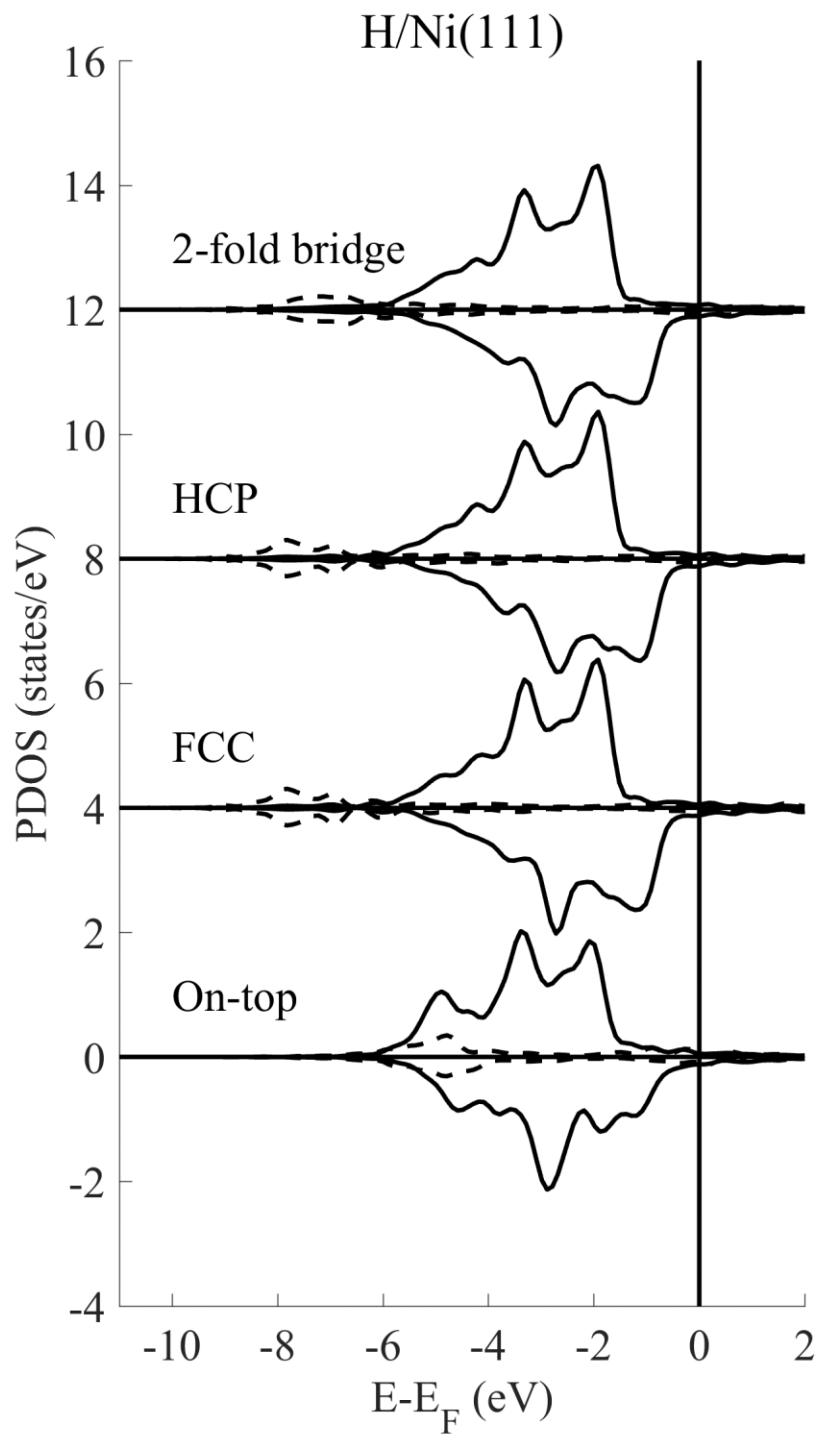
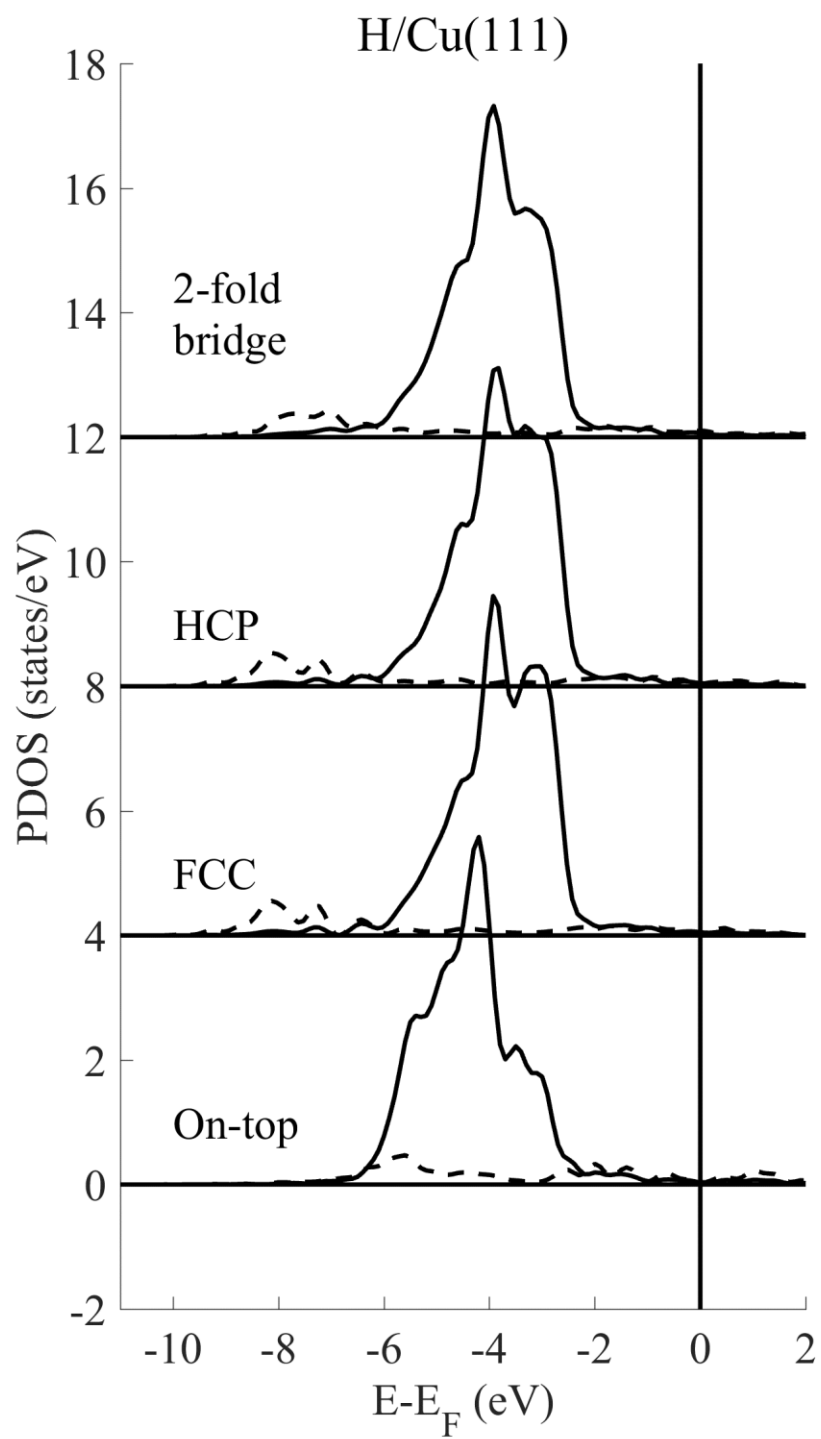


Fig. S5. The projected density of states (PDOS) at equilibrium ($\sigma=0\%$) for the hydrogenated (a-g) FCC (111), (h-o) FCC (100), and (p-q) HCP(0001) surfaces. The dashed (solid) curves denote H s (metal d) states. The labels denote the hydrogen binding position which are defined in Fig. 1. Curves for different hydrogen binding sites are offset vertically for clarity.

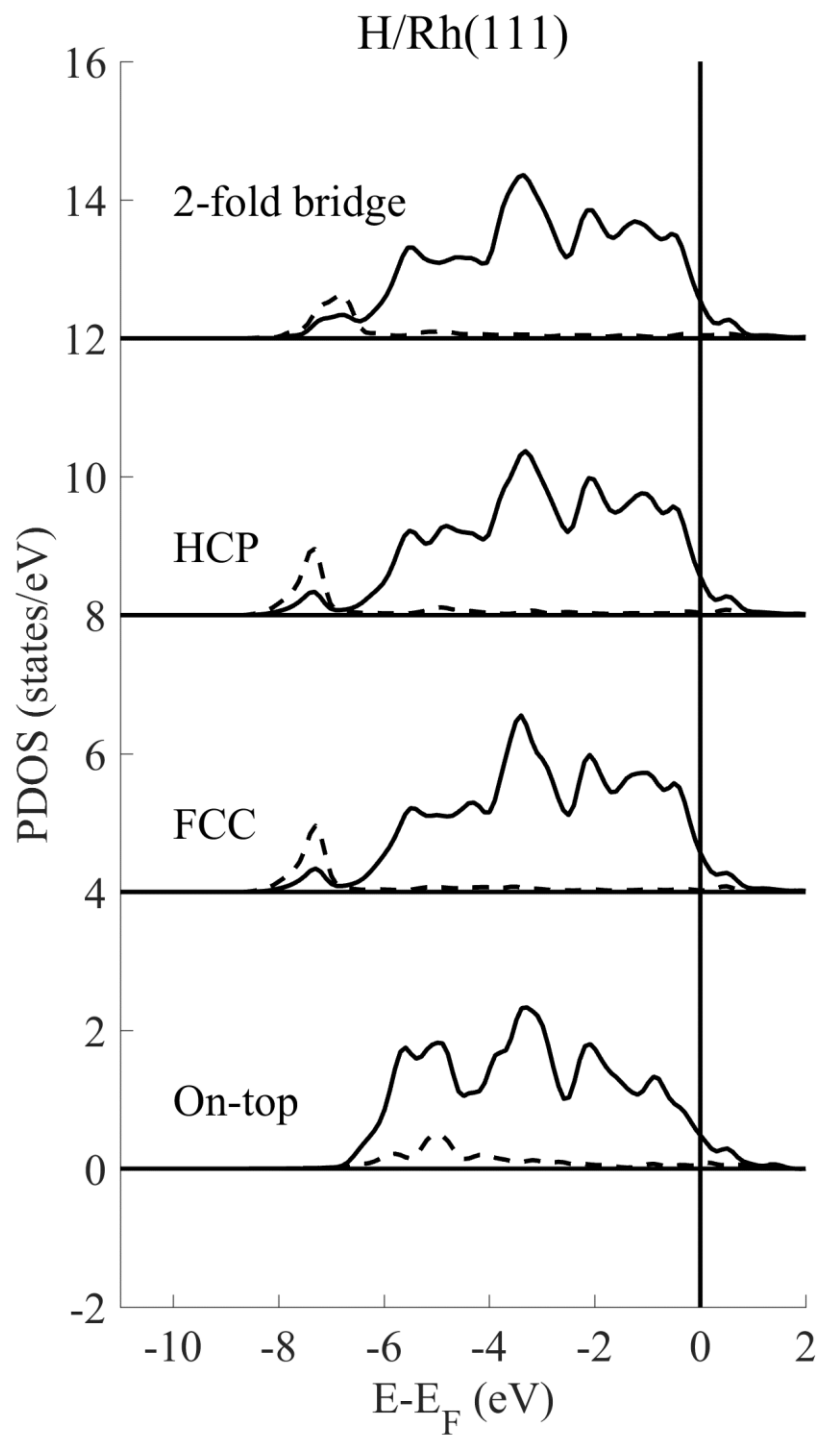
(a)



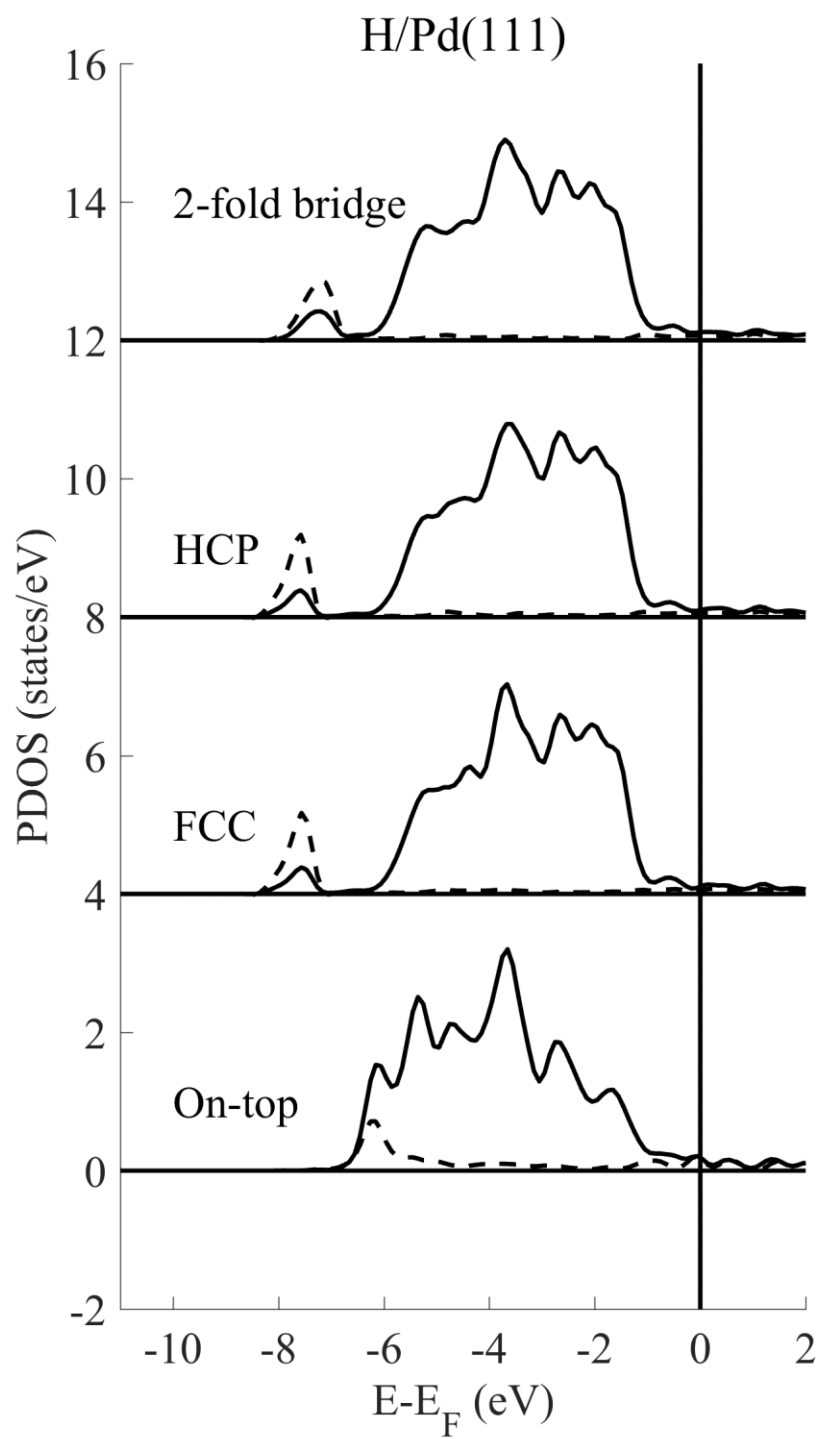
(b)



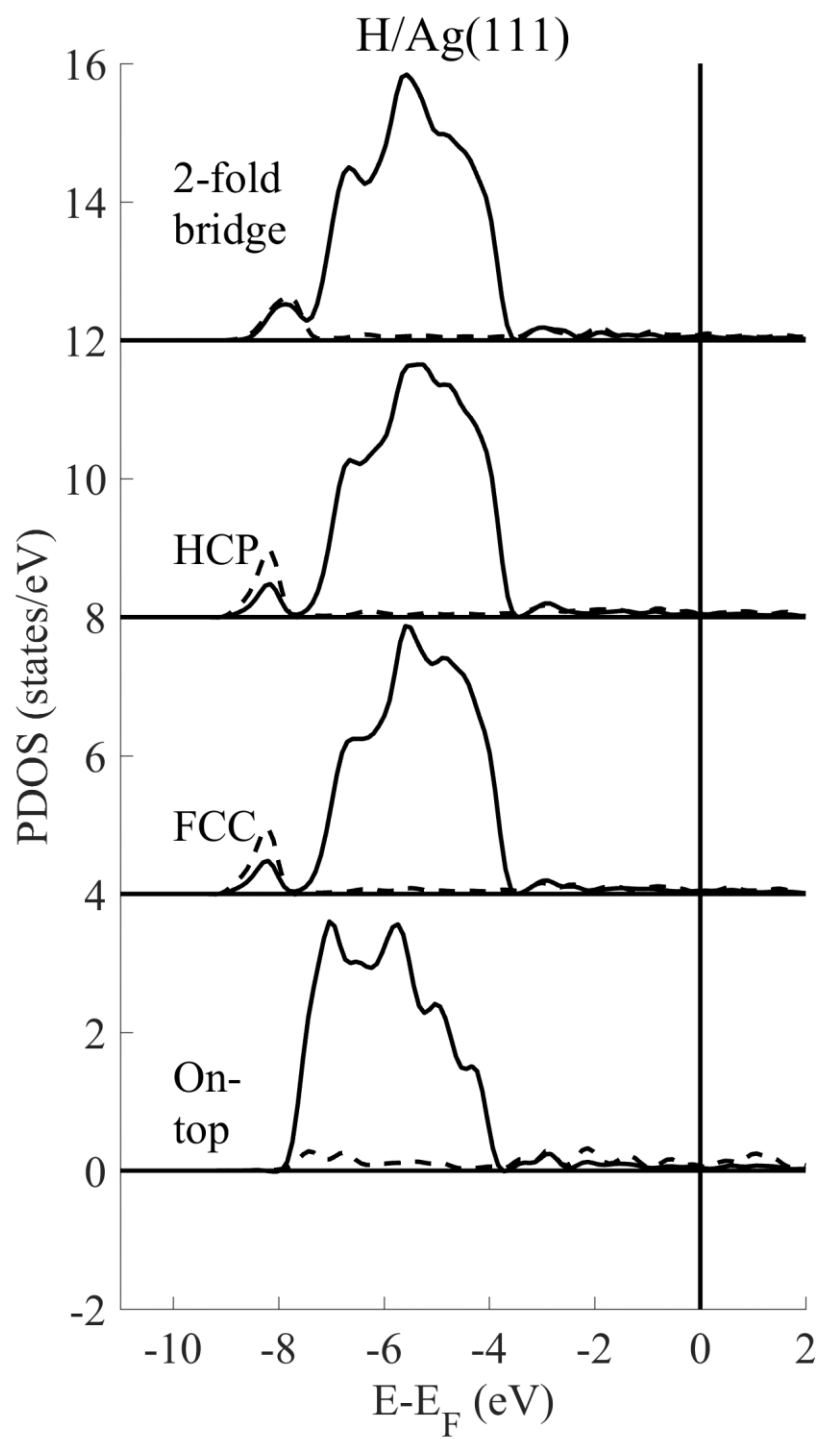
(c)



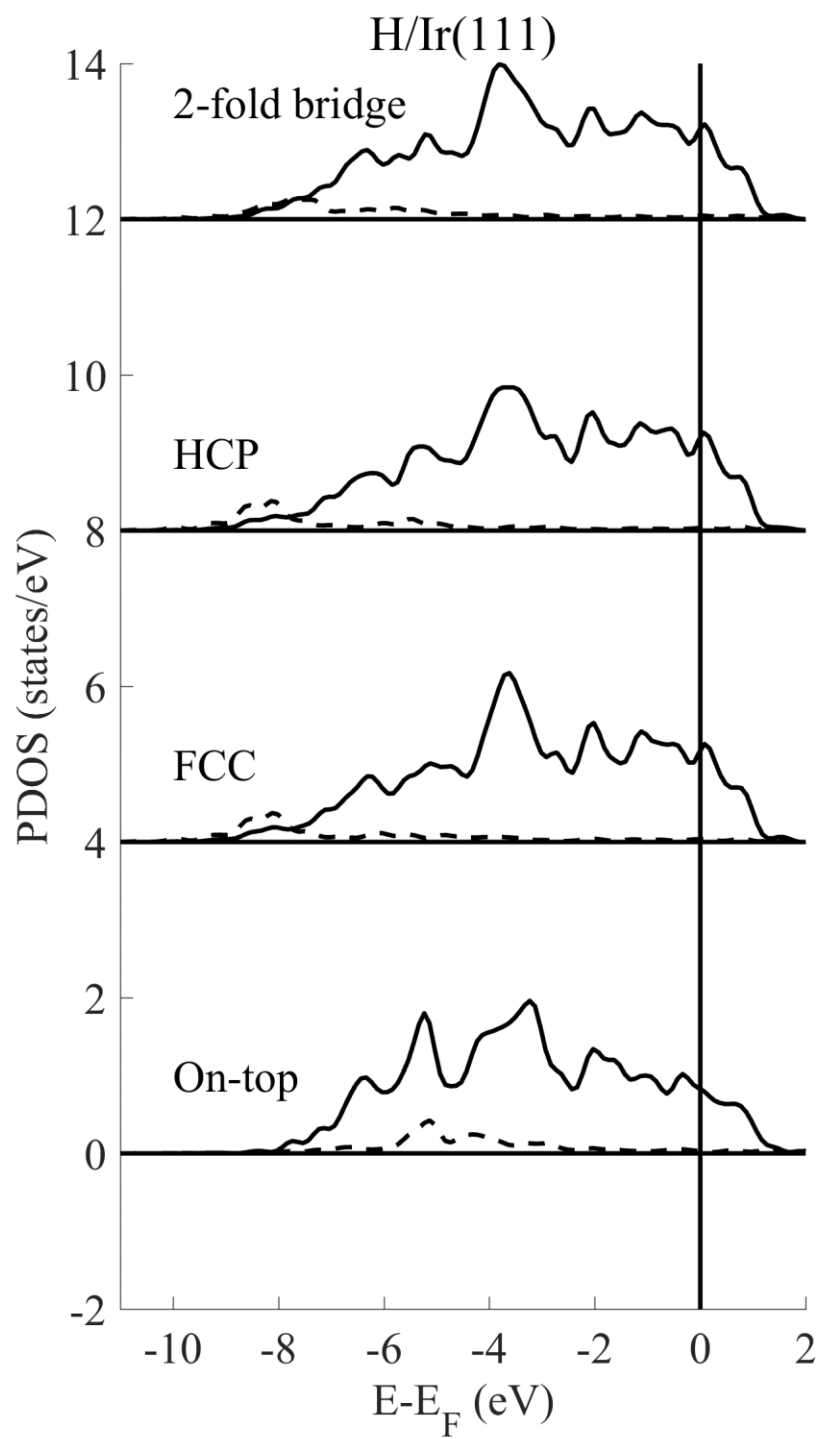
(d)



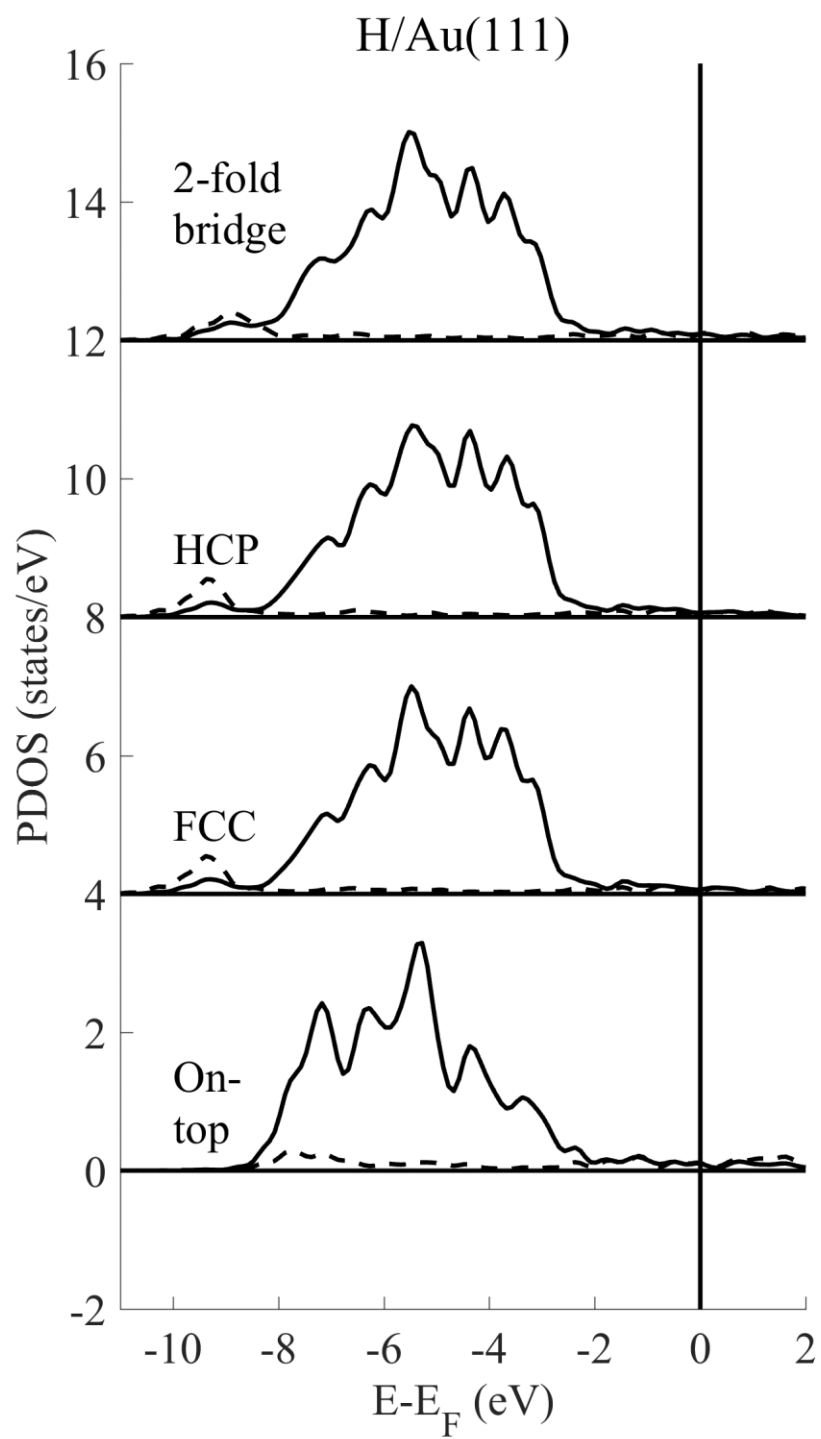
(e)



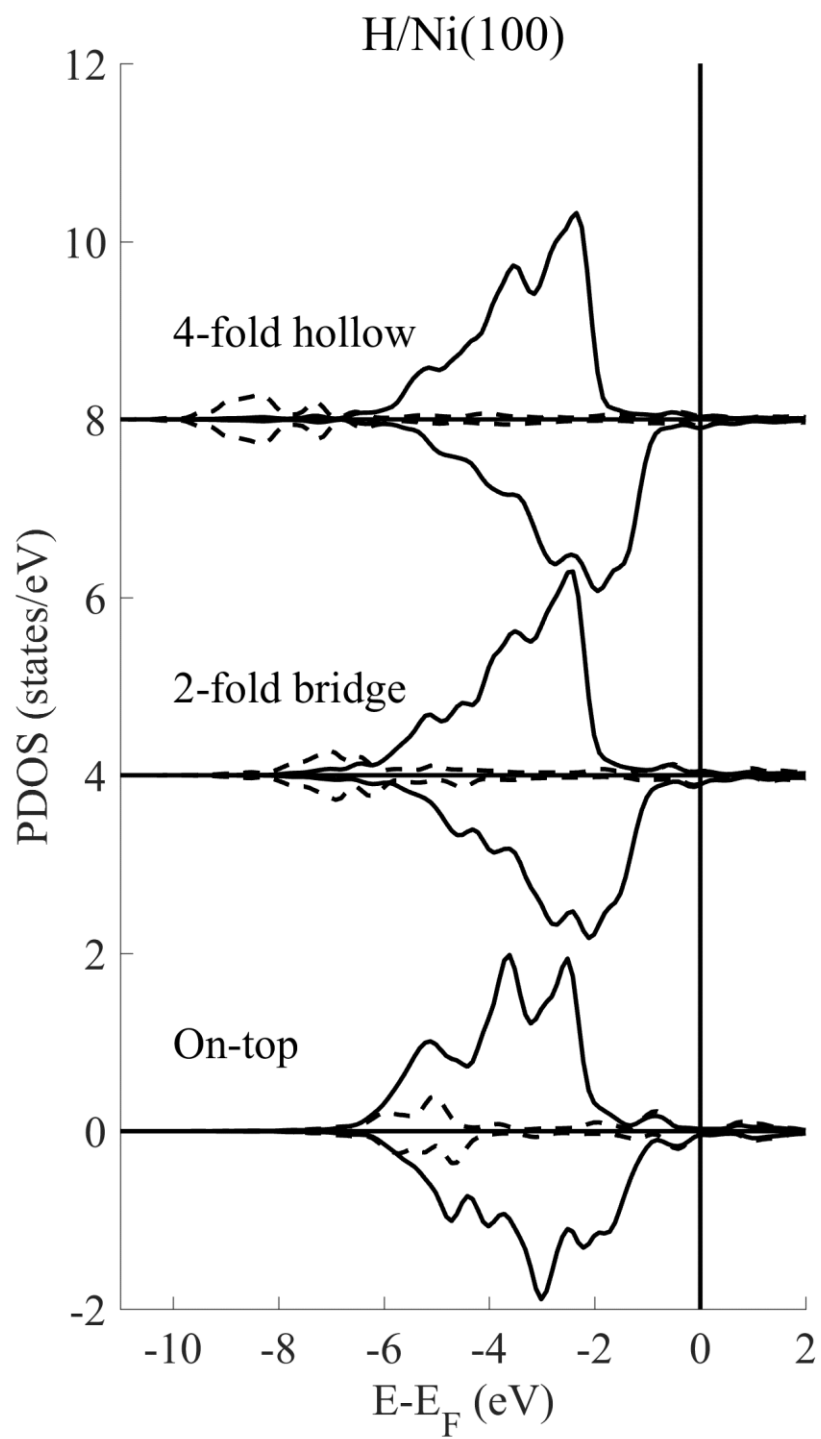
(f)



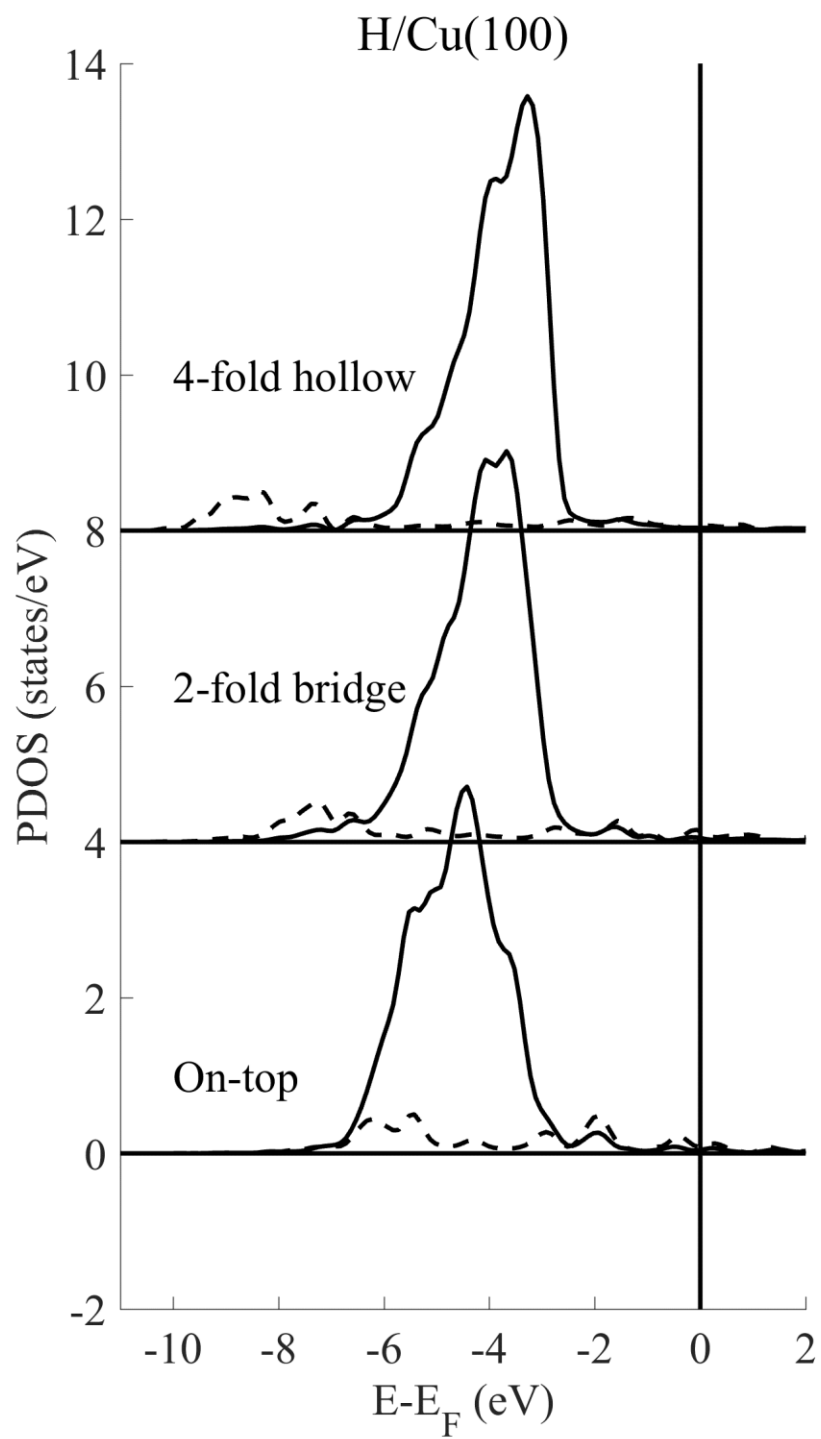
(g)



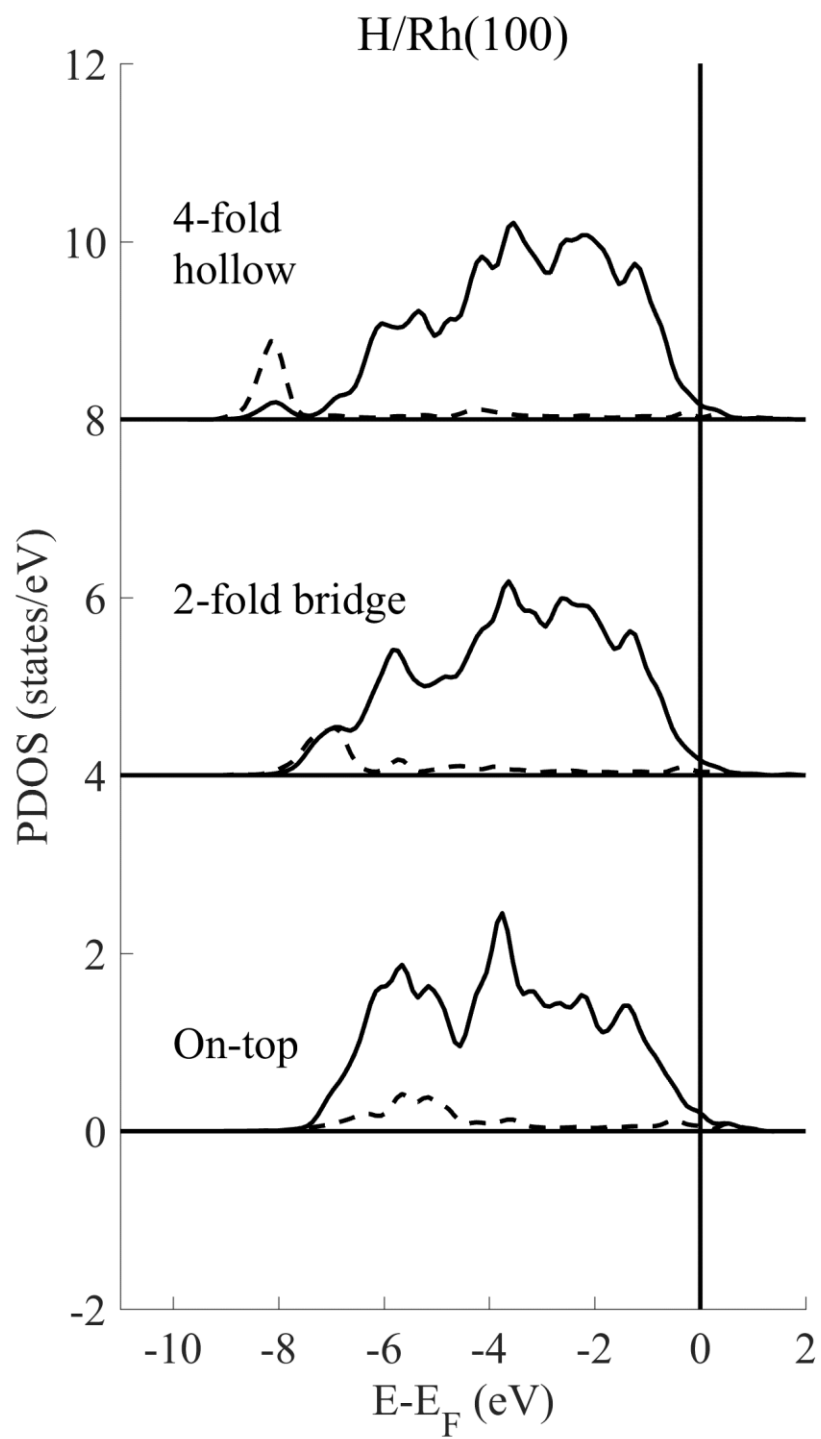
(h)



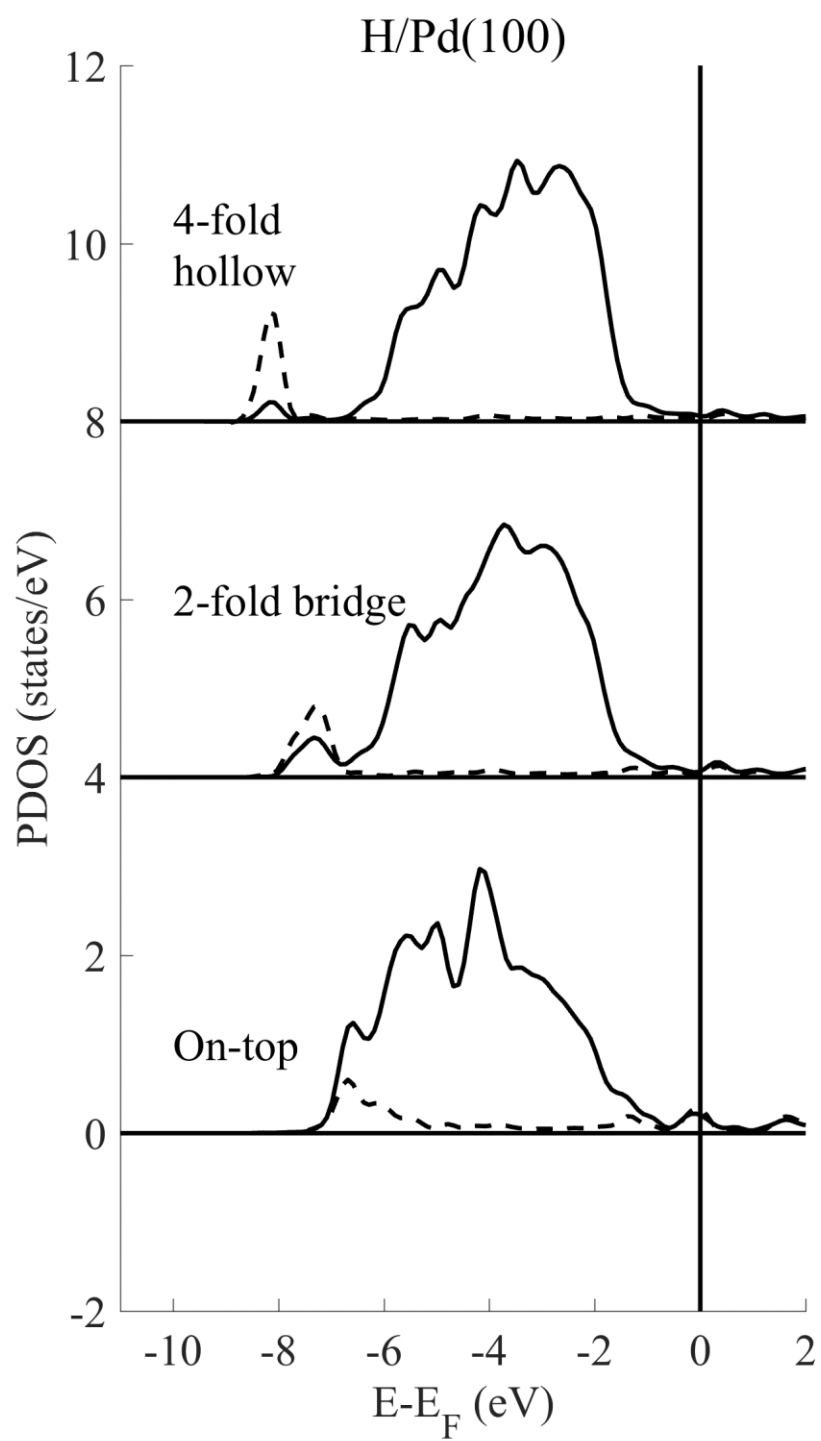
(i)



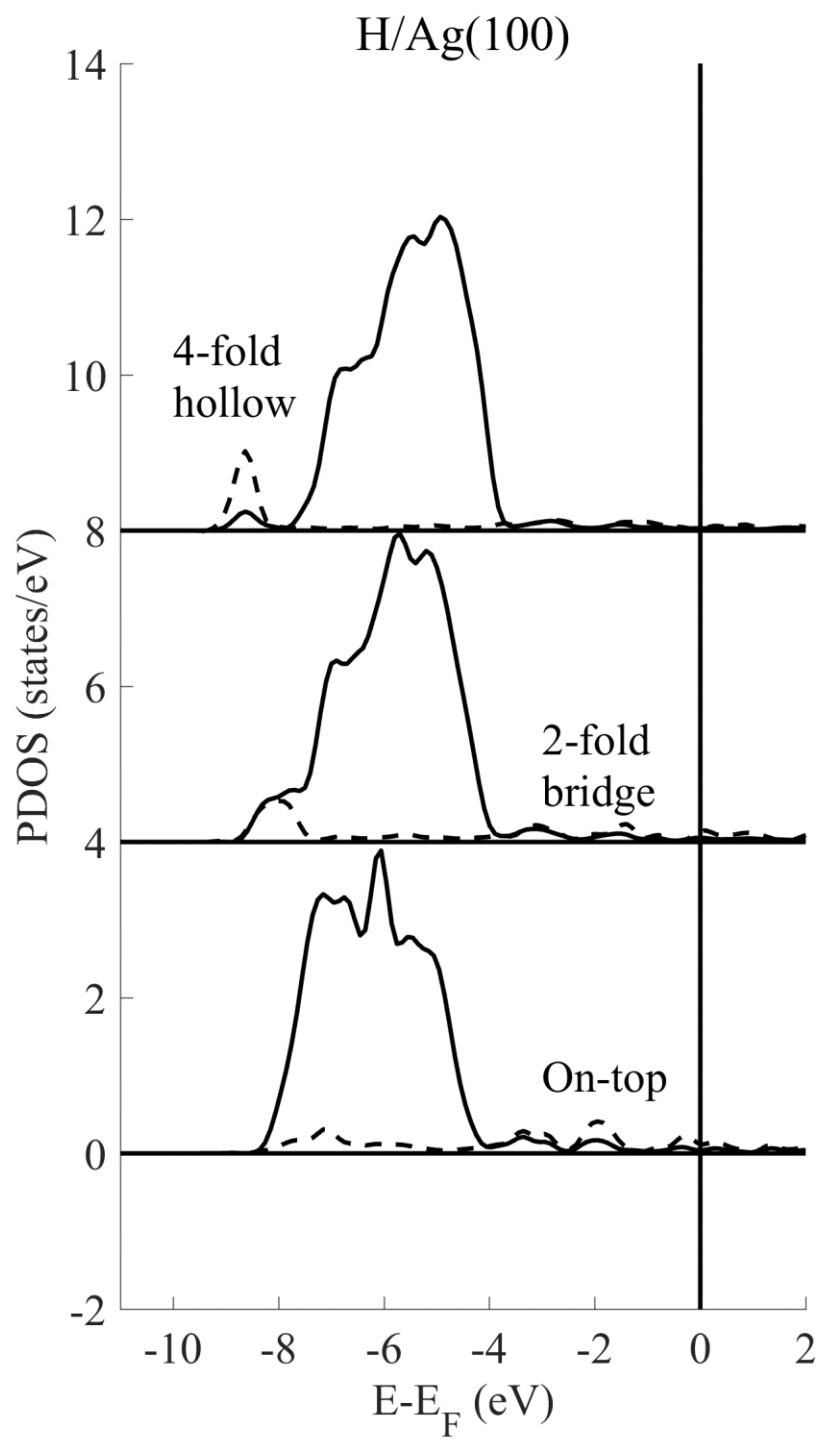
(j)



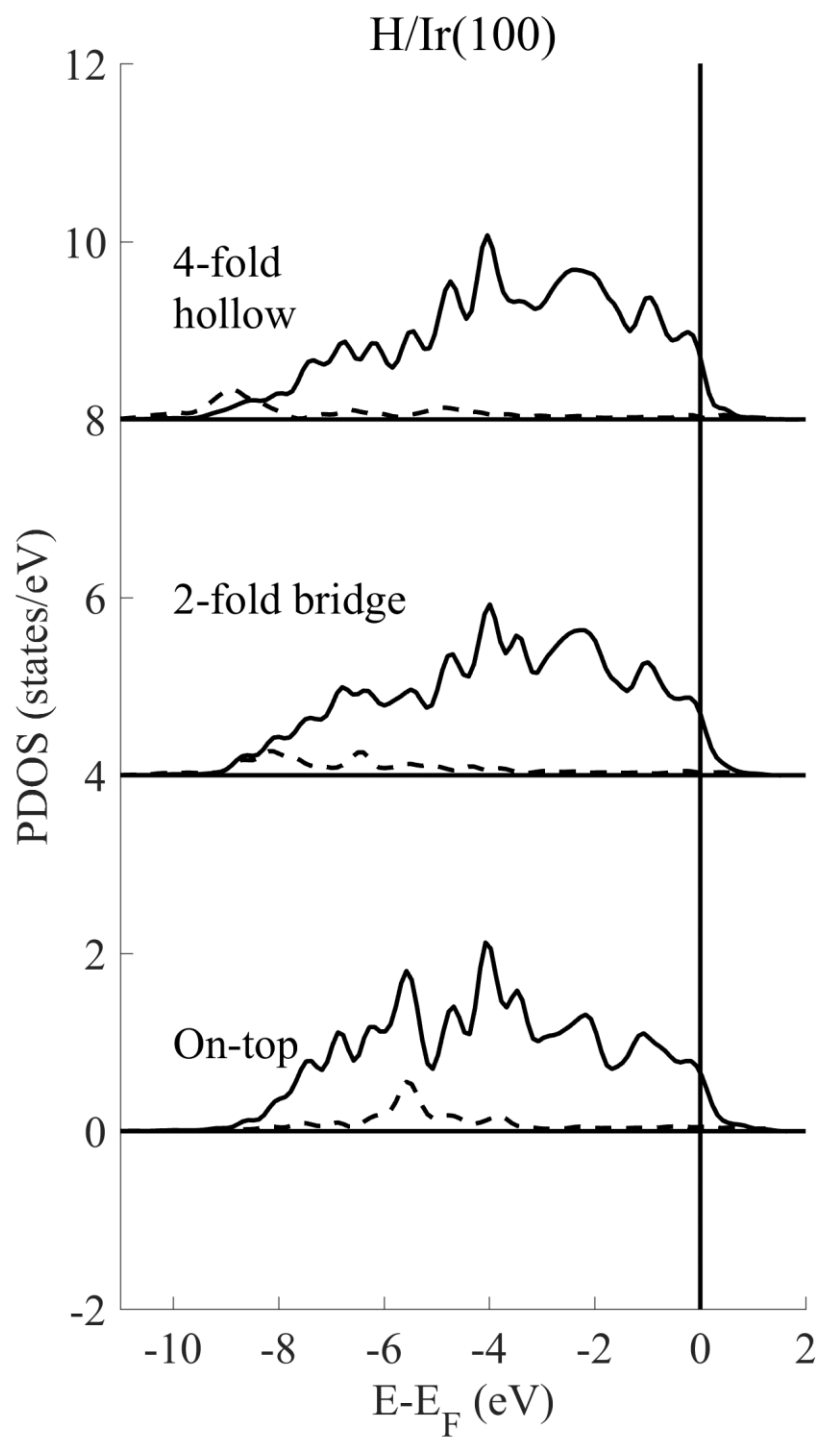
(k)



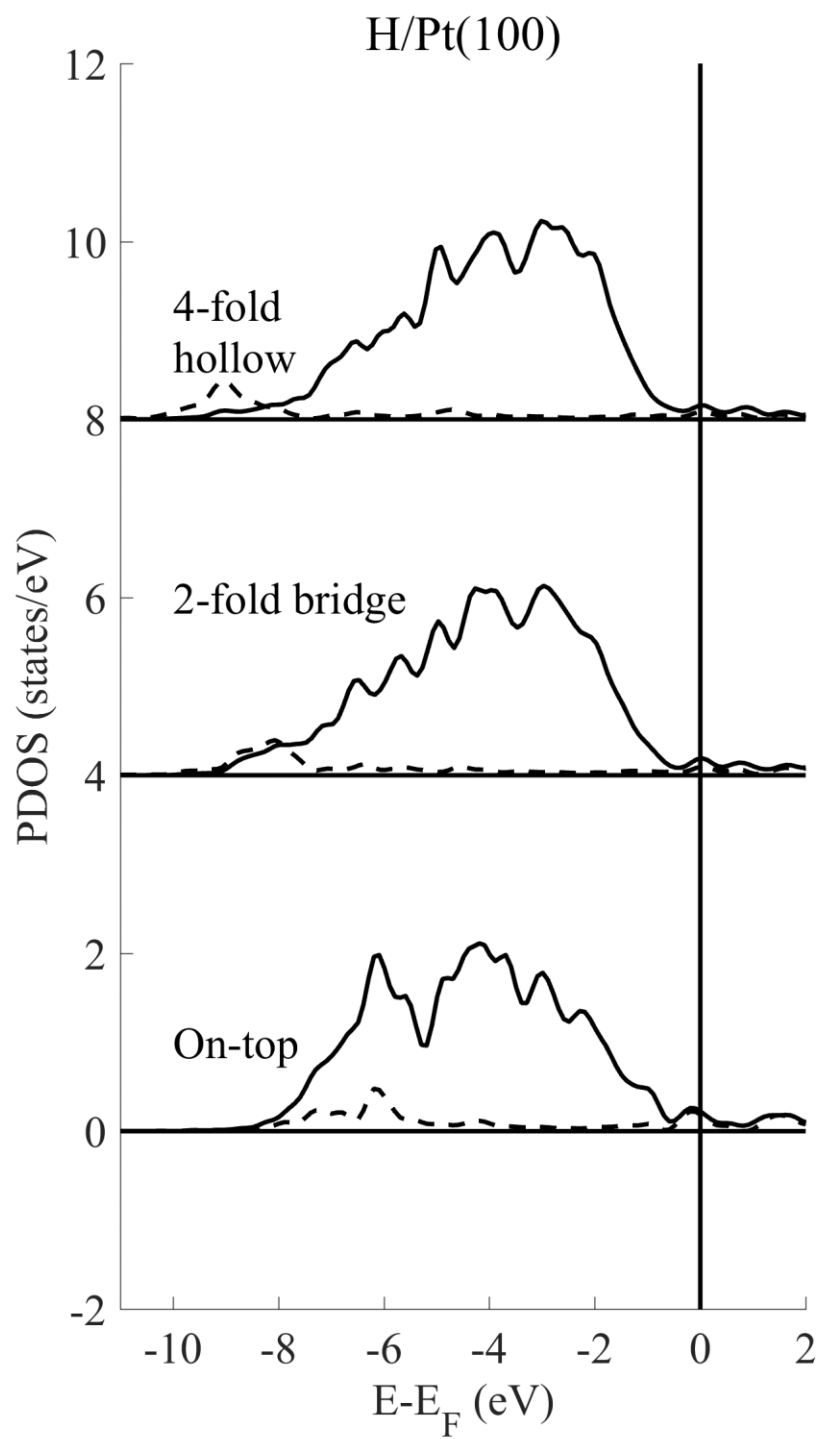
(1)



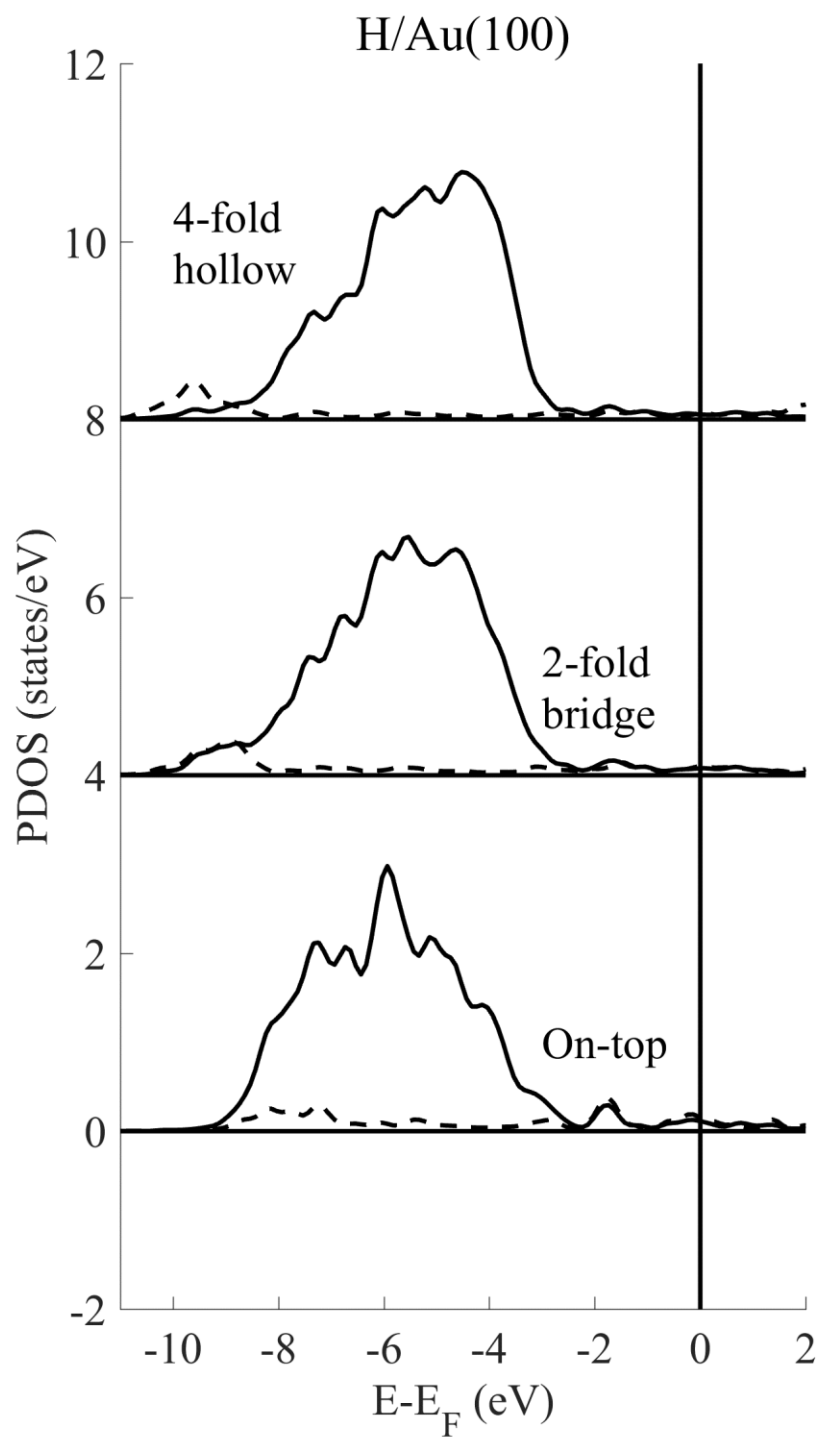
(m)



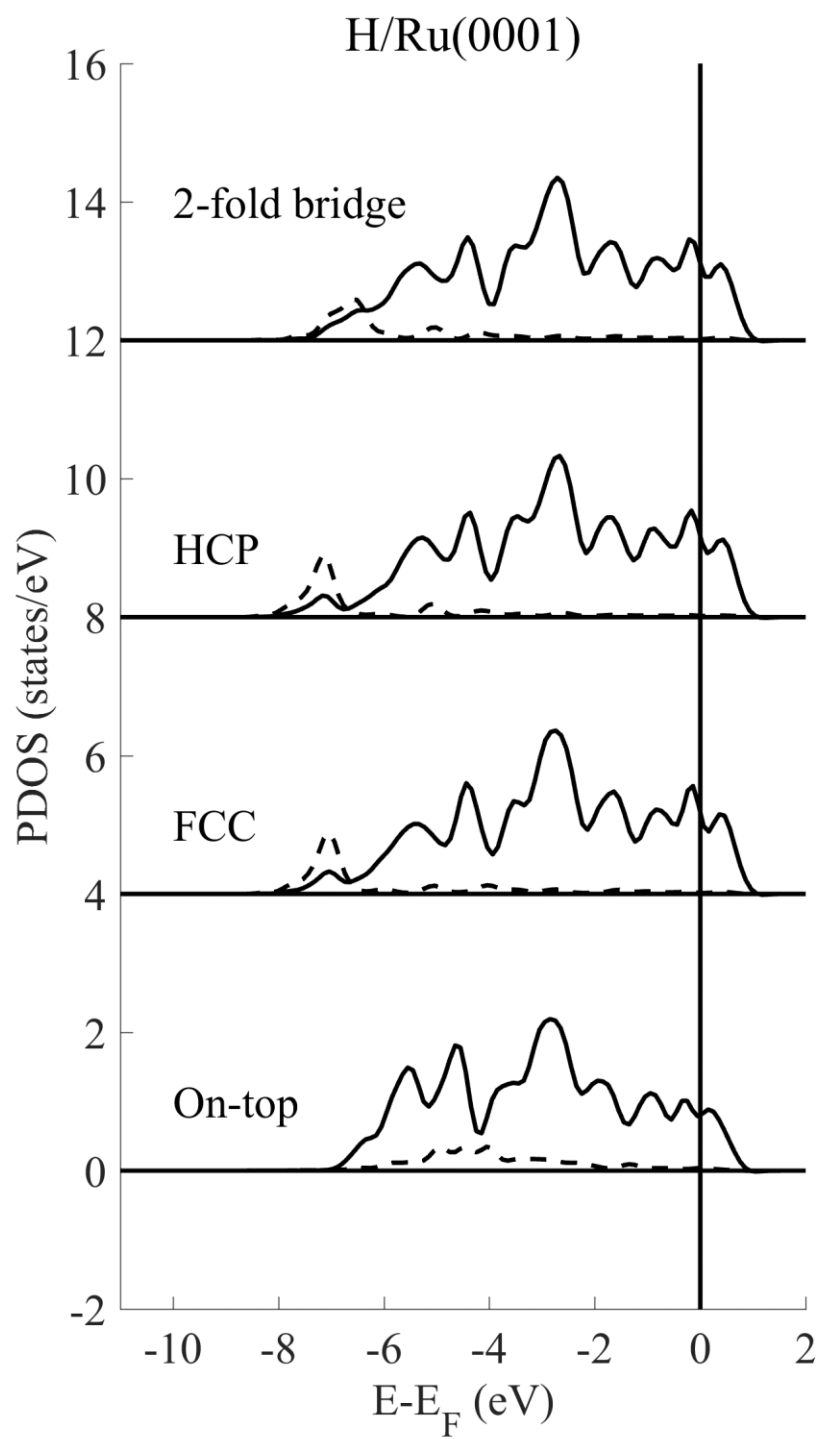
(n)



(c)



(p)



(q)

